

1 2 9 0



UNIVERSIDADE D
COIMBRA

Paulo David Nunes Barradas

**The chemistry and photochemistry of chitosan randomly
labeled polymers and cationic Ladder-type polymers
containing pyrene as fluorescence probe**

Dissertação no âmbito do Mestrado em Química, na área de especialização de Química
Avançada e Industrial variante Química-Física Experimental e Teórica orientada pelo
Professor Doutor João Sérgio Seixas de Melo e apresentada ao Departamento de Química da
Faculdade de Ciências e Tecnologia da Universidade de Coimbra.

September 2023

Faculdade de Ciências e Tecnologia da Universidade de Coimbra

The chemistry and photochemistry of chitosan
randomly labeled polymers and cationic
Ladder-type polymers containing pyrene as
fluorescence probe

Paulo David Nunes Barradas

Dissertação no âmbito do Mestrado em Química, na área de especialização de Química
Avançada e Industrial variante Química-Física Experimental e Teórica orientada pelo Professor
Doutor João Sérgio Seixas de Melo e apresentada ao Departamento de Química da Faculdade de
Ciências e Tecnologia da Universidade de Coimbra.

September 2023



UNIVERSIDADE D
COIMBRA

*“Progress is made by trial and failure;
the failures are generally a hundred times more numerous than successes,
yet they are usually left unchronicled.”*

Sir William Ramsay

Acknowledgments

If someone had ever told me what I would have to do to reach the point where I am now, I probably would not have trusted him. The challenges I have faced, the obstacles I have overcome, and the opportunities to connect with new and diverse people, cultures, and experiences all have brought me to where I am now. While words and pages fall short of expressing my gratitude to all those who have crossed my path, I want to extend my heartfelt appreciation to those who have, in various ways, contributed to my current standing in my academic, professional, and personal life.

I would like to begin by expressing my deep gratitude to my supervisor, Professor Dr. Sérgio Seixas de Melo, for his unwavering support, understanding, availability, trust, and guidance. I am thankful for the insightful scientific discussions and the challenges he presented to me. His encouragement of my scientific curiosity, the opportunities he has provided me, and his preparation for the challenges that lie ahead have been invaluable and have led me to this point. To you, Professor, my sincerest thanks!

To Professor Dr. Ullrich Scherf, I am grateful for the warm welcome, and positive environment that I could find in his research group. To my colleagues at the Macromolecular Chemistry Laboratory at the University of Wuppertal – Tobias, Marvim, Felix, and Hauke – I extend my appreciation for their patience and assistance during my time in Germany. Vielen Dank!

I wish to express my deep thankfulness to Dr. João Pina for his availability, positive demeanor, and assistance with the use and training of several equipment facilities, namely, the fs-TA, and ps-TCSPC. His patient approach to addressing my uncertainties and his encouragement to delve into the mechanics behind the concepts, rather than passively accepting them, have been immensely valuable.

To my colleagues and friends from the Photochemistry Group at the University of Coimbra – Ana Clara, Telma, Carlita, Mariana, Ricardo, Catarina, Daniela S., Simone, Estefânia, Carla 'Whiskies', and Gabriel – I express my gratitude for the enriching moments, valuable advice, availability, and camaraderie. A special mention goes to Carlita, who has consistently been there to help when needed and to ground me when things got overly complicated. Thank you for your friendship and support throughout this journey. To Ana Clara, thank you for patiently addressing my questions and sharing your knowledge and experiences. To Mariana, I am grateful for your cheerful presence and camaraderie, both within and outside the laboratory. To you three 'Flores', my heartfelt Obrigado!

My appreciation goes to Dr. Bernardo Albuquerque for his assistance in acquiring and analyzing Raman spectra, as well as his availability and support.

I extend my thanks to the Center for Chemistry of Coimbra (CQC) for funding my research scholarships.

To the family, I have met in Coimbra and to my dear friends – Carol, Rita, Victor, Rodrigo, and João – thank you for the countless coffees and hours of conversation, your unwavering support, friendship, and genuine concern. Please know that I hold each of you in high regard, and regardless of the physical distance, you're with me for life!

I am deeply grateful to those who have crossed my path and, in their ways, imparted wisdom and contributed to my personal growth. I also extend my gratitude to the new people life has introduced me to recently, individuals who have offered their support and belief in me.

A heartfelt thank you to my parents, sisters, grandmother, and uncles – those I left behind in Venezuela to pursue my goal of becoming a chemist. Your trust in me and your constant words of encouragement and life advice, despite the physical separation, means the world. You've consistently supported my journey to become a better person and have motivated me to reach for my aspirations. Your unconditional support has been the cornerstone of my journey. Muchas Gracias!

Once again, to every one of you, thank you!

*Coimbra tem mais encanto na hora da despedida,
pena que ainda não é tempo de ir embora porque ainda há mais por conseguir!*

Paulo David Nunes Barradas

Table of Contents

TABLE OF CONTENTS	I
SCHEMES	V
FIGURES	VI
ABBREVIATIONS & SYMBOLS	IX
ABSTRACT	XI
RESUMO	XIII
CHAPTER 1: INTRODUCTION	1
1.1 PHOTOCHEMISTRY AND PHOTOPHYSICS	3
1.2 PYRENE	4
1.3 POLYMERS	6
1.3.1 Chitosan	7
1.3.2 Ladder Polymers	8
1.4 OBJECTIVES AND METHODOLOGIES	9
BIBLIOGRAPHY	12
CHAPTER 2: CHITOSAN POLYMER RANDOMLY LABELED WITH PYRENE	15
SUMMARY	17
2.1 SYNTHESIS AND STRUCTURAL CHARACTERIZATION	17
2.1.1 Reagents and solvents	17
2.1.2 Experimental procedure	17
2.2 RESULTS AND DISCUSSION	19
2.2.1 Degree of pyrene in ChiNPy polymers	19
2.2.2 FTIR and Raman characterization	24
2.2.3 UV-Vis and fluorescence characterization	26
2.2.4 Interaction with metals	32
CONCLUSION	35
BIBLIOGRAPHY	36
CHAPTER 3: DIAZACATIONIC LADDER-TYPE POLYMERS WITH PYRENE	37
SUMMARY	39
3.1 SYNTHESIS AND STRUCTURAL CHARACTERIZATION	39

3.1.1 Reagents and solvents	39
3.1.2 Experimental procedure	39
3.2 RESULTS AND DISCUSSION	48
3.2.1 FTIR Characterization	48
3.2.2 EPR measurements	49
3.2.3 UV-Vis and fluorescence characterization	50
MonPy	50
PolyNPy	53
DiazaPy	56
3.2.4 Temperature dependence studies of PolyNPy and DiazaPy polymers	63
CONCLUSION	66
BIBLIOGRAPHY	68
CHAPTER 4: EXPERIMENTAL TECHNIQUES	69
SUMMARY	71
INSTRUMENTATION AND TECHNIQUES	71
4.1.1 Nuclear Magnetic Resonance	71
4.1.2 Liquid Chromatography - Mass Spectrometry	72
4.1.3 Fourier Transform Infrared and Raman Spectroscopy	73
4.1.4 Electron Paramagnetic Resonance	74
4.1.5 UV-visible spectrophotometry and Steady-State Fluorescence measurements	75
4.1.6 Time-Correlated Single Photon Counting Techniques	77
4.1.7 Pump-probe femtosecond Transient Absorption	79
4.1.8 Theoretical Calculations	79
BIBLIOGRAPHY	82
CHAPTER 5: APPENDIX	85
Appendix A. ¹ H NMR of ChiNPy Polymers	87
Appendix B. Determination of molar extinction coefficient	88
Appendix C. Determination of %DS _{Py} by UV-Vis techniques	88
Appendix D. Fluorescence quenching	91
Appendix E. Statistical parameter of Stern-Volmer plots	92
Appendix F. Prediction of electronic transitions of MonPy, PolyNPy, and DiazaPy	92

Appendix G. 2D-NMR of MonPy

95

BIBLIOGRAPHY

97

Schemes

Scheme 1.1 Pyrene molecule with identification of its positions and showing its three different planes of symmetry. Groups with chemically identical sites are represented with the same color.	4
Scheme 1.2 Chitosan structure. DA – Deacetylated unit; AC – Acetylated unit.	7
Scheme 1.3 Pyrene-containing polymeric systems studied in the current work.	9
Scheme 1.4 Generic mechanism for the formation of a Schiff base.	10
Scheme 1.5 Schematic presentation of the Buchwald-Hartwig Cross-Coupling catalytic cycle.	11
Scheme 2.1 Schematic synthesis of the ChiNPy polymers	18
Scheme 2.2 Structures of all possible monomer units present in ChiNPy polymers.	20
Scheme 3.1. Synthesis of MonPy molecule by Buchwald-Hartwig amination.	40
Scheme 3.2 Polymerization of MonPy with (2,5-dibromo-1,4-phenylene)bis((4-decylphenyl)methanone).	42
Scheme 3.3 Synthesis of diazocationic ladder-type polymer DiazaPy from PolyNPy.	46
Scheme 3.4 Illustration of possible structures in DiazaPy sample produced by defects in the polymer. These are highlighted to help in the discussion; see text for more details.	60

Figures

Figure 1.1 Simplified Jablonski-Perrin diagram. <i>vr</i> – vibrational relaxation; IC – Internal Conversion; ISC – Intersystem Crossing.....	3
Figure 1.2 (Left) Normalized absorption and emission spectrum of a diluted solution of pyrene in THF. Relevant electronic transitions are indicated. (Right) Normalized absorption spectrum of pyrene (black) and 1-pyrenecarboxyaldehyde (green) in THF at T=293 K.....	5
Figure 2.1 ¹ H NMR of (top) Chitosan and (bottom) ChiNPy-B at 50 °C in D ₂ O: DCl 1% solution. The chemical shift values (δ) of the main peaks of each compound are shown as inset.....	21
Figure 2.2 Graphical representation of the different species presents in ChiNPy polymers. UV-Vis spectra of amine pyrene units in chitosan were estimated by subtraction of ChiNPy-B to ChiNPy-Imine spectra.....	22
Figure 2.3 FTIR spectra of (A) Chitosan, (B) ChiNPy-A, (C) ChiNPy-B and (D) ChiNPy-Imine. Key bands pertinent to the rapid analysis of %DD are highlighted for easy reference.....	25
Figure 2.4 (Left) Theoretical Raman spectra obtained for Acetylated (AC), Deacetylated (DA), Amine, and Imine pyrene monomers model within ChiNPy polymers. These spectra were obtained using the Gaussian® 16 package employing the b3pw91 functional. (Right) Normalized experimental Raman spectra of (A) Chitosan, (B) ChiNPy-A, (C) ChiNPy-B, and (D) ChiNPy-Imine.....	26
Figure 2.5 Representation of the proposed monomers utilized for computational previsions of the electronic characteristics of ChiNPy polymers. At the right, the optimized structure obtained by DFT is presented.....	27
Figure 2.6 Prediction of absorption spectra with TD-DFT with the BPBE functional in water for model monomers of (red) Amino and (Black) Imine structures in the ChiNPy polymers. Experimental absorption spectra are also shown as dashed lines for comparison.....	27
Figure 2.7 Normalized (A) absorption and (B) emission spectra of ChiNPy polymers in HAc 5% of ChiNPy-A (black line), ChiNPy-B (dashed-red line) and ChiNPy-Imine (Dashed green line). Emission spectra were recorded using $\lambda_{exc} = 350$ nm.....	28
Figure 2.8 Comparison of normalized excitation spectra of (A) ChiNPy -A,(B) ChiNPy-B, and (C) ChiNPy-Imine at different emission wavelengths, (dashed-black line) $\lambda_{exc} = 380$ nm, (dashed red line) $\lambda_{exc} = 430$ nm, and (dashed green line) $\lambda_{exc} = 500$ nm. The absorption spectra (gray line) are also shown.....	29
Figure 2.9 (Left) Fluorescence decay adjusted using a method of the sum of exponential and (Right) lifetime distribution obtained by the method of maximum entropy of (A) ChiNPy-A and (B) ChiNPy-B. Weighted residues (W.R) and autocorrelation function(A.C) are shown as an inset in the fluorescence decay as parameters of the fitting. Residues of the function are shown in the case of MEM as inset.....	31
Figure 2.10 Fluorescence decay of ChiNPy-Imine in HAc 5% at 20 °C. Analysis of each λ_{em} was made individually by the method of sum of exponential. Weighted residues (W.R) and autocorrelation function (A.C) are shown as an inset in the fluorescence decay as parameters of the fitting.....	32
Figure 2.11 Normalized emission spectra of ChiNPy-B with $\lambda_{exc} = 350$ nm, at 25 °C and continuous stirring at 250 rpm with the addition of different metals and anions in HAc 5 %v/v. Each spectrum was recorded 3 min after the addition of the quencher to the solution.....	33
Figure 2.12 Stern-Volmer plot for the addition of different (left) metals and (right) anions to a solution c.a. 1 ppm of ChiNPy-B at 25 °C and continuous stirring at 250 rpm. Each measurement was performed in an interval of 3	

min after the addition of the quencher and each experiment was done by triplicate. Gray lines in classic SV are meant to be a guideline to the eye to highlight the downward curvature observed.	34
Figure 2.13 Alternative Stern-Volmer plots for the addition of different metals (left) and anions (right) to a solution with approximately 1 ppm of ChiNPy-B at 25 °C. Further details and insights regarding the experimental outcomes are provided in Appendix E.	34
Figure 3.1 ¹ H NMR of MonPy in deuterated chloroform. The peak attribution is made in Table 3.1.	41
Figure 3.2 ¹³ C NMR of MonPy in deuterated chloroform. The peak attribution is made in Table 3.1.	41
Figure 3.3 Soxhlet apparatus used for extraction of the different fractions of the PolyNPy polymers.	43
Figure 3.4 ¹ H NMR of PolyNPy in 1,1,2,2-Tetrachloroethane-d ₂ . Expansion of the aromatic zone showed as inset. The colors match the attribution in Table 3.2.	44
Figure 3.5 ¹³ C NMR of PolyNPy in 1,1,2,2-Tetrachloroethane-d ₂	45
Figure 3.6 ¹ H NMR of DiazaPy in 1,1,2,2-Tetrachloroethane-d ₂ . Peaks marked as gray are residual solvents.	47
Figure 3.7 ¹³ C NMR of DiazaPy in 1,1,2,2-Tetrachloroethane-d ₂	47
Figure 3.8 FTIR-ATR spectra of (black line) MonPy, (blue line) PolyNPy, and (green line) DiazaPy.	49
Figure 3.9 EPR spectra of DiazaPy in CHCl ₃ (right) under exposition to room light and (left) and avoiding any type of radiation at time (red) 0 h and (green) 96 h.	50
Figure 3.10 Normalized absorption, excitation and fluorescence emission of MonPy in (A) 2MeTHF, (B) CHCl ₃ and (C) toluene. The fluorescence spectra were acquired using an excitation wavelength (λ_{exc}) of 350 nm, while the excitation spectra were obtained with an emission wavelength (λ_{em}) of 450 nm. Each spectrum is accompanied by an inset, providing an enlarged view of the S ₀ →S ₁ transition and highlighting the mirrored relationship between absorption and fluorescence spectra.	51
Figure 3.11 Absorption spectra predicted using TD-DFT with BPBE functional in toluene for MonPy, alongside inset of optimized structure. Dashed lines represent experimental absorption spectra for comparative analysis.	52
Figure 3.12 Time-resolved femtosecond transient absorption (fs-TA) of MonPy obtained with $\lambda_{exc} = 380$ nm in deaerated toluene at room temperature. Representative kinetic traces with fits from global analysis are presented as inset.	53
Figure 3.13 Normalized absorption, excitation and fluorescence emission of PolyNPy in (A) 2MeTHF, (B) CHCl ₃ and (C) toluene. The fluorescence spectra were acquired using an excitation wavelength (λ_{exc}) of 390 nm, while the excitation spectra were obtained with an emission wavelength (λ_{em}) of 570 nm.	54
Figure 3.14 Absorption spectra predicted using TD-DFT with BPBE functional in toluene for PolyNPy, alongside inset of optimized structure. Dashed lines represent experimental absorption spectra for comparative analysis. ..	55
Figure 3.15 Time-resolved femtosecond transient absorption (fs-TA) of PolyNPy obtained with $\lambda_{exc} = 380$ nm in deaerated toluene at room temperature. Representative kinetic traces with fits from global analysis are presented as inset.	56
Figure 3.16 Normalized spectra of DiazaPy compound with a concentration of 35 ppm in different solvents.	56
Figure 3.17 Normalized absorption, excitation and fluorescence emission of DiazaPy in (A) 2MeTHF, (B) CHCl ₃ and (C) toluene. The fluorescence spectra were acquired using an excitation wavelength (λ_{exc}) of 350 nm, while the excitation spectra were obtained with an emission wavelength (λ_{em}) of (dashed purple) 510 nm and (dashed yellow) 780 nm.	57

Figure 3.18 Absorption spectra of various concentrations of DiazaPy in toluene at 20 °C.	58
Figure 3.19 Emission spectra of different concentrations of DiazaPy in toluene at 20 °C using excitation wavelengths of (right) 350 nm and (left) 700 nm. A Gaussian fit was applied to the right spectrum to show the complete spectral profile since the correction factor is no longer valid for $\lambda > 810$ nm.	58
Figure 3.20 Absorption spectra predicted using TD-DFT with BPBE functional in toluene for DiazaPy, alongside inset of optimized structure. Dashed lines represent experimental absorption spectra for comparative analysis. ..	59
Figure 3.21 Time-resolved femtosecond transient absorption (fs-TA) of DiazaPy obtained with $\lambda_{exc} = 380$ nm in deaerated toluene at room temperature. Representative kinetic traces with fits from global analysis are presented as inset.	61
Figure 3.22 Emission spectra of PolyNPy at different temperatures with $\lambda_{exc} = 390$ nm.	63
Figure 3.23 (Left) Depiction of maximum emission intensity and corresponding emission wavelength as functions of temperature for PolyNPy in toluene with excitation wavelength (λ_{exc}) of 390 nm. (Right) Arrhenius plot illustrating experimental data for PolyNPy tracked at emission wavelength (λ_{em}) of 573 nm.	64
Figure 3.24 Emission spectra of DiazaPy at different temperatures with $\lambda_{exc} = 350$ nm.	65
Figure 3.25 (A) Depiction of maximum emission intensity in the first emission band of DiazaPy and corresponding emission wavelength as functions of temperature in toluene with excitation wavelength (λ_{exc}) of 350 nm. (B) Arrhenius plot illustrating experimental data of first emission band for DiazaPy tracked at emission wavelength (λ_{em}) of 488 nm. (C) Depiction of maximum emission intensity in the second emission band of DiazaPy and corresponding emission wavelength as functions of temperature in toluene with excitation wavelength (λ_{exc}) of 350 nm. (D) Arrhenius plot illustrating experimental data of second emission band for DiazaPy tracked at emission wavelength (λ_{em}) of 780 nm.	65
Figure 5.1 ¹ H NMR of ChiNPy-A at 50 °C in D ₂ O: DCl 1% solution. The degree of substitution determined by this technique is shown as inset.	87
Figure 5.2 ¹ H NMR of ChiNPy-A at 50 °C in D ₂ O: DCl 1% solution. The degree of substitution determined by this technique is shown as inset.	87
Figure 5.3 Representation of UV-Vis spectra of 1-pyrenecarboxyaldehyde for determination of molar extinction coefficient in methanol at 20 °C.	88
Figure 5.4 Determination of molar extinction coefficient of 1-pyrenecarboxyaldehyde in methanol at (A) 340 nm and (B) 393 nm.	88
Figure 5.5 Absorption spectra of ChiNPy-A solutions used for determination of %DS _{Py}	89
Figure 5.6 Absorption spectra of ChiNPy-B solutions used for determination of its %DS _{Py}	90
Figure 5.7 Absorption spectra of ChiNPy-Imine solutions used for determination of its %DS _{Py}	90
Figure 5.8 ¹ H- ¹ H COSY NMR spectra of MonPy in CDCl ₃	95
Figure 5.9 ¹ H- ¹³ C HSQC NMR spectra of MonPy in CDCl ₃	95
Figure 5.10 ¹ H- ¹³ C HMBC NMR spectra of MonPy in CDCl ₃	96
Figure 5.11 ¹⁹ F NMR spectra of MonPy in CDCl ₃	96

Abbreviations & Symbols

TSP-d4	3-(Trimethylsilyl)propionic-2,2,3,3 acid sodium salt
HAc	Acetic Acid
AC	Acetylated Unit in Chitosan Monomer
a.u.	Arbitrary Units
ATR	Attenuated Total Reflectance
A.C	Autocorrelation Function
¹³ C NMR	Carbon Nuclear Magnetic Resonance
CT	Charge Transfer
ChiNPy	Chitosan Randomly Labeled with Pyrene
DA	Deacetylated Unit in Chitosan Monomer
%DD	Degree of Deacetylation in Chitosan Polymers
%DS _{Py}	Degree of Substitution with Pyrene In Chitosan Polymer
DFT	Density Functional Theory
DiazaPy	Diazacationic Ladder-Type Polymer with Pyrene
DCM	Dichloromethane
EPR	Electronic Paramagnetic Resonance
$\Delta E_{(S_1 - T_1)}$	Energy Splitting Between the Lowest Singlet and Triplet Excited State
ESA	Excited State Absorption
φ_F'	Fluorescence Quantum Efficiency
φ_F	Fluorescence Quantum Yield
¹⁹ F NMR	Fluorine Nuclear Magnetic Resonance
FRET	Föster Resonance Energy Transfer
FTIR	Fourier-Transform Infrared Spectroscopy
f_a	Fraction of accessible fluorophore to the quencher
FC	GAMESS-US Franck Condon
GPC	Gel Permeation Chromatography
GAMESS	General Atomic and Molecular Electronic Structure System
GSB	Ground-State Bleaching
HMBC NMR	Heteronuclear Multiple Bond Correlation NMR
HSQC NMR	Heteronuclear Single Quantum Correlation NMR
HOMO	Highest Occupied Molecular Orbital
COSY	Homonuclear Correlation Spectroscopy
IUPAC	International Union of Pure and Applied Chemistry
LC-MS	Liquid Chromatography-Mass Spectrometry
LE	Locally Excited
LUMO	Lower Unoccupied Molecular Orbital

MEM	Maximum Entropy Method
ϵ	Molar Extinction Coefficient
M_w	Molecular weight
MonPy	N2,N7-Bis(2,6-Difluorophenyl)Pyrene-2,7-Diamine
OD	Optical Density
OLEDs	Organic Light-Emitting Diodes
f	Oscillator Strength
PolyNPY	Polymer Precursor of Diazacationic Ladder-Type Polymer
$^1\text{H NMR}$	Proton Nuclear Magnetic Resonance
ϵ_{ss}	Singlet Extinction Coefficient
SV	Stern-Volmer
K_a	Stern-Volmer Quenching Constant
SE	Stimulated Emission
Δ_{ss}	Stokes Shift
TCSPC	Time-Correlated Single Photon Counting
TDDFT	Time-Dependent Density Functional Theory
TA	Transient Absorption
ϵ_{TT}	Triplet Extinction Coefficient
TICT	Twisted Intramolecular Charge Transfer
λ_{em}	Wavelength of Emission
λ_{exc}	Wavelength of Excitation
W.R.	Weighted Residues

Abstract

In the last century, the industry underwent a revolution due to the introduction of polymeric systems. Year after year, extensive hours of research and investments were dedicated to developing new materials that could be applied in a wide range of applications. This master's thesis aims to propose the development of two novel polymeric systems containing pyrene in their structures, to harness the advantageous electronic characteristics of this molecule.

The first polymeric systems studied were two chitosan polymers. These polymers, known as ChiNPy-A and ChiNPy-B, possess degrees of pyrene substitution (%DS_{Py}) with values of 0.5% and 4.5%, respectively, and determined by ¹H NMR and UV-Vis techniques. The resulting polymers comprised four distinct units, as evidence indicated the presence of both pyrene amine units and residual pyrene imine units after reduction.

Time-resolved measurements were conducted in an aqueous solution of 5% acetic acid, resulting in a triple exponential decay pattern that characterizes the fluorescence properties of both pyrene units (amine and imine), as well as certain self-quenching pyrene units.

Fluorescence quenching of pyrene amine units in the ChiNPy polymer was explored as a potential method for sensing anions and cations. The results indicated that lead(II) and mercury(II) ions exhibited the highest degree of fluorescence quenching. These experiments highlighted the presence of two distinct populations of fluorophores, leading to a curved pattern in the Stern-Volmer plots. Overall, these findings underscore the potential of pyrene-labeled chitosan as sensitive fluorescent probes.

The second polymeric system investigated was a novel ladder-type polymer containing pyrene, designated as DiazaPy. This polymer was obtained through an acid-mediated post-polymerization cyclization of a specific conjugated polymer, PolyNPy, which was also synthesized for the first time in this work. Both polymers were derived from a 2,7-diamino-substituted pyrene monomer, MonPy.

The synthesis of MonPy yielded a 60% yield, and this molecule exhibited a relatively low Stokes shift in various solvents with a ϕ_F value of 0.48 ± 0.02 and a monoexponentially fluorescence lifetime of 20.6 ns in deaerated toluene. PolyNPy was obtained in two different fractions, with the larger polymer obtained by extraction with chloroform having a molecular weight of 11,800 g/mol. This polymer demonstrated a substantial Stokes shift when compared to its monomeric counterpart and a lower ϕ_F value of 0.190 ± 0.008 . Time-resolved techniques indicated a bi-exponential decay behavior with relatively close values of the two decay times. Thermally-activated twisted intermolecular charge transfer (TICT) was also observed in this polymer at 70 °C, which is an uncommon feature that enhances its fluorescence emission.

For DiazaPy, a radical cation was observed instead of a simple cation. This was determined from NMR and EPR measurements. DiazaPy also exhibited solvent-dependent emission characteristics, indicating a significant number of defects in its structure. In toluene, a two-absorption and dual-emission band was observed, characterized by the presence of more than one absorbing chromophoric unit and respective fluorescence. Quantum Chemical calculations confirmed that the second emission band results from a dicationic structure of the ladder polymer, which still retains its ladder structure. Experimental results suggest that the polymer has undergone a type of bond cleavage, resulting in a new fluorophore part resembling the MonPy structure. The data was further rationalized from time-resolved fluorescence and fs-TA techniques, indicating the presence of four different fluorescence lifetimes, highlighting the complexity of its structural and electronic behavior.

Resumo

No último século, a indústria passou por uma revolução devido à introdução de sistemas poliméricos. Ano após ano, extensas horas de pesquisa e investimento foram dedicados ao desenvolvimento de novos materiais que podem ser utilizados numa ampla gama de aplicações. Esta tese de mestrado tem como objetivo propor o desenvolvimento de dois novos sistemas poliméricos com pireno na sua estrutura, aproveitando as características eletrônicas dessa molécula.

Os primeiros sistemas poliméricos estudados foram dois polímeros de quitosano. Esses polímeros, conhecidos como ChiNPy-A e ChiNPy-B, possuem graus de substituição de pireno (%DSPy) com valores de 0,5% e 4,5%, respetivamente, determinados por técnicas de RMN de ^1H e UV-Vis. Os polímeros resultantes compreendem quatro unidades distintas, como evidenciado pela presença de unidades de amino pireno e unidades de imino pireno residual após a redução.

As medições resolvidas no tempo foram realizadas numa solução aquosa de ácido acético 5% (v/v), resultando num padrão de decaimento triexponencial que caracteriza as propriedades de fluorescência de ambas as unidades de pireno (amina e imina), bem como certas unidades de pireno que sofrem auto supressão de fluorescência.

A supressão de fluorescência das unidades de amino pireno no polímero ChiNPy foi explorada como potencial método de deteção de aniões e catiões. Os resultados indicaram que os iões de chumbo (II) e mercúrio (II) exibiam um maior grau de supressão de fluorescência. Essas experiências destacaram a presença de duas populações distintas de fluoróforos, levando a um padrão curvo concavo para baixo nos gráficos de Stern-Volmer. De um modo geral, estes resultados destacam o potencial dos polímeros de quitosano marcados com pireno como sondas fluorescentes.

O segundo sistema polimérico investigado foi um novo polímero em ‘escada’ (do inglês, *ladder polymer*) contendo pireno, designado como DiazaPy. Este polímero foi obtido através de uma pós-polimerização mediada por ácido, de um polímero conjugado, PolyNPy, que também foi sintetizado pela primeira vez neste trabalho. Ambos os polímeros foram derivados de um monómero de 2,7-diamino- pireno, MonPy.

Na síntese de MonPy foi obtido um rendimento de 60%, e essa molécula exibiu um desvio de Stokes relativamente baixo em vários solventes, com um valor de φ_F de $0,48 \pm 0,02$ e um tempo de vida de fluorescência monoexponencial de 20,6 ns em tolueno saturado com N_2 . O PolyNPy foi obtido em duas frações diferentes, com o polímero maior obtido por extração com clorofórmio, com um peso molecular de 11,800 g/mol. Este polímero demonstrou um substancial desvio de Stokes quando comparado ao seu homólogo

monomérico e um valor de φ_F de $0,190 \pm 0,008$. As técnicas resolvidas temporalmente indicaram um decaimento biexponencial com valores relativamente próximos entre os dois tempos de vida. Transferência de carga intermolecular por torção (TICT; do inglês, '*Twisted intermolecular charge transfer*') ativada termicamente também foi observada neste polímero a partir dos 70 °C, o que é uma característica incomum que aumenta a emissão de fluorescência.

Para o DiazaPy, observou-se um catião radical em vez do um simples catião. Isso foi determinado pela análise de seus espectros de RMN e medidas de EPR. O DiazaPy também apresentou características de emissão dependentes do solvente, indicando um número significativo de defeitos na sua estrutura. Em tolueno, uma dupla absorção e emissão foi observada. Caracterizada pela presença de mais de uma unidade cromófora e a sua respectiva fluorescência. Cálculos computacionais confirmaram, que a segunda banda de emissão é resultado de uma estrutura dicatiônica no polímero, que ainda retém a sua estrutura em forma de 'escada'. Resultados experimentais sugerem que o polímero sofreu algum tipo de clivagem de ligação, resultando numa nova parte fluorescente com semelhanças à estrutura do MonPy. Estes dados foram logo racionalizados a partir de técnicas de fluorescência resolvida no tempo de absorção transiente, indicando a presença de quatro tempos de vida de fluorescência diferente, reafirmando a complexidade estrutural e eletrônica da amostra.

Chapter 1:

Introduction

1.1 Photochemistry and Photophysics

Life, as we understand it, would be untenable without a series of intricate and diverse photochemical processes. Light, with its dual nature as both a wave and a particle, interacts with matter through various mechanisms, triggering a multitude of events. Upon electronic excitation, in the excited state, molecules become entirely new entities, often displaying distinct characteristics from their ground electronic state. However, these excited electronic states typically have a brief duration, with a lifetime ranging from picoseconds to nanoseconds for singlet states and from microseconds to milliseconds for triplet states.¹

Photochemistry entails the examination of the interplay between light and matter, a dynamic that initiates novel routes for chemical reactions. Conversely, photophysics encompasses the exploration of the complex mechanisms involved in the excitation and subsequent deactivation of a molecule, covering both radiative (luminescent) and non-radiative phenomena. The fusion of these two domains offers significant benefits, enabling a comprehensive characterization of the array of processes a molecule can undergo when subjected to photoexcitation. The excited state is thus a distinct entity with its unique characteristics.¹⁻³

The Jablonski-Perrin diagram⁴ works as an illustrative tool depicting all processes occurring upon absorption and emission of light. A conventional representation of the Jablonski-Perrin diagram is shown in **Figure 1.1**, where the singlet electronic states (S_n) and the triplet electronic states (T_n) are represented, together with the deactivation routes, radiative and non-radiative processes, of the excited state.

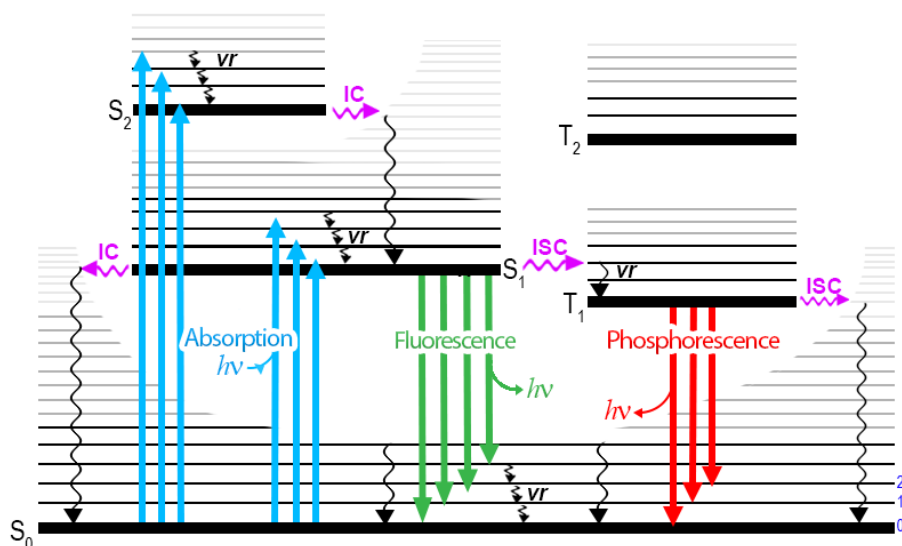
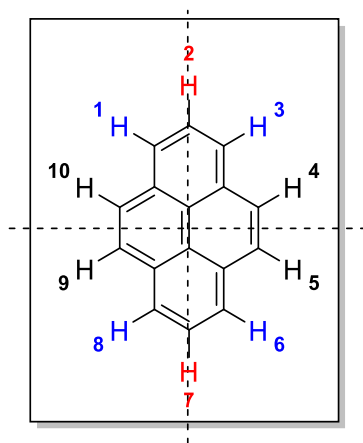


Figure 1.1 Simplified Jablonski-Perrin diagram. *vr* – vibrational relaxation; IC – Internal Conversion; ISC – Intersystem Crossing.

Fluorescence, denoting the radiative deactivation from the first electronic excited state to the ground electronic state ($S_1 \rightarrow S_0$), has garnered extensive investigation through both steady-state and time-resolved methodologies. Fluorescent compounds, often called fluorophores, have versatile utility across chemical and biological sciences. Their applications range from pH and polarity sensors, in cellular imaging, enabling single-molecule detection, etc. This multifaceted role of fluorescent sensors underlines the significance of advancing new fluorescent materials, elevating the research on this subject as a pivotal endeavor.⁵

1.2 Pyrene

Pyrene, a polycyclic aromatic hydrocarbon, **Scheme 1.1**, possesses a high degree of symmetry, characterized by the presence of three distinct planes of symmetry. This unique symmetry arrangement results in three discrete positions, each exhibiting a different chemical reactivity. Notably, 1, 3, 6, and 8 positions are predisposed to electrophilic aromatic substitution hence these positions are particularly electron-rich, facilitating electrophilic reactions. In contrast, the 2 and 7 positions exhibit relatively lower reactivity, except when a bulky electrophile is employed. However, synthesizing derivatives involving the 2 and 7 positions often demands multi-step synthetic routes. Significantly, the so-called K-region, encompassing the 4, 5, 9, and 10 positions, remains inaccessible through Friedel-Craft-type reactions in non-previously functionalized pyrene derivatives.⁶⁻⁷



Scheme 1.1 Pyrene molecule with identification of its positions and showing its three different planes of symmetry. Groups with chemically identical sites are represented with the same color.

Due to its symmetry and electronic configuration, pyrene exhibits remarkable photochemical and photophysical properties. It can undergo $\pi \rightarrow \pi^*$ electronic transitions, leading to well-defined absorption bands in the ultraviolet and visible (UV-Vis) spectrum. Moreover, this molecule shows two relevant low-lying electronic transitions. Firstly, the transition from the ground state to the first electronic excited state ($S_0 \rightarrow S_1$), is strongly

forbidden. Secondly, the transition from the ground state to the second electronic excited state ($S_0 \rightarrow S_2$) is symmetry allowed, exhibiting a pronounced intensity, often observed around 340 nm as depicted in **Figure 1.2**.⁸

The emission of pyrene is also characterized by its intense blue emission and notably long-lived excited singlet state lifetime. Additionally, its ability to form excimers enhances its distinct characteristics. Furthermore, pyrene exhibits exceptional chemical stability and charge-carrier mobility. These unique characteristics make pyrene a highly favored chromophore, making it the preferred choice for a diverse range of applications across scientific domains. For instance, pyrene finds utility in crafting field-effect transistors and organic light-emitting diodes (OLEDs), thereby enabling the development of electronic devices. Moreover, pyrene's versatility extends to creating supramolecular photosensors, facilitating precise detection and analysis. It also serves in measuring solvent polarity and detecting simple molecules, highlighting its flexibility for various research applications.⁷⁻⁹

Importantly, pyrene's electronic characteristics can be effectively manipulated through the strategic incorporation of specific functional groups. An illustrative example is found in 1-pyrenecarboxaldehyde. The inclusion of a carbonyl group, inherently possessing π character, significantly enhances pyrene's π -system. This change allows to breaking up of the forbidden nature of the $S_0 \rightarrow S_1$ transition making it symmetry allowed, resulting in a complete transformation of the spectral profile, as shown in **Figure 1.2**. This example highlights how distinct functional groups can finely tune pyrene's electronic properties, with the consequence of promoting a substantial influence on its photochemical/photophysical behavior.¹⁰

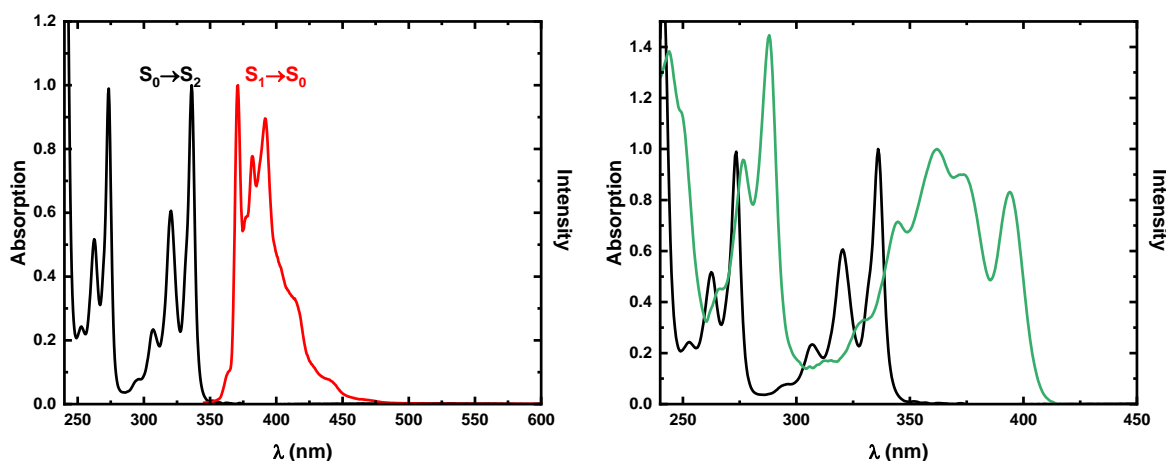


Figure 1.2 (Left) Normalized absorption and emission spectrum of a diluted solution of pyrene in THF. Relevant electronic transitions are indicated. **(Right)** Normalized absorption spectrum of pyrene (black) and 1-pyrenecarboxaldehyde (green) in THF at T=293 K.

1.3 Polymers

Since the year 1907, when Bakelite, the first synthetic plastic polymer, was obtained because of a controlled chemical reaction, an industrial revolution began. Polymers, which are macromolecules composed of repeating units known as monomers, linked together through one or more covalent bonds, exhibit various characteristics due to the accumulation of a significant number of inter- and intramolecular interactions. This gives these materials appealing properties for use in a wide range of applications. Therefore, the development of new polymeric materials has been a primary focus of study for many researchers over the years.

Polymers can be categorized as natural or synthetic. Natural polymers, also referred to as biopolymers, encompass substances such as proteins and polysaccharides and are found in nature, i.e., DNA, silk, and cellulose. In contrast, synthetic polymers are obtained through chemical processes. Examples of synthetic polymers include nylon and epoxy glue.¹¹

Polymers can be classified based on their structure, composition, and specific characteristics of the monomer units. They fall into categories such as linear, branched, or cross-linked, depending on their structural arrangement. In terms of composition, they are categorized as either homopolymers, composed of a single monomer unit, or heteropolymers, formed by two or more distinct monomer units. Within heteropolymers, monomeric units can exhibit regular or non-regular arrangements.⁸

In modern society, polymers play an immensely significant role and are found to be extensively used in various domains such as housewares, packaging, biomedical supplies, fabrics, and more. Their popularity arises from their ease of processing and the broad spectrum of mechanical properties they can offer. Consequently, the modulation of polymer characteristics and capabilities, as well as the development of novel polymeric materials, form a flourishing research area.

Despite the substantial advantages of polymer systems, some drawbacks have added new challenges, in particular, the study of the stability of these macromolecules and their extended degradation times have become an increasingly concerning ecological issue year after year. Hence, the necessity arises for the utilization and development of more sustainable polymer systems, with natural-origin polymers, biopolymers, providing the swifter solution to this issue.

In parallel, there has been a pronounced demand for fluorescent materials. Consequently, the preparation of new fluorescent polymers has emerged as a prominent topic in the last decades. Much like fluorescent molecules, fluorescent polymers have gained widespread attention due to their multifaceted applications in areas such as optoelectronics, molecular imaging, organic light-emitting diodes (OLEDs), anti-counterfeiting

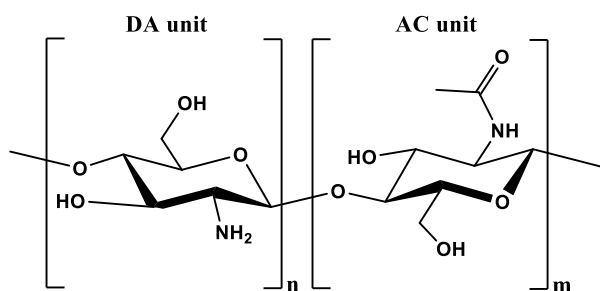
materials, environmental sensing, and more. This reflects the broad and dynamic nature of the field and its potential impact on various technological advancements.¹²

1.3.1 Chitosan

One of the most significant concerns, associated with the extensive utilization of polymers, concerns the pollution stemming from the degradation of conventional polymeric systems, specifically plastics. This issue raises environmental questions and poses an increasing threat to human health. This is the primary reason behind the recent surge in the search for more ecologically friendly systems, which have become of paramount importance. Biopolymers represent a noteworthy alternative as they are derived from natural resources and have a low carbon footprint.¹³

Following cellulose, chitin (the primary constituent of the shells of shrimps, lobsters, and other crustaceans) stands as the second most abundant biopolymer on Earth. Chitin can be processed into chitosan through a deacetylation procedure conducted under alkaline conditions.¹⁴

Chitosan, as depicted in **Scheme 1.2**, is a linear copolymer comprising 2-amino-2-deoxy-D-glucopyranose units (also known as deacetylated units, DA) alongside residual units of 2-acetamino-2-deoxy-D-glucopyranose (referred to as acetylated units, AC). The chemical functionalization of this biopolymer can be achieved without changing the degree of polymerization, originating either from the amino group (-NH₂) or from its secondary hydroxyl group (-OH). Including in the most prevalent techniques for chitosan functionalization is the creation of a Schiff base. This process involves the direct reaction of the polymeric material with an aldehyde, followed by a subsequent reduction step to yield an amino-substituted group (-NHR).¹⁵⁻¹⁷



Scheme 1.2 Chitosan structure. DA – Deacetylated unit; AC – Acetylated unit.

Chitosan, and its derivatives, have found value in various applications such as drug delivery,¹⁸ aromatic compound removal,¹⁹ antimicrobial agents,²⁰ and the removal of heavy and toxic metals. This versatility arises from chitosan's inherent chelating ability, facilitated by the hydroxyl and amino groups within its structure.

These groups are either intrinsically present or can be incorporated through structural modifications, enabling the creation of effective adsorbents.²¹⁻²²

1.3.2 Ladder Polymers

Most polymers are usually linked through single, double, or even triple bonds. However, a unique category exists, known as ladder polymers, wherein the polymer chains are designed with a special double-stranded structure. The concept of ladder polymers was formally introduced by IUPAC in 1993.²³ According to this definition, a ladder polymer is characterized by an uninterrupted sequence of rings, with adjacent rings sharing two or more atoms in common.

There are two primary approaches for obtaining ladder polymers: direct ladder polymerization and zipping of a linear pre-polymer.²⁴ In direct ladder polymerization, cyclic monomer units are simultaneously linked, forming two new bonds between them. Alternatively, ladder polymers can be synthesized by zipping a linear pre-polymer, which contains regular functional groups and side groups that facilitate the formation of the second bond in the polymer structure. However, it is worth noting that both synthesis methods can potentially lead to undesired structural defects. Therefore, meticulous consideration is needed when selecting monomers to prevent such structural defects.

Conjugated ladder polymers have gained significant attention due to their potential in optical and electronic applications. This heightened interest is a result of their distinct attributes, including a rigid and coplanar structure. This structural arrangement, combined with efficient electron delocalization, contributes to their ability to exhibit intense luminescence, high carrier mobility, and an extended exciton diffusion length.

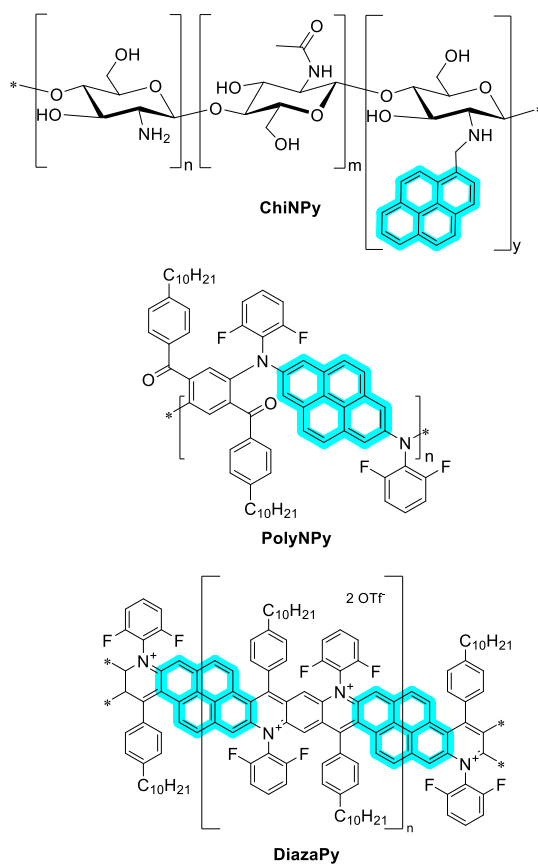
Moreover, this class of polymers possesses reasonable thermal stability and demonstrates greater π - π stacking interactions. These enhanced interactions facilitate the formation of aggregates, further enhancing their potential in various applications.²⁴⁻²⁵

The synthesis of ladder polymers presents a significant challenge due to various technical obstacles that need to be surmounted to achieve the desired product. These polymers are recognized for their inherent rigidity and substantial molecular size. This structural composition entails limited conformational freedom, thereby leading to a swift decline in solubility as the molecular weight (M_w) of the polymer escalates.²⁴

Ideal ladder polymers are free from torsional defects, maximizing the extent of π -electron delocalization. This characteristic results in an improved electronic performance compared to conventional conjugated polymers. However, it is important to acknowledge that most reported ladder polymers exhibit structural defects. These defects stem from unreacted sites or side reactions, compromising the ideal polymer structure.²⁶

1.4 Objectives and Methodologies

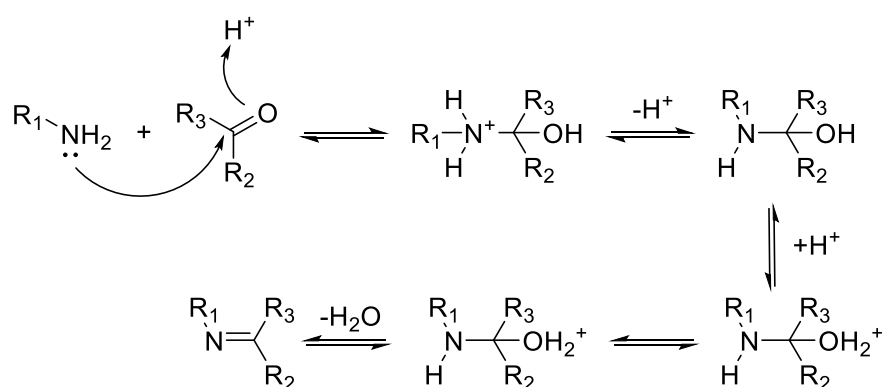
The current study integrates the aforementioned concepts to create novel fluorescent polymeric systems, with each sample being comprehensively analyzed using various spectroscopic techniques. Three distinct polymeric systems were synthesized, all sharing the common feature of incorporating pyrene as the central fluorescent core. **Scheme 1.3** illustrates the three distinct proposed polymeric systems designated for investigation.



Scheme 1.3 Pyrene-containing polymeric systems studied in the current work.

Chapter 2 provides a comprehensive discussion of the synthesis, characterization, and potential applications of the ChiNPy polymer. The polymer was obtained from the functionalization of a commercially available chitosan sample. The selected approach for the synthesis of this polymer involved the formation of an imine intermediate, commonly known as Schiff base, followed by the subsequent reduction of this intermediate using sodium borohydride (NaBH_4) to yield a secondary amine. This synthetic method, which has previously been reported for other functionalized chitosan derivatives, offers the advantage of mild reaction conditions. Furthermore, this method ensures the structural integrity of the primary polymer backbone while facilitating the incorporation of the newly introduced component of the molecule.^{15, 22, 27}

As illustrated in **Scheme 1.4** the formation of the Schiff base follows a two-step reversible reaction. In the initial step, a primary amine acts as a nucleophile, reacting with an aldehyde or ketone (functioning as the electrophile) through its carbonyl group. This leads to the formation of a carbinolamine intermediate. Subsequently, dehydration of the intermediate occurs. The progress of this reaction is contingent upon pH, with the optimal range being between 3 and 4. This pH range is favorable to both the nucleophilic addition and elimination of water. It is important to note that water, as a byproduct of this reaction, can shift the equilibrium towards the initial products, through the back-reaction.²⁸ Consequently, considering that the reaction with chitosan occurs in an aqueous medium due to its limited solubility in alternative solvents, it is anticipated that the reaction yield will be relatively modest.



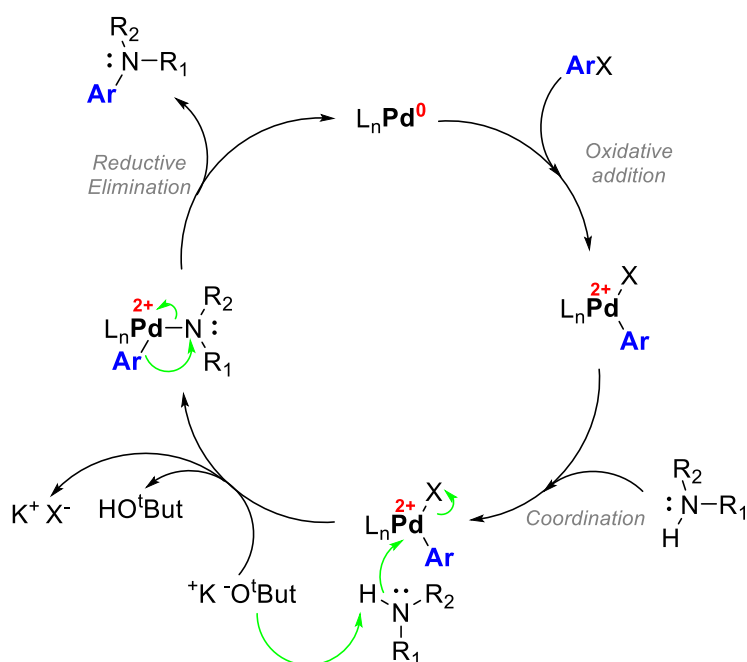
Scheme 1.4 Generic mechanism for the formation of a Schiff base.

Chapter 3 will extensively cover the methodological approach and related investigations regarding the other two synthesized polymers. The central aim of this chapter is to synthesize a novel ladder polymer belonging to the diazaacenes family, with the incorporation of pyrene within its core structure. This polymer, named DiazaPy, is depicted in **Scheme 1.3**. As established in the preceding section, the synthesis of ladder polymers is inherently intricate. Consequently, the chosen route to obtain this compound involved a post-polymerization step of a meticulously designed conjugated polymer, the PolyNPY. The methodology employed for the synthesis of DiazaPy closely resembled that of previously described ladder polymers in the literature.²⁹⁻³⁰

The initial pyrene building block adopted was a 2,7-disubstituted derivative. This selection aimed to maximize the potential of pyrene in facilitating an acid-mediated post-polymerization cyclization. This capability arises from the electron-rich nature of the non-K region position of pyrene, enabling electrophilic aromatic reactions. Both the 2,7-amino-substituted pyrene and PolyNPY were synthesized through a Buchwald-Hartwig cross-coupling amination reaction.

The Buchwald-Hartwig reaction involves a Pd-catalyzed interaction between an amine and an aryl halide substrate in the presence of a strong base. The catalytic cycle, elucidated in **Scheme 1.5**, outlines the initiation

reaction with the oxidative addition of the aryl halide to the palladium(0) species. This is followed by the coordination of the amine to the catalyst. At this stage, the potent base abstracts a proton from the amine, resulting in the formation of an amide. This amide reacts with the palladium catalyst, displacing the halide as a leaving group. A reductive elimination process follows, yielding the aryl amine product and regenerating the active palladium(0) catalyst.³¹⁻³³



Scheme 1.5 Schematic presentation of the Buchwald-Hartwig Cross-Coupling catalytic cycle.

This work aimed at the synthesis and thorough analytical spectroscopic and photophysical characterization of each sample. To achieve this, NMR, FTIR, UV-Vis, time-resolved, and steady-state fluorescence techniques were used. Supplementary techniques were also employed when needed. Furthermore, a theoretical computational approach was integrated into the methodology to gain additional insights into the molecular properties of the synthesized polymers. All the experimental procedures described in **Chapter 2** were conducted at the Center of Chemistry of the University of Coimbra (CQC-UC) in Portugal. The polymers discussed in **Chapter 3** were studied as a result of a collaboration between the Macromolecular Group of the University of Wuppertal (Makro-BUW) in Germany and the Photochemistry Group at CQC-UC.

Bibliography

1. Balzani, V.; Ceroni, P.; Juris, A., *Photochemistry and photophysics: concepts, research, applications*. John Wiley & Sons: 2014.
2. Seixas de Melo, J. S.; Pina, J.; Dias, F. B.; Maçanita, A. L., Experimental Techniques for Excited State Characterisation. In *Applied Photochemistry*, Evans, R. C.; Douglas, P.; Burrow, H. D., Eds. Springer Netherlands: Dordrecht, 2013; pp 533-585.
3. Lakowicz, J. R., *Principles of fluorescence spectroscopy*. Springer: 2006.
4. Jabłoński, A., Über den mechanismus der photolumineszenz von farbstoffphosphoren. *Zeitschrift für Physik* **1935**, *94* (1-2), 38-46.
5. Valeur, B.; Berberan-Santos, M. N., *Molecular fluorescence: principles and applications*. John Wiley & Sons: 2012.
6. Casas-Solvas, J. M.; Howgego, J. D.; Davis, A. P., Synthesis of substituted pyrenes by indirect methods. *Org. Biomol. Chem.* **2014**, *12* (2), 212-232.
7. Zöphel, L. J. Chemical transformations of the pyrene K-region for functional materials. MPI for Polymer Research, Max Planck Society, 2012.
8. Seixas de Melo, J. S.; Costa, T.; de Castro, C. S.; Macanitab, A. L., Photophysics of fluorescently labeled oligomers and polymers. *Photochemistry: Volume 41* **2013**, *41*, 59.
9. Barry, N. P.; Therrien, B., Pyrene: The guest of honor. In *Organic Nanoreactors*, Elsevier: 2016; pp 421-461.
10. Sahoo, G. P.; Das, D.; Sheet, P. S.; Beg, H.; Salgado-Morán, G.; Misra, A., Morphology directing synthesis of 1-pyrene carboxaldehyde microstructures and their photo physical properties. *RSC Advances* **2014**, *4* (21).
11. Carraher Jr, C. E., *Carraher's polymer chemistry*. CRC press: 2017.
12. Ahumada, G.; Borkowska, M., Fluorescent Polymers Conspectus. *Polymers (Basel)* **2022**, *14* (6).
13. Ivleva, N. P.; Wiesheu, A. C.; Niessner, R., Microplastic in aquatic ecosystems. *Angewandte Chemie International Edition* **2017**, *56* (7), 1720-1739.
14. Negm, N. A.; Hefni, H. H. H.; Abd-Elaal, A. A. A.; Badr, E. A.; Abou Kana, M. T. H., Advancement on modification of chitosan biopolymer and its potential applications. *International Journal of Biological Macromolecules* **2020**, *152*, 681-702.
15. Tommeraas, K.; Strand, S. P.; Tian, W.; Kenne, L.; Varum, K. M., Preparation and characterisation of fluorescent chitosans using 9-anthraldehyde as fluorophore. *Carbohydr Res* **2001**, *336* (4), 291-6.
16. Ghorai, S.; Jana, B.; Pan, D.; Ramasamy, T.; Parshi, N.; Arumugam, G.; Ganguly, J., Evaluation of nanofibril chitosan@ 8-formyl-7-hydroxy-coumarin hydrogel having distinct auto-fluorescence efficiency: Structure-properties relation, improved antioxidant, and cellular imaging. *Journal of Applied Polymer Science* **2022**, e52908.
17. Chen, H.; Hu, X.; Chen, E.; Wu, S.; McClements, D. J.; Liu, S.; Li, B.; Li, Y., Preparation, characterization, and properties of chitosan films with cinnamaldehyde nanoemulsions. *Food Hydrocolloids* **2016**, *61*, 662-671.

18. Manna, S.; Seth, A.; Gupta, P.; Nandi, G.; Dutta, R.; Jana, S.; Jana, S., Chitosan Derivatives as Carriers for Drug Delivery and Biomedical Applications. *ACS Biomater Sci Eng* **2023**, *9* (5), 2181-2202.
19. Filho, C. M. C.; Bueno, P. V. A.; Matsushita, A. F. Y.; Vilsinski, B. H.; Rubira, A. F.; Muniz, E. C.; Murtinho, D. M. B.; Valente, A. J. M., Uncommon Sorption Mechanism of Aromatic Compounds onto Poly(Vinyl Alcohol)/Chitosan/Maleic Anhydride-beta-Cyclodextrin Hydrogels. *Polymers (Basel)* **2020**, *12* (4).
20. Yan, D.; Li, Y.; Liu, Y.; Li, N.; Zhang, X.; Yan, C., Antimicrobial Properties of Chitosan and Chitosan Derivatives in the Treatment of Enteric Infections. *Molecules* **2021**, *26* (23).
21. Varma, A. J.; Deshpande, S. V.; Kennedy, J. F., Metal complexation by chitosan and its derivatives: a review. *Carbohydrate Polymers* **2004**, *55* (1), 77-93.
22. Matias, P. M. C.; Sousa, J. F. M.; Bernardino, E. F.; Vareda, J. P.; Duraes, L.; Abreu, P. E.; Marques, J. M. C.; Murtinho, D.; Valente, A. J. M., Reduced Chitosan as a Strategy for Removing Copper Ions from Water. *Molecules* **2023**, *28* (10).
23. Metanomski, W.; Bareiss, R.; Kahovec, J.; Loening, K.; Shi, L.; Shibaev, V., Nomenclature of regular double-strand (ladder and spiro) organic polymers (IUPAC Recommendations 1993). *Pure and applied chemistry* **1993**, *65* (7), 1561-1580.
24. Teo, Y. C.; Lai, H. W. H.; Xia, Y., Synthesis of Ladder Polymers: Developments, Challenges, and Opportunities. *Chemistry* **2017**, *23* (57), 14101-14112.
25. Lupton, J. M.; Scherf, U., Conjugated, Aromatic Ladder Polymers: From Precision Synthesis to Single Chain Spectroscopy and Strong Light-Matter Coupling. *Ladder Polymers: Synthesis, Properties, Applications, and Perspectives* **2023**, 13-58.
26. Lee, J.; Kalin, A. J.; Yuan, T.; Al-Hashimi, M.; Fang, L., Fully conjugated ladder polymers. *Chemical Science* **2017**, *8* (4), 2503-2521.
27. Triana-Guzmán, V. L.; Ruiz-Cruz, Y.; Romero-Peñaloza, E. L.; Zuluaga-Corrales, H. F.; Chaur-Valencia, M. N., New chitosan-imine derivatives: from green chemistry to removal of heavy metals from water. *Revista Facultad de Ingeniería Universidad de Antioquia* **2018**, (89), 34-43.
28. Akitsu, T., *Schiff Base in Organic, Inorganic and Physical Chemistry*. BoD—Books on Demand: 2023.
29. Wetterling, D.; Forster, M.; AC, B. R.; Seixas de Melo, J. S.; Scherf, U., Cationic Diazapentacenium Polymers Made in a Sequence of C-N Cross Coupling Polymerization and Acid-Mediated Postpolymerization Cyclization. *Macromol Rapid Commun* **2021**, *42* (19), e2100370.
30. Rudnick, A.; Kass, K. J.; Preis, E.; Scherf, U.; Bassler, H.; Kohler, A., Interplay of localized pyrene chromophores and pi-conjugation in novel poly(2,7-pyrene) ladder polymers. *J Chem Phys* **2017**, *146* (17), 174903.
31. Dorel, R.; Grugel, C. P.; Haydl, A. M., The Buchwald–Hartwig Amination After 25 Years. *Angewandte Chemie* **2019**, *131* (48), 17276-17287.
32. Guram, A. S.; Buchwald, S. L., Palladium-Catalyzed Aromatic Aminations with in situ Generated Aminostannanes. *Journal of the American Chemical Society* **1994**, *116* (17), 7901-7902.
33. Paul, F.; Patt, J.; Hartwig, J. F., Palladium-catalyzed formation of carbon-nitrogen bonds. Reaction intermediates and catalyst improvements in the hetero cross-coupling of aryl halides and tin amides. *Journal of the American Chemical Society* **2002**, *116* (13), 5969-5970.

Chapter 2:

**Chitosan Polymer
Randomly Labeled
with Pyrene**

Summary

In this chapter, we will describe how the random labeling of low molecular chitosan with pyrene, through the formation of new C=N and C-N bonds, was obtained. These polymers were designated as ChiNPy (Chi- from *Chitosan* and -Py from *Pyrene*). The obtained ChiNPy polymers are also different from each other by the pyrene substitution degree (%DS_{Py}) or by the bond type connected to the chitosan skeleton, ChiNPy-Imine, and ChiNPy-amine. All polymers were carefully investigated by different spectroscopic techniques and were also tested as potential probes in the detection of different metal cations and anions in an aqueous solution.

2.1 Synthesis and structural characterization

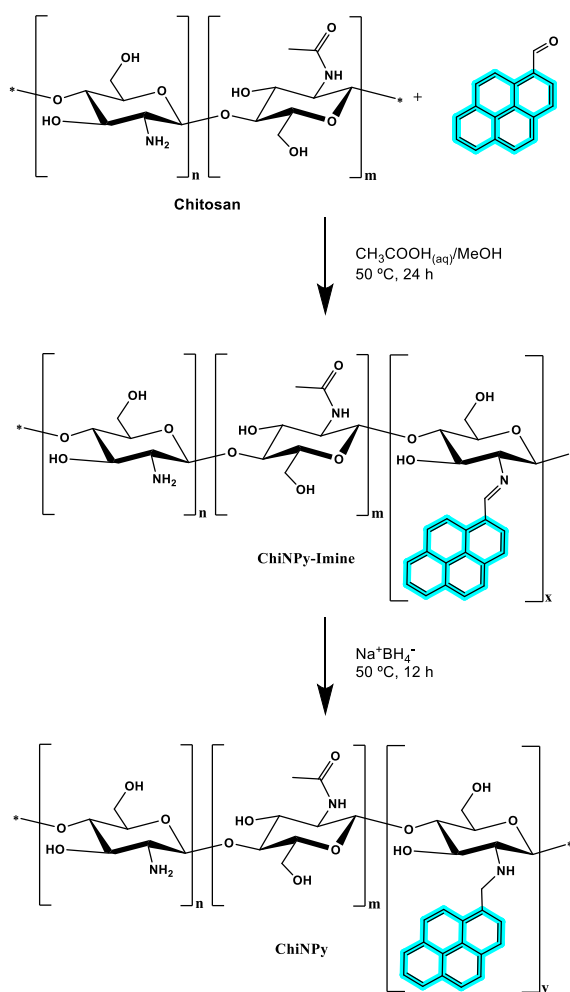
2.1.1 Reagents and solvents

To achieve the labeling of chitosan with pyrene, the following reagents were used. Low molecular chitosan (50.000 – 190.000 Da), 1-pyrenecarboxyaldehyde (99% purity), and sodium borohydride (NaBH₄) were purchased from Sigma-Aldrich. The solvents, methanol, and dichloromethane (DCM) HPLC grade from Fischer-chemicals, were used as received, and a solution of Acetic acid (HAc) 5% v/v from Chem-Lab was prepared by the corresponding dilution of acid with water *Milli-Q*.

For the quenching experiments, the following salts were used: tetrabutylammonium nitrate (with a purity of 97%), tetrabutylammonium chloride (with a purity of 97%), tetrabutylammonium iodide (with a purity of 97%), mercury(II) chloride, lead(II) perchlorate hydrate (with a purity of 98%), and copper(II) trifluoromethanesulphonate (with a purity of 98%).

2.1.2 Experimental procedure

The approach used to obtain the final ChiNPy polymers involved a two-step reaction process, **Scheme 2.1** where firstly the Schiff base is formed involving chitosan with pyrene, and, subsequently, the new imine bond in the Schiff base was reduced by the addition of sodium borohydride to obtain the C-N bond.



Scheme 2.1 Schematic synthesis of the ChiNPy polymers

The hardest part in the synthesis of ChiNPy polymers was related to the solubilities of the reagents involved in the reaction. Chitosan is well-known to be soluble only in diluted acid solution, and in contrast, 1-pyrenecarboxaldehyde, like most organic compounds, is insoluble in aqueous media due to its hydrophobic nature. This fact increased the difficulty of the formation of the so-called ChiNPy-Imine intermediate polymer. Mixtures of ethanol and methanol with HAc, in different proportions, were tested to retain as much as possible of the chitosan and pyrene derivative in solution during the reaction time. A methanol: HAc (5%) mixture in a proportion of 1:1 at 50 °C was the most promisor mixture and was used to obtain the desired products.

Two ChiNPy polymers were obtained and identified as ChiNPy-A and ChiNPy-B for the polymer with the lower and higher pyrene percentage, %DS_{Py}, respectively. It was also synthesized and isolated, in an independent way, a ChiNPy-Imine precursor polymer and used as a reference. The detailed synthesis of the ChiNPy polymers is described below.

1 equivalent of commercial chitosan was dissolved in HAc 5% v/v, the proportion of polymer to solvent of 1 g per 100 mL, by continuous stirring at 50 °C for 5 hours. A solution of 1 equivalent/2 equivalent (ChiNPy-A/ ChiNPy-B, respectively) in methanol was added drop-by-drop to the chitosan solution; methanol was added till the final volume mixture was 1:1 HAc: methanol. The reaction was running for 24 h at 50 °C with continuous stirring. Then, the reaction crude was allowed to cool to room temperature in continuous stirring, and an excess of 10 times sodium borohydride was added slowly and left to stir for another 12 h.

Methanol was evaporated under vacuum and the aqueous remanent solution was extracted with DCM (3 x 20 mL) for the removal of any excess of non-bonded pyrene. The aqueous phase was then concentrated by evaporation and a few drops of sodium hydroxide (NaOH) 5 M were added till a pH of c.a. 8 was obtained. The final polymer was precipitated by the addition of acetone. The solid was sieved and left to dry in a stove for one week at 70 °C.

The final powder was again washed using a Soxhlet apparatus for 4 hours using acetone and methanol as solvent. There was no evidence of the presence of pyrene (by Uv-Vis) in the washing solvents used in this last step.

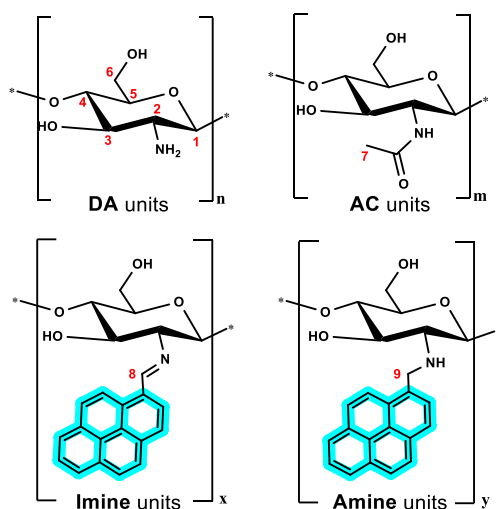
For the case of ChiNPy-Imine, the same procedure was performed (as for ChiNPy-A) but avoided the addition of NaBH₄.

2.2 Results and Discussion

2.2.1 Degree of pyrene in ChiNPy polymers

Chitosan polymers are obtained through the deacetylation of natural chitin by treating it with a strong alkaline solution. The determination of the degree of deacetylation (%DD) of the resulting chitosan is commonly performed using ¹H NMR spectroscopy, potentiometric titrations, or conductometric titrations ¹.

In this study, the %DD of the commercially purchased chitosan was determined using ¹H NMR. This was made by considering the monomer units of acetylated (AC) and deacetylated (DA) forms in chitosan, as depicted in **Scheme 2.2**. The signal arising from the three protons in the methyl of the acetylated unit has a lower chemical shift than the six protons present in the glucopyranose structure, which are common to both units. The former protons exhibit a narrow signal at around 2.07 ppm, in contrast to the latter, which displays a broad band ranging from 3.00 to 4.20 ppm. Based on this, it is possible to define **Equation 2.1** where "I" represents the integration of the signal at the respective chemical shift. From three independent measurements, the %DD of chitosan used for the synthesis was found to be 80 ± 1%.



Scheme 2.2 Structures of all possible monomer units present in ChiNPy polymers.

$$\%DD = \left(1 - \frac{1/3 \times I_{2.07 \text{ ppm}}}{1/6 \times I_{3.00-4.20 \text{ ppm}}} \right) \times 100 \quad 2.1$$

Figure 2.1 presents the ^1H NMR spectra of the ChiNPy-B polymer in comparison to the raw chitosan, while the spectra of the other ChiNPy polymers can be found in **Appendix A**. Notably, **Figure 2.1** reveals the appearance of two new signals: one at 2.20 ppm and a broad peak centered at 8.31 ppm. These signals, absent in the raw chitosan, are attributed to the 1-methyl pyrene moiety in the amine pyrene units of the ChiNPy polymers.

Similarly, the $\%DS_{\text{Py}}$ (degree of substitution with pyrene) can be determined using an analogous methodology to the one employed for $\%DD$. The nine protons of pyrene units, with their distinct signals in the aromatic region, are distinguishable from the six protons present in the glucopyranose ring. This distinction enables the use of **Equation 2.2** to quantify the $\%DS_{\text{Py}}$ using ^1H NMR.

$$\%DS_{\text{Py}} = \left(\frac{1/9 \times I_{\text{aromatic peaks}}}{1/6 \times I_{3.00-4.20 \text{ ppm}}} \right) \times 100 \quad 2.2$$

Nonetheless, within this study, an alternative approach, using UV-Vis spectroscopy, was employed to determine the $\%DS_{\text{Py}}$ making use of the distinctive spectral characteristics of pyrene. This method involved the molar extinction coefficients of 1-pyrenemethylamine and 1-pyrenecarboxaldehyde, thoughtfully selected as parent compounds for the amine and imine units in ChiNPy polymers.

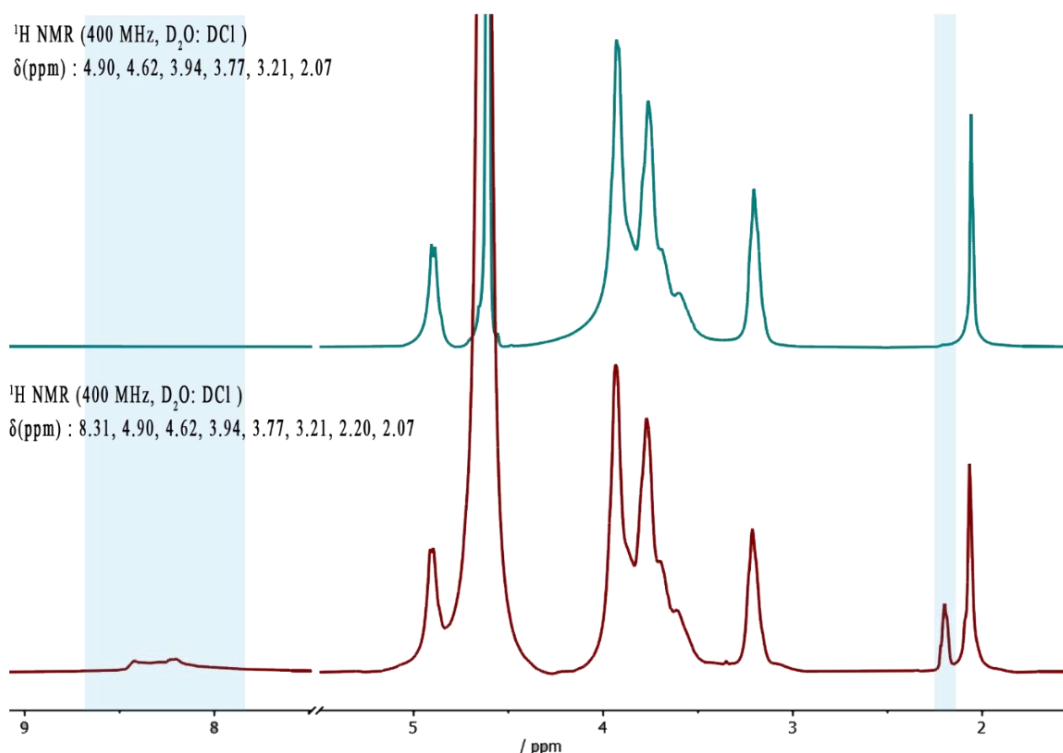


Figure 2.1 ^1H NMR of (top) Chitosan and (bottom) ChiNPy-B at 50 °C in D_2O : DCl 1% solution. The chemical shift values (δ) of the main peaks of each compound are shown as inset.

As will be described later in this section, both ChiNPy-A and ChiNPy-B were found to possess a blend of amine and imine pyrene units within their molecular frameworks, even after the use of an excess of tenfold equivalents of the reducing agent. Nonetheless, it became possible to approximate the UV-Vis spectra of the amine pyrene unit by deducting the experimental ChiNPy-Imine spectra from those of ChiNPy-A and ChiNPy-B polymers, **Figure 2.2**. This approach is viable due to the distinct absorption range of the pyrene when linked to amine or imine units.

The methodology employed for determining the values of $\%DS_{\text{Py}}$ through UV-Vis spectroscopy required the preparation of a ChiNPy solution by dissolving a specific mass of the polymer (denoted as m_{ChiNPy}) in a final volume (v_f) of 5% HAc. The solution was stirred for 24 hours at 50 °C and kept in darkness. Absorption spectra of the samples were recorded at room temperature. By using the molar extinction coefficient of 1-pyreneamine ($\epsilon = 37.070 \text{ M}^{-1}\cdot\text{cm}^{-1}$ at 340 nm)² and 1-pyrenecarboxaldehyde ($\epsilon = 16.680 \text{ M}^{-1}\cdot\text{cm}^{-1}$ at 393 nm and $\epsilon = 13.680 \text{ M}^{-1}\cdot\text{cm}^{-1}$ at 340 nm) in methanol, which are provided in **Appendix B** and chosen as parent compounds for amine and imine pyrene units, respectively, the $\%DS_{\text{Py}}$ were determined from **Equation 2.15**, see below.

The concentration of imine pyrene units ($[Py^{imine}]$) in the samples was determined using the Beer-Lambert law, represented by **Equation 2.3**. The theoretical absorption of the imine pyrene unit at 340 nm was calculated and subtracted from the experimental absorption to estimate the value required for calculating the concentration of amine pyrene units, as defined by **Equation 2.4**. Subsequently, the number of moles of pyrene units ($n_T Py$) present in the ChiNPy samples was calculated using the initial mass of chitosan, used in the synthesis of ChiNPy ($m_{chitosan}$), as described by **Equations 2.5** and **2.6**.

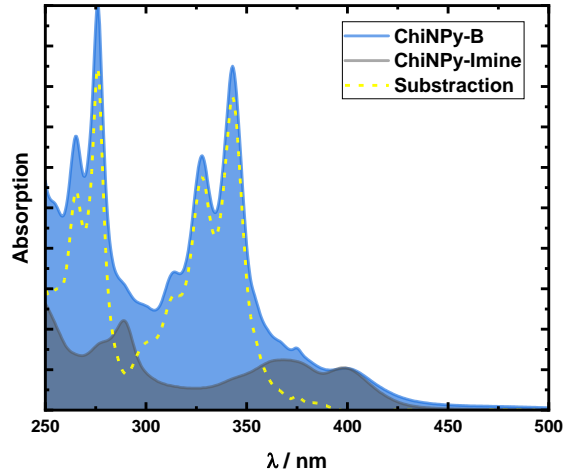


Figure 2.2 Graphical representation of the different species present in ChiNPy polymers. UV-Vis spectra of amine pyrene units in chitosan were estimated by subtraction of ChiNPy-B to ChiNPy-Imine spectra.

$$[Py^{imine}] = \frac{Abs_{398nm}^{ChiNPy}}{\epsilon_{393nm}^{PyCOH}} \quad 2.3$$

$$[Py^{amine}] = \frac{Abs_{340nm}^{ChiNPy} - \epsilon_{340nm}^{PyCOH} \cdot [Py^{imine}] \cdot l}{\epsilon_{393nm}^{PyCOH} \cdot l} \quad 2.4$$

$$n_T Py^{amine} = [Py^{amine}] \cdot v_f \cdot \frac{m_{chitosan}}{m_{ChiNPy}} \quad 2.5$$

$$n_T Py^{imine} = [Py^{imine}] \cdot v_f \cdot \frac{m_{chitosan}}{m_{ChiNPy}} \quad 2.6$$

The amount, in moles of chitosan, of original monomers was determined using the molar weights of the structural units: DA monomer ($M_w^{DA} = 161.16$ g/mol), AC monomer ($M_w^{AC} = 203.19$ g/mol), and the molar weights of chitosan-pyrene units ($M_w Py^{amine} = 375.42$ g/mol and $M_w Py^{imine} = 373.41$ g/mol). By employing the

previously determined %DD through ^1H NMR and recognizing that AC units are not involved in the pyrene incorporation reaction, the amount of this unit (m_T^{AC}) remains constant in the post-synthesis and can be calculated from **Equation 2.7**.

$$m_T^{\text{AC}} = m_{\text{chitosan}} \cdot \left(1 - \frac{\%DD}{100}\right) \quad 2.7$$

The quantity of DA (m_T^{DA}) is derived from the difference between the initial mass and the mass of the other units, as expressed in **Equation 2.8**. By using the respective molar weights, it becomes feasible to determine the number of moles for each unit, as indicated in **Equations 2.9** and **2.10**.

$$m_T^{\text{DA}} = m_{\text{chitosan}} - (m_T^{\text{AC}} + n_T \text{Py}^{\text{amine}} \cdot M_w \text{Py}^{\text{amine}} + n_T \text{Py}^{\text{imine}} \cdot M_w \text{Py}^{\text{imine}}) \quad 2.8$$

$$n_T^{\text{DA}} = \frac{m_T^{\text{DA}}}{M_w^{\text{DA}}} \quad 2.9$$

$$n_T^{\text{AC}} = \frac{m_T^{\text{AC}}}{M_w^{\text{AC}}} \quad 2.10$$

The %DS_{py} was obtained from the normalization of the number of moles for each unit, following the description provided by **Equations 2.11-2.14**, and subsequently substituting these values into **Equation 2.15**.

$$y(\text{Py}^{\text{imine units}}) = \frac{n_T \text{Py}^{\text{imine}}}{n_T \text{Py}^{\text{imine}}} = 1 \quad 2.11$$

$$x(\text{Py}^{\text{amine units}}) = \frac{n_T \text{Py}^{\text{amine}}}{n_T \text{Py}^{\text{imine}}} \quad 2.12$$

$$w(\text{DA}) = \frac{n_T^{\text{DA}}}{n_T \text{Py}^{\text{imine}}} \quad 2.13$$

$$p(\text{AC}) = \frac{n_T^{\text{AC}}}{n_T \text{Py}^{\text{imine}}} \quad 2.14$$

$$\%DS_{Py} = \left(\frac{y(Py^{imine\ units}) + x(Py^{amine\ units})}{y(Py^{imine\ units}) + x(Py^{amine\ units}) + w(DA) + p(AC)} \right) \times 100\% \quad 2.15$$

For the determination of the %DS_{Py} of ChiNPy-Imine, the [Py^{amine}] is set equal to zero and the equation above is still valid. Detailed results for each ChiNPy polymer are presented in **Appendix C**.

Table 2.1 presents the %DS_{Py} outcomes obtained through both the ¹H NMR and UV-Vis techniques, revealing a clear proximity between the results obtained from these two methods. However, the distinct advantage of UV-Vis lies in its capacity to offer, not only information about the overall pyrene content within the polymers, akin to ¹H NMR, but also to estimate the count of units for each monomer present within the polymer. This estimation is possible due to the capacity to differentiate between the two types of pyrene units throughout their respective molar extinction coefficients.

The results yielded by the UV-Vis technique, particularly in the case of ChiNPy-A, indicate an approximate ratio of one pyrene unit for every 200 non-pyrene units. This reveals a proportion of amine to imine pyrene units within this polymer of 6:1. On the other hand, for ChiNPy-B, the pyrene content is nearly tenfold higher compared to ChiNPy-A, suggesting at least one pyrene unit for every 20 units of other units. Additionally, the ratio of amine to imine pyrene units in ChiNPy-B stands at 2:1.

Table 2.1 Value of %DSPy obtained for ChiNPy polymers by ¹H NMR and UV-Vis.

Polymer	¹ H NMR / % ^a	UV-Visible / % ^b	Proportion Pyrene: other units ^c	Proportion Amine: Imine Pyrene units ^c
ChiNPy-A	0.5 ± 0.1	0.46 ± 0.02	c.a. 1:200	6:1
ChiNPy-B	4.5 ± 0.3	4.4 ± 0.2	c.a. 1:20	2:1
ChiNPy-Imine	0.13 ± 0.05	0.13 ± 0.01	c.a. 1:830	0:1

^a Error was reported as the standard deviation of three independent measurements. ^b Error reported as confidence limit for a small population with 95% confidence for five independent measurements. ^c Values obtained by UV-Vis method.

2.2.2 FTIR and Raman characterization

Fourier-transform infrared spectroscopy (FTIR) has demonstrated its utility as a rapid method to determine whether any substantial changes occur in the %DD of chitosan during the process of functionalization. This evaluation can be readily conducted by measuring the intensities between the amide I peak, located at around 1660 cm⁻¹, and the NH₂ bending band at 1600 cm⁻¹. These spectral features are intricately linked to the quantities of AC and DA units characteristic in the polymer backbone.³

As illustrated in **Figure 2.3**, the FTIR spectra of ChiNPy polymers exhibit no discernible shifts within the bands associated with the different %DD. Furthermore, the band at approximately 3300 cm⁻¹, corresponding

to the stretching vibrations of N-H and O-H, shows a broadening which is attributed to the formation of intramolecular hydrogen bonds. Similarly, the band at around 2900 cm^{-1} , encompassing symmetric and asymmetric C-H stretching, as well as the region spanning 1400-1300 cm^{-1} , confirming the presence of CH_2 bending and CH_3 deformation, alongside the robust band at approximately 1000 cm^{-1} corresponding to C-O stretching, reveal no substantive modifications when compared with the initial chitosan material.⁴

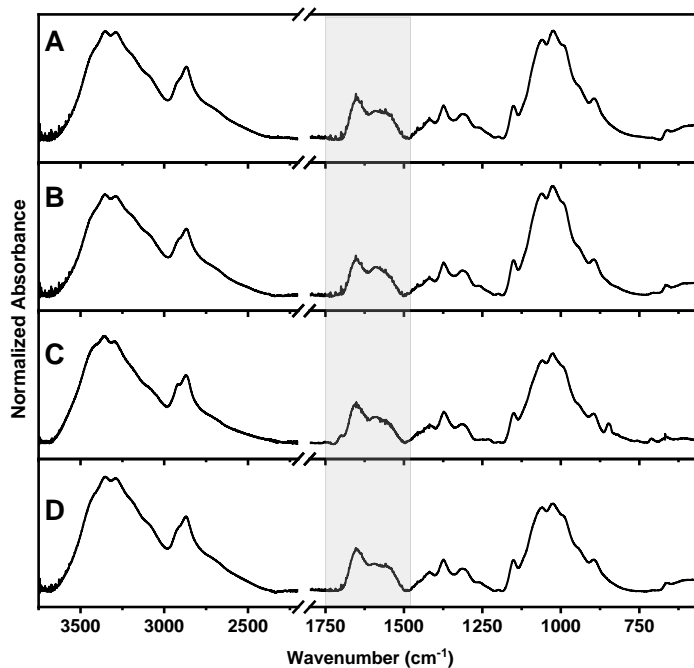


Figure 2.3 FTIR spectra of (A) Chitosan, (B) ChiNPy-A, (C) ChiNPy-B and (D) ChiNPy-Imine. Key bands pertinent to the rapid analysis of %DD are highlighted for easy reference.

In contrast to FTIR, Raman spectroscopy offers a more complex insight into the newly formed covalent bonds resulting from the incorporation of pyrene into the chitosan backbone. Through Density Functional Theory (DFT) calculations, the relative intensities of Raman signals, for the proposed monomers corresponding to AC, DA, amine, and imine pyrene units within ChiNPy polymers, were investigated. **Figure 2.4** illustrates that the anticipated relative intensities for the pyrene-substituted units were expected to surpass those of AC and DA units. These theoretical predictions are aligned with the experimentally observed peaks at 590 cm^{-1} , 1237 cm^{-1} , 1525 cm^{-1} , and 1625 cm^{-1} . Each of these peaks is associated with the combination of bending and stretching vibrations inherent to the pyrene structure and N-H bonding. Remarkably, these peaks exhibited significantly enhanced intensity compared to those observed in the initial chitosan material as predicted by DFT calculations.

Furthermore, the relative intensities of the peaks, attributed to the amine pyrene unit, exhibited an increased prominence in the ChiNPy-B when compared to ChiNPy-A polymer. This disparity suggests a higher %DS_{Py} in the former, aligning with the preceding findings obtained through ¹H NMR and UV-Vis techniques.

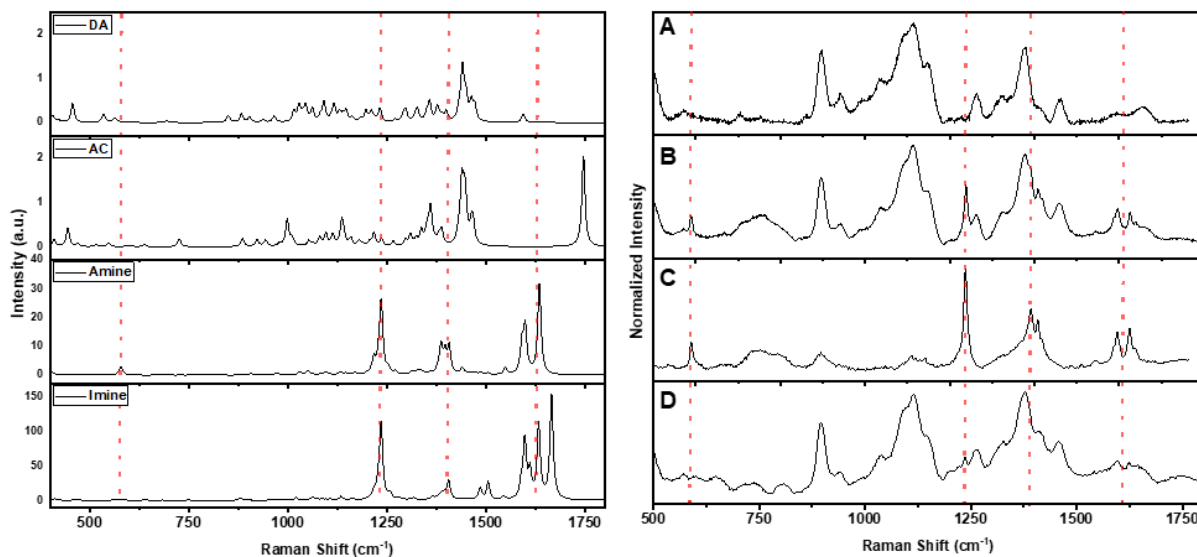


Figure 2.4 (Left) Theoretical Raman spectra obtained for Acetylated (AC), Deacetylated (DA), Amine, and Imine pyrene monomers model within ChiNPy polymers. These spectra were obtained using the Gaussian® 16 package employing the b3pw91 functional. (Right) Normalized experimental Raman spectra of (A) Chitosan, (B) ChiNPy-A, (C) ChiNPy-B, and (D) ChiNPy-Imine.

2.2.3 UV-Vis and fluorescence characterization

As explained in the introductory chapter, pyrene in its ground state exhibits two distinct electronic transitions: the forbidden $S_0 \rightarrow S_1$ transition and the allowed $S_0 \rightarrow S_2$ transition. However, any change or substitution in the pyrene core can result in a modification of its electronic behavior, potentially leading to significant differences in the spectrum of the pyrene derivative.

By utilizing the quantum chemical package GAMESS, Density Functional Theory (DFT) and Time-Dependent Density Functional Theory (TD-DFT) calculations were carried out employing the BPBE functional.⁵ These calculations were focused on the two different monomers representing the amine and imine pyrene units found within various ChiNPy polymers (Figure 2.5). Theoretical absorption spectra, depicted in Figure 2.6 and obtained through TD-DFT calculations, show a remarkable proximity to the experimental spectra. Notably, these predictions accurately anticipated the occurrence of a hypochromic shift in the first electronic transition, when the double bond in the C=N linkage is reduced to C-N in the final phase of the synthesis.

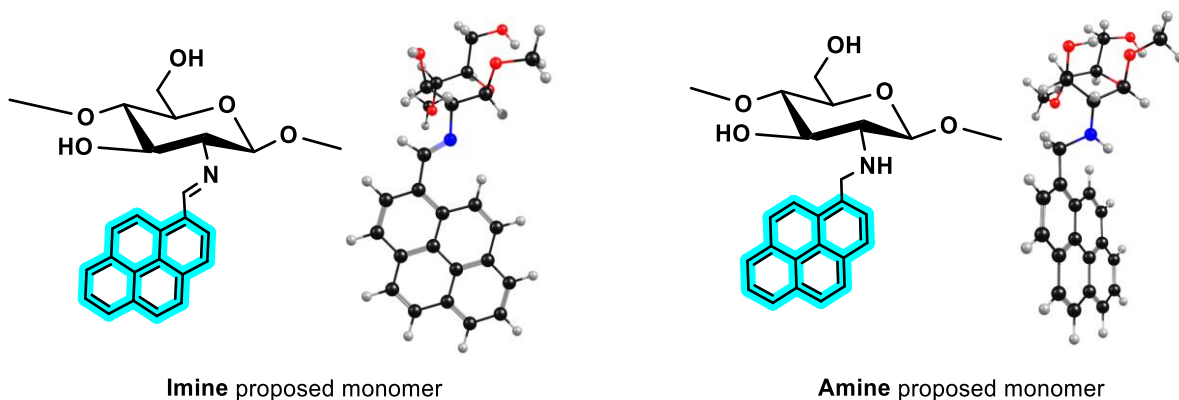


Figure 2.5 Representation of the proposed monomers utilized for computational previsions of the electronic characteristics of ChiNPy polymers. At the right, the optimized structure obtained by DFT is presented.

The outcomes of UV-Vis properties, foreseen through DFT and TD-DFT calculations, unveil that the presence of a double bond within the imine group facilitates π -electron delocalization (thus extending π - π conjugation), a phenomenon illustrated in the representation of the HOMO-LUMO orbitals in **Table 2.2**. This delocalization contributes to a reduction of the HOMO-LUMO bandgap ($\Delta E_{\text{LUMO-HOMO}}$). Consequently, the transition associated to the pyrene-imine units shows, at lower energy levels (corresponding to higher wavelengths), a departure from the pyrene-amine units that are located at lower wavelength values.

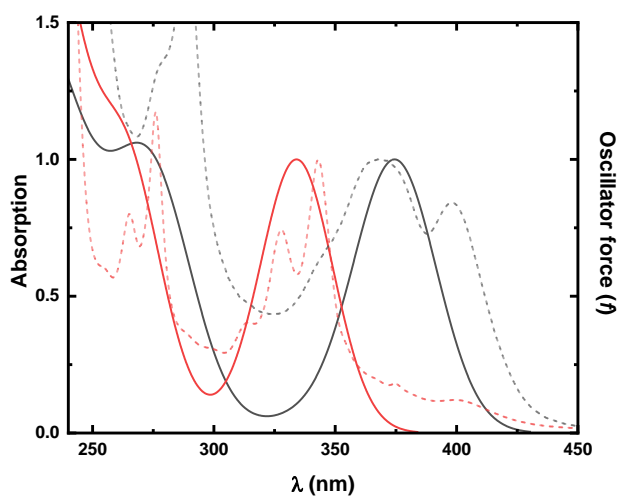
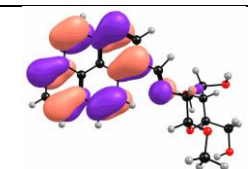
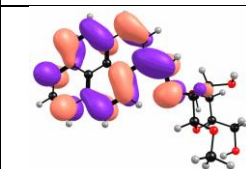
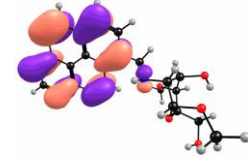
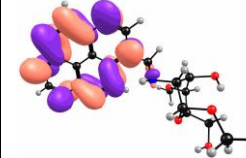


Figure 2.6 Prediction of absorption spectra with TD-DFT with the BPBE functional in water for model monomers of (red) Amino and (Black) Imine structures in the ChiNPy polymers. Experimental absorption spectra are also shown as dashed lines for comparison.

Table 2.2 Values predicted by DFT of the spectral characteristic for amine and imine pyrene monomers in water.

Structure	λ_{abs}^* (nm)	$\lambda_{\text{abs}}^{**}$ (nm)	f	Electronic transition	HOMO	LUMO
Imine unit	367	380	0.7139	HOMO \rightarrow LUMO		
Amine unit	343	339	0.5751	HOMO \rightarrow LUMO		

*Experimental value from ChiNPy polymers; ** Theoretical maxima absorption predicted though TD-DFT//LC-BPBE/SBKJC level of theory.

The absorption and steady-state fluorescence spectra of the ChiNPy polymers are presented in **Figure 2.7**. A comparison of the absorption spectra of the polymers shows a blue shift in the absorption maxima on going from ChiNPy-Imine to ChiNPy-A or ChiNPy-B. Nevertheless, the absorption spectra of ChiNPy-A and ChiNPy-B still exhibit evidence for the presence of residual imine pyrene units in the polymer even after the reduction with NaBH₄. This is expressed by an additional absorption band at around 400 nm, not observed in amino 1-methylpyrene derivatives.

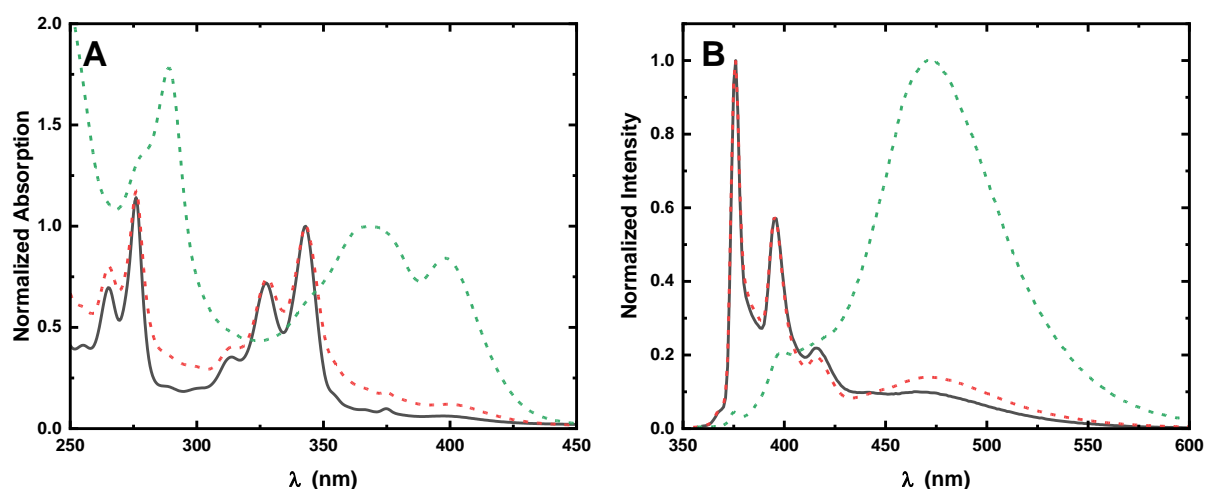


Figure 2.7 Normalized (A) absorption and (B) emission spectra of ChiNPy polymers in Hac 5% of ChiNPy-A (black line), ChiNPy-B (dashed-red line) and ChiNPy-Imine (Dashed green line). Emission spectra were recorded using $\lambda_{\text{exc}} = 350$ nm.

Moreover, the emission spectra, also in **Figure 2.7**, and recorded with excitation at 350 nm, where both amino and imine pyrene units absorb, show the emission of two bands. The first band is characteristic of pyrene-labeled polymers in an aqueous environment, with a peak at 380 nm with vibrational resolution, the pyrene

monomer emission.² In contrast, the second band is notably broader, centered around 470 nm, matching the emission wavelength maximum of the ChiNPy-Imine.

Nonetheless, the attribution of the origin of this second emission band can be made from the emission originating from imine pyrene units and not from the presence of an excimer or exciplex. This could be established for ChiNPy-A and ChiNPy-B polymers from a comprehensive analysis of their excitation spectra obtained with various emission wavelengths, as depicted in **Figure 2.8**. Indeed, the excitation spectra obtained by collecting the spectra at lower wavelengths yield a spectrum similar to the absorption of the amino pyrene units. In contrast, collecting the spectra at higher emission wavelengths leads to an excitation spectra of imine pyrene units. The excitation spectra collected with intermediate emission wavelengths result in a combined representation of the two (imine- and amine-pyrene) absorption spectra.

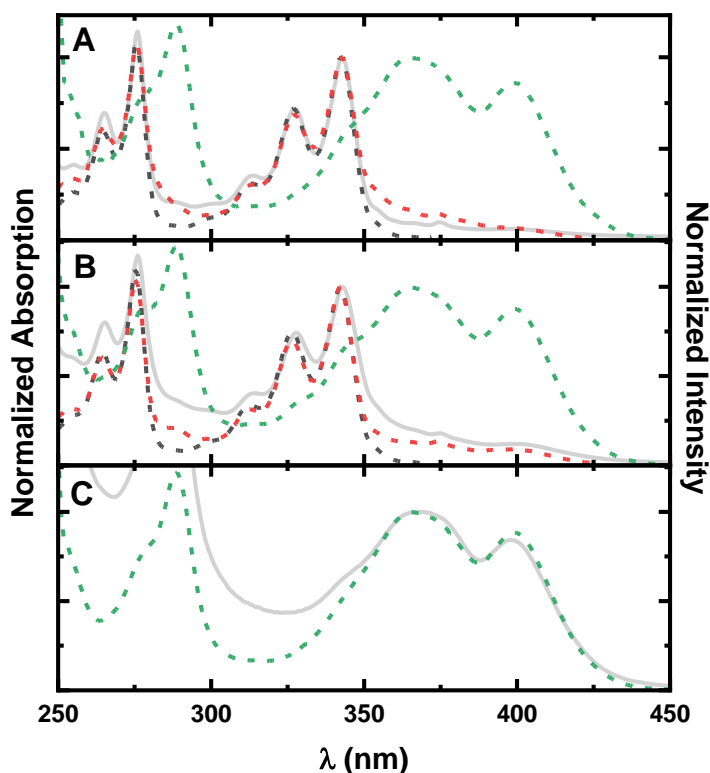


Figure 2.8 Comparison of normalized excitation spectra of (A) ChiNPy -A,(B) ChiNPy-B, and (C) ChiNPy-Imine at different emission wavelengths, (dashed-black line) $\lambda_{\text{exc}}= 380$ nm, (dashed red line) $\lambda_{\text{exc}}= 430$ nm, and (dashed green line) $\lambda_{\text{exc}}= 500$ nm. The absorption spectra (gray line) are also shown.

Steady-state fluorescence measurements support the composition of ChiNPy-A and ChiNPy-B polymers, consisting of four distinct monomeric units. These units include the inherent DA and AC units within the chitosan backbone. Additionally, two additional units result from pyrene incorporation through the formation of an intermediate Schiff base, which remains partially reducible. It is noteworthy that some degree of hydrolysis

of the imine unit, yielding 1-pyrenecarboxyaldehyde and DA units, is expected due to the use of acidic aqueous conditions.⁶⁻⁷

Fluorescence decay analyses were conducted for the ChiNPy-A and ChiNPy-B polymers using nanosecond time-correlated single photon counting (ns-TCSPC). The excitation was carried out at 339 nm, and the emission decays recorded at 377 nm, where the predominant emission from the amino pyrene unit arises. Additionally, measurements with emission collected at 430 nm, where a coexistence of both pyrene-containing units is present, were also obtained. For the analysis of ChiNPy-Imine, a similar approach was employed, albeit using equipment with picosecond time resolution (ps-TCSPC). In this scenario, the excitation was set at 393 nm. This specific excitation wavelength was selected to ensure preferential excitation of the imine pyrene units and minimize the excitation of amino pyrene units. The emission was subsequently measured at 490 nm.

Error! Reference source not found. shows the decay analysis for ChiNPy-A and B. The analyses unveiled the presence of three distinct excited state species. The first species is characterized by a fast decay component of approximately 5 ns and is attributed to the emission of the imine pyrene units. This is supported by the fact that this decay time component is also observed in the decay of ChiNPy-Imine (**Figure 2.10**). Notably, this component solely emerges when analyzing the decays obtained at 430 nm, a wavelength where both imine- and amine-pyrene units in the ChiNPy polymers emit.

The second species is characterized by a long fluorescence decay time of around 100 ns, with a value that is similar to the amino pyrene compounds. This is further corroborated by the constancy of this decay time at both λ_{em} (377 nm and 430 nm), where steady-state measurements have shown the presence of the amino pyrene.

Interestingly, a third decay time, of approximately 20 ns, was obtained in the analysis at 377 nm. This decay time contribution is relatively modest, accounting for approximately 1% of the total fluorescence in ChiNPy-A. However, its contribution increases to 3% in ChiNPy-B. It is noteworthy that ChiNPy-B shows to have nearly tenfold more pyrene units per gram than ChiNPy-A. The increase in the contribution of this intermediate decay suggests potential quenching of amino pyrene units by nearby non-excited pyrene units. This quenching phenomenon emerges at short distances and can lead to a reduction in the fluorescence lifetimes. Considering that ChiNPy-B has a higher pyrene content, the prevalence of these interactions is magnified, thus resulting in a higher contribution.

It is important to note that the contribution of the longest lifetime in ChiNPy-A, where the ratio of amine to imine pyrene units is 6:1, remains almost constant, decreasing only slightly from 99% to 98% as the emission wavelength changes from 377 nm to 430 nm. In contrast, in ChiNPy-B, where this ratio is only 2:1, a noticeable effect on the fluorescence decay contribution, of the longer-lived component, is observed, decreasing from 97% to 75% as the emission wavelength changes from 377 nm to 430 nm.

In macromolecular systems labeled with fluorescent probes, the process of random labeling (and the inherent polydispersity of the polymer) introduces heterogeneity, allowing the fluorescent probe to interact with various local environments. This complexity gives rise to more intricate fluorescence decay patterns. Consequently, describing the fluorescence decay of polymers may not be straightforwardly achieved by summing discrete exponentials. A more realistic approach involves considering the observed behavior in terms of a distribution of lifetimes, a concept well-discussed in the literature.⁸

In the case of ChiNPy, where the fluorescent probe is covalently randomly bonded to the chitosan skeleton, a distribution of lifetimes occurs. To analyze the fluorescence decays of ChiNPy polymers, the Maximum Entropy Method (MEM) was employed. The analysis revealed a distribution with maxima that aligns with the sum of discrete exponentials, as depicted in Error! Reference source not found. for ChiNPy-A and ChiNPy-B, respectively. This proximity between the results obtained from the MEM analysis and the sum of discrete exponentials underscores the robustness and consistency of the experimental findings.

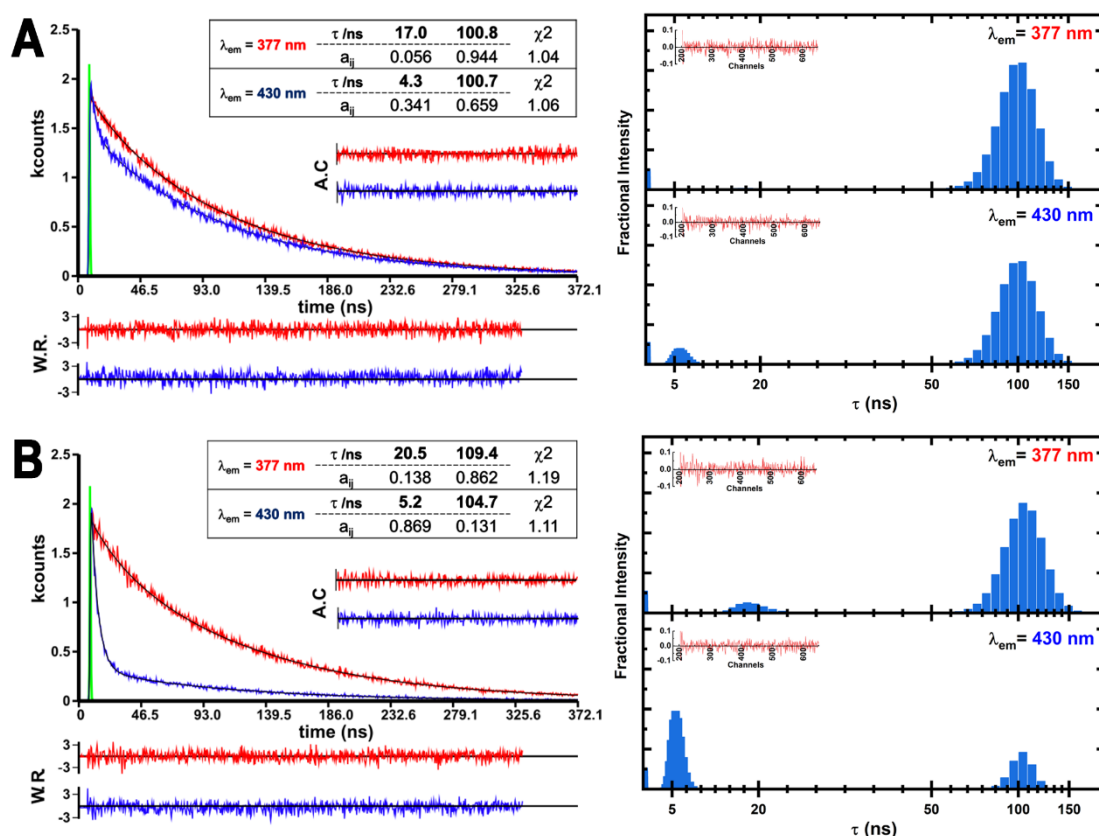


Figure 2.9 (Left) Fluorescence decay adjusted using a method of the sum of exponential and (Right) lifetime distribution obtained by the method of maximum entropy of (A) ChiNPy-A and (B) ChiNPy-B. Weighted residues (W.R) and autocorrelation function(A.C) are shown as an inset in the fluorescence decay as parameters of the fitting. Residues of the function are shown in the case of MEM as inset.

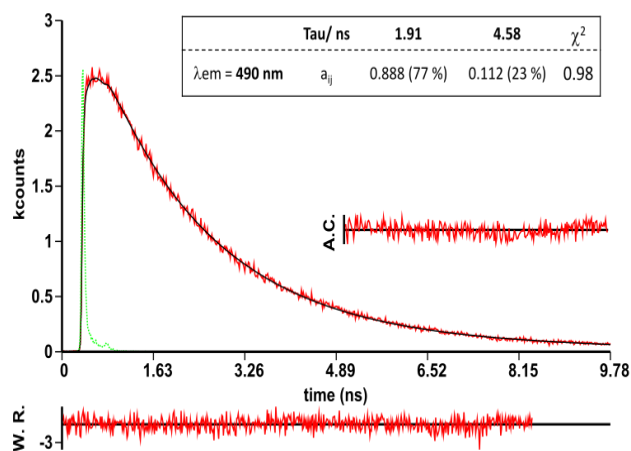


Figure 2.10 Fluorescence decay of ChiNPy-Imine in HAc 5% at 20 °C. Analysis of each λ_{em} was made individually by the method of sum of exponential. Weighted residues (W.R) and autocorrelation function (A.C) are shown as an inset in the fluorescence decay as parameters of the fitting.

2.2.4 Interaction with metals

The investigation aimed to explore the potential applicability of ChiNPy polymers for directly determining a distinct group of metal ions and anions. For this purpose, the fluorescence emission of ChiNPy-B, the higher pyrene-labeled ChiNPy polymer, was observed in the 375-600 nm spectral range. As illustrated in **Figure 2.11**, a notable phenomenon was observed where the fluorescence of ChiNPy-B was quenched upon the introduction of either metal ions or anions.

Figure 2.12 displays the corresponding Stern-Volmer (SV) plots, obtained with emission at 380 nm, which depict the fluorescence quenching of the amine pyrene unit of the chitosan polymer. Importantly, with all metals and anions studied a downward curvature on their respective SV plots was observed. As shown in **Appendix B**, this characteristic curvature mirrors the presence of two distinct populations of fluorophores, wherein one of these populations remains inaccessible to the quenching process and is commonly observed in macromolecular systems.

The underlying rationale for this behavior stems from the hydrophobic nature of the pyrene moieties present in the ChiNPy polymers. The working solvent, an aqueous solution of acetic acid, facilitates the solubilization of the chitosan backbone through the protonation of its amino groups. Subsequently, the pyrene-containing units tend to self-enclose due to their inherent hydrophobicity, effectively shielding themselves from the solvent.

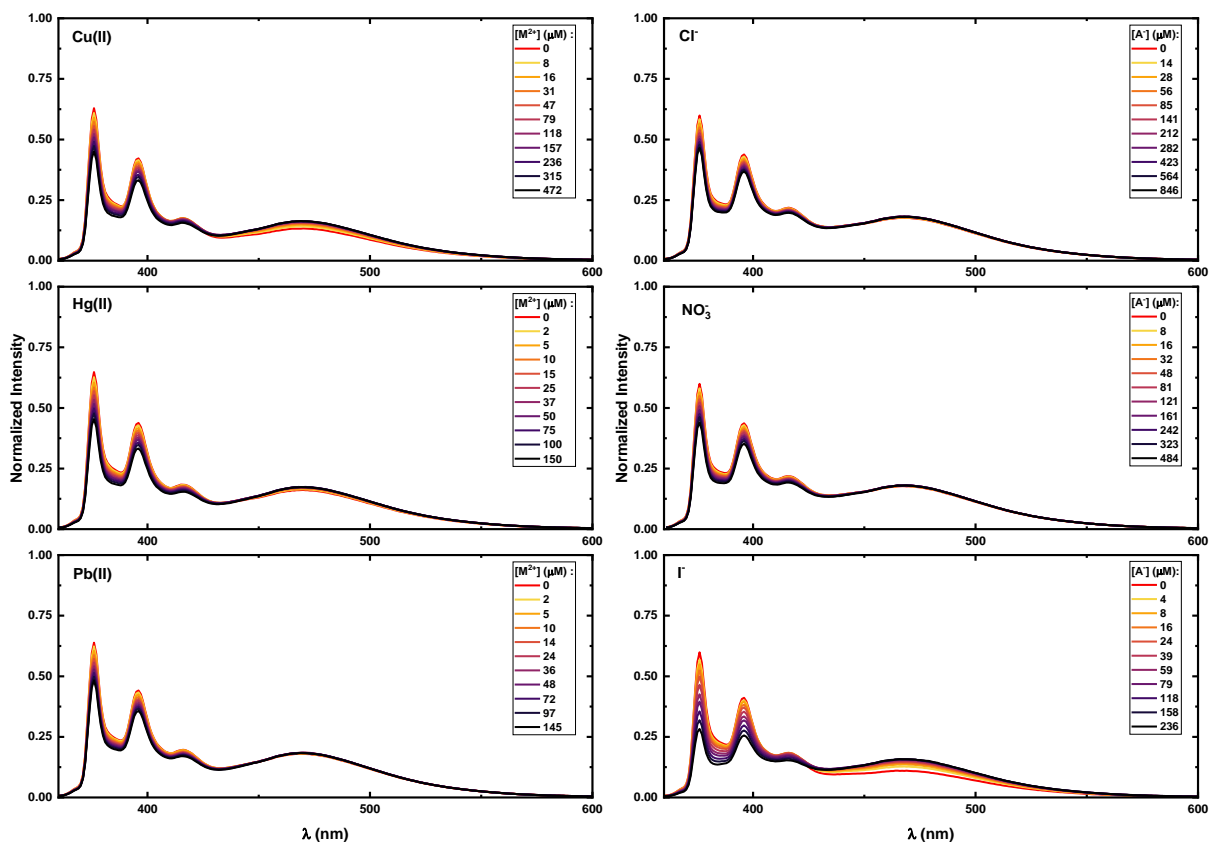


Figure 2.11 Normalized emission spectra of ChiNPy-B with $\lambda_{exc} = 350$ nm, at 25 °C and continuous stirring at 250 rpm with the addition of different metals and anions in Hac 5 %v/v. Each spectrum was recorded 3 min after the addition of the quencher to the solution.

To provide a comprehensive explanation for this phenomenon, alternative SV type plots (**Figure 2.13**) were obtained with **Equation 5.4** in **Appendix B**. This approach allows for a more comprehensive understanding of the intricate fluorescence quenching dynamics observed within the ChiNPy-B polymer.

Table 2.3 illustrates a noteworthy trend: the fraction of accessible fluorophores to the quencher, given by the parameter f_a , increases with the size of the latter. This phenomenon finds its rationale in the primary interaction occurring between the quencher and the chitosan backbone, with the fluorophore itself assuming a spectator role. Upon introduction of the respective ionic species, the chitosan chain engages with the charged entities, inducing closer proximity to the randomly labeled pyrene groups. This spatial proximity facilitates the quenching of pyrene likely through Förster resonance energy transfer (FRET).

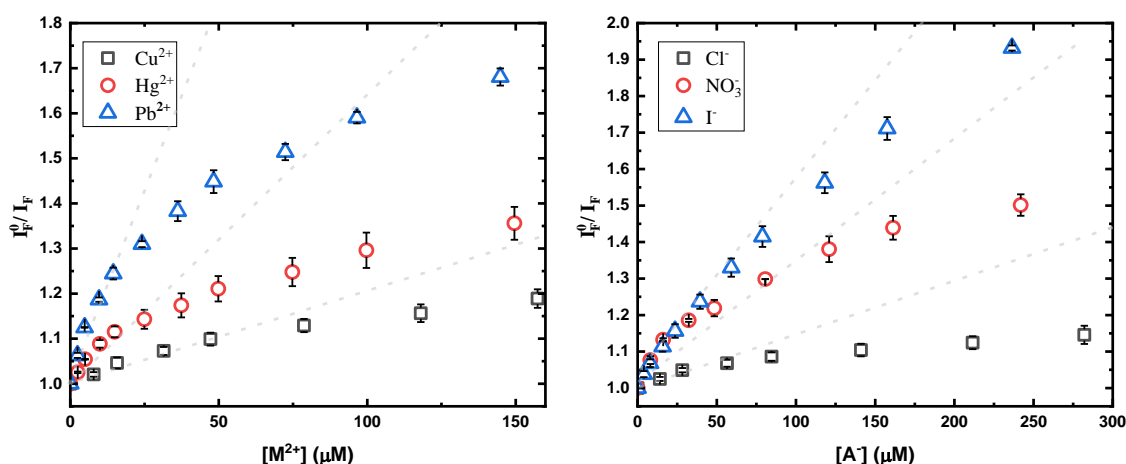


Figure 2.12 Stern-Volmer plot for the addition of different (left) metals and (right) anions to a solution c.a. 1 ppm of ChiNPy-B at 25 °C and continuous stirring at 250 rpm. Each measurement was performed in an interval of 3 min after the addition of the quencher and each experiment was done by triplicate. Gray lines in classic SV are meant to be a guideline to the eye to highlight the downward curvature observed.

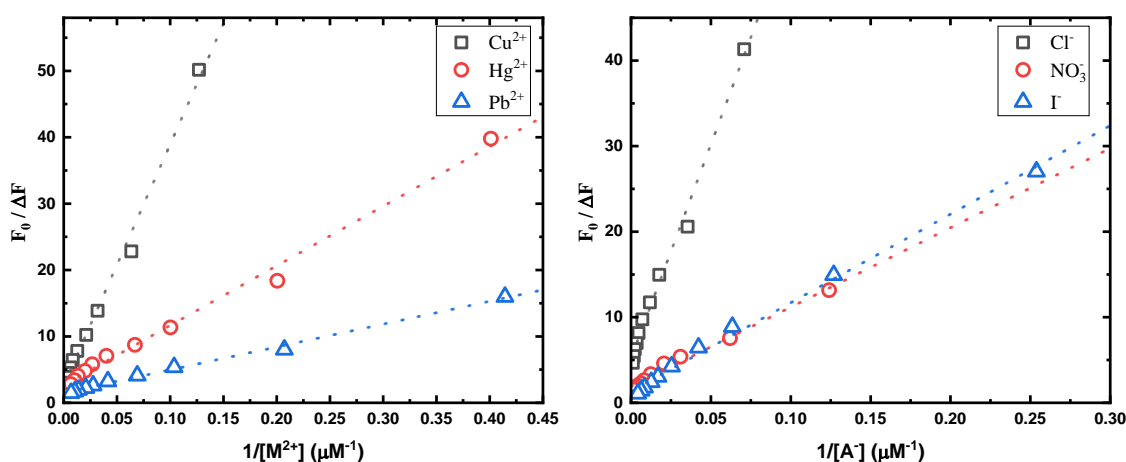


Figure 2.13 Alternative Stern-Volmer plots for the addition of different metals (left) and anions (right) to a solution with approximately 1 ppm of ChiNPy-B at 25 °C. Further details and insights regarding the experimental outcomes are provided in Appendix E.

As the ionic species expands in size, a greater number of pyrene molecules become accessible and engage with the quencher, leading to an increase in the level of accessibility. Consequently, it follows that larger ions such as iodine and lead (II) would exhibit a higher fraction of accessible fluorophores. This insight into the fraction of accessible fluorophores further enables the determination of the Stern-Volmer quenching constant (K_a) for the different analytes (metal ions and anions). A close examination of these K_a values unveils that the interaction of ChiNPy polymers with lead (II) and mercury (II) shows heightened sensitivity. This heightened sensitivity is indicated by their elevated K_a values in comparison to other quenchers.

Table 2.3 Values of the fraction of fluorophore accessible to the quencher (f_a) and Stern-Volmer quenching constant (K_a) of different anions and cations tested with ChiNPy-B

Quencher	f_a	K_a (mol^{-1})
Cl ⁻	0.19	0.010
NO ₃ ⁻	0.53	0.020
I ⁻	0.76	0.013
Cu ²⁺	0.38	0.007
Hg ⁺²	0.38	0.030
Pb ⁺²	0.66	0.044

Conclusion

Chitosan polymers functionalized with pyrene, denoted as ChiNPy, were synthesized and characterized through a range of spectroscopic methods. The extent of substitution with pyrene quantified as %DS_{py}, was obtained via ¹H NMR and UV-Visible spectroscopy. Two distinct labeled polymers denoted A and B were obtained, with %DS_{py} values of 0.5% and 4.4% respectively. The polymers are composed of four fundamental units: deacetylated and acetylated segments intrinsic to the chitosan backbone, together with the amine and imine pyrene units attained during functionalization. In the presence of acidic aqueous environments, discernible hydrolysis of the imine units occurred, culminating in the regeneration of the initial 1-pyrenecarboxyaldehyde reagent.

From the fluorescence decays a tri-exponential system associated with the amine and imine units was observed. The amine unit shows a relatively long lifetime of approximately 100 ns, while the imine-pyrene unit exhibits a shorter lifetime of around 5 ns. Moreover, with a higher pyrene content %DS_{py}, an additional lifetime component, possibly linked to quenching induced by neighboring non-excited pyrene units, was observed.

Exploring the interaction of ChiNPy polymers with various metals and anions unveiled a characteristic downward trajectory in Stern-Volmer plots, indicating the presence of distinct fluorophore populations. Notably, one subset remained impervious to the introduced quencher, resulting in a persistent fluorescence signal. This observation is in line with the notion that the primary interaction takes place between the charged species and the chitosan structure, with the pyrene moiety assuming a secondary role. A more efficient quenching was observed with lead (II) and mercury (II).

Bibliography

1. Pérez-Álvarez, L.; Ruiz-Rubio, L.; Vilas-Vilela, J. L., Determining the Deacetylation Degree of Chitosan: Opportunities To Learn Instrumental Techniques. *Journal of Chemical Education* **2018**, *95* (6), 1022-1028.
2. Costa, T.; Seixas de Melo, J. S.; Castro, C. S.; Gago, S.; Pillinger, M.; Goncalves, I. S., Picosecond dynamics of dimer formation in a pyrene labeled polymer. *J Phys Chem B* **2010**, *114* (39), 12439-47.
3. Dimzon, I. K. D.; Knepper, T. P., Degree of deacetylation of chitosan by infrared spectroscopy and partial least squares. *International Journal of Biological Macromolecules* **2015**, *72*, 939-945.
4. Fernandes Queiroz, M.; Melo, K. R.; Sabry, D. A.; Sasaki, G. L.; Rocha, H. A., Does the use of chitosan contribute to oxalate kidney stone formation? *Mar Drugs* **2014**, *13* (1), 141-58.
5. Barca, G. M. J.; Bertoni, C.; Carrington, L.; Datta, D.; De Silva, N.; Deustua, J. E.; Fedorov, D. G.; Gour, J. R.; Gunina, A. O.; Guidez, E.; Harville, T.; Irle, S.; Ivanic, J.; Kowalski, K.; Leang, S. S.; Li, H.; Li, W.; Lutz, J. J.; Magoulas, I.; Mato, J.; Mironov, V.; Nakata, H.; Pham, B. Q.; Piecuch, P.; Poole, D.; Pruitt, S. R.; Rendell, A. P.; Roskop, L. B.; Ruedenberg, K.; Sattasathuchana, T.; Schmidt, M. W.; Shen, J.; Slipchenko, L.; Sosonkina, M.; Sundriyal, V.; Tiwari, A.; Galvez Vallejo, J. L.; Westheimer, B.; Wloch, M.; Xu, P.; Zahariev, F.; Gordon, M. S., Recent developments in the general atomic and molecular electronic structure system. *J Chem Phys* **2020**, *152* (15), 154102.
6. Cordes, E. H.; Jencks, W. P., The Mechanism of Hydrolysis of Schiff Bases Derived from Aliphatic Amines. *Journal of the American Chemical Society* **2002**, *85* (18), 2843-2848.
7. Pramanik, B.; Das, D., Aggregation-Induced Emission or Hydrolysis by Water? The Case of Schiff Bases in Aqueous Organic Solvents. *The Journal of Physical Chemistry C* **2018**, *122* (6), 3655-3661.
8. Siemiarczuk, A.; Wagner, B. D.; Ware, W. R., Comparison of the maximum entropy and exponential series methods for the recovery of distributions of lifetimes from fluorescence lifetime data. *The Journal of Physical Chemistry* **1990**, *94* (4), 1661-1666.

Chapter 3:

**Diazacationic Ladder-
type Polymers with
Pyrene**

Summary

In this chapter, a comprehensive synthetic approach was undertaken to yield a new ladder-type polymer derived from the diazaacenes family, incorporating pyrene as a key structural core, herein abbreviated to DiazaPy. To accomplish this, the synthesis required an appropriate amino pyrene monomer as well as an alternating copolymer precursor, denoted as MonPy and PolyNPy, respectively.

The compounds (DiazaPy, MonPy, and PolyNPy) were systematically isolated, purified, and subjected to characterization employing an NMR, FTIR, and UV-Vis.

After the characterization process, the electronic and photophysical properties of these compounds were systematically investigated. This was achieved from a comprehensive approach involving both DFT quantum chemical calculations and time-resolved techniques.

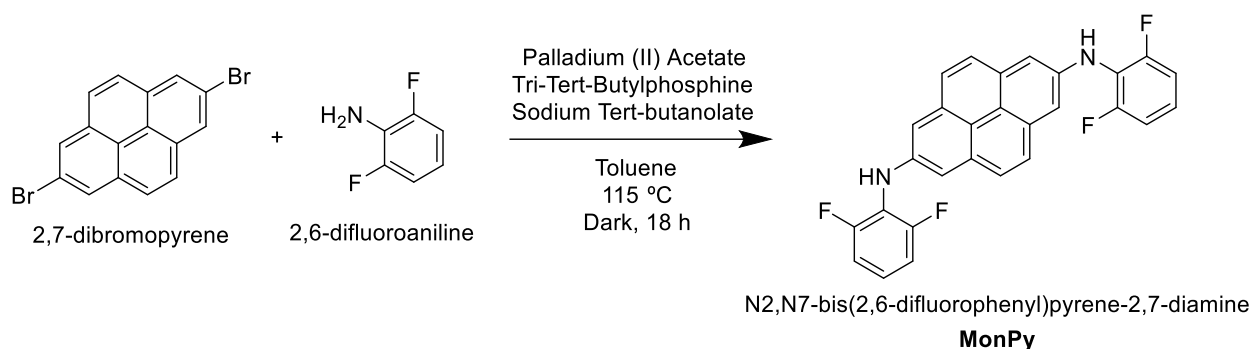
3.1 Synthesis and structural characterization

3.1.1 Reagents and solvents

The synthesis of the compounds required the following reagents: 2,7-dibromopyrene (95% purity, obtained from BLDPharmatech), tri-tert-butylphosphine (98%), sodium tert-butoxide (99%) purchased from Sigma Aldrich, palladium (II) acetate (98%), 2,6-difluoroaniline (98%) from TCI Chemical, and trifluoromethanesulfonic acid (98%, from Alfa Aesar). Technical grade solvents, including toluene, chloroform, acetone, hexane, and ethyl acetate, were used for the different synthesis and purification steps. Spectroscopical grade solvents were used for UV-visible and fluorescence measurements.

3.1.2 Experimental procedure

To complete the synthesis of the cationic ladder-type polymer containing pyrene moieties, a three-step reaction was conducted following a protocol similar to that reported by Wetterling et al.¹ Initially, a 2,7-di-substituted amine pyrene monomer (abbreviated as MonPy, Mon- for monomer) was obtained through a Buchwald-Hartwig amination reaction, as depicted in **Scheme 3.1**. The detailed synthetic procedure is described below.



Scheme 3.1. Synthesis of MonPy molecule by Buchwald-Hartwig amination.

In a head-dried two-neck flask, 1 equivalent of 2,7-dibromopyrene, sodium tert-butoxide (4 equivalents), tri-tert-butyl phosphine (1.5 equivalents), and palladium (II) acetate (0.05 equivalent) were dissolved in 30 mL of deaerated, under an argon atmosphere, toluene. Subsequently, 2.5 equivalents of 2,6-difluoroaniline were added dropwise, and the mixture was stirred for approximately 18 hours in the absence of light at 115 °C.

The reaction mixture was then extracted with dichloromethane and washed twice with water and once with an aqueous solution of NaCl. The organic phase was dried over magnesium sulfate, and the solvent was removed using a rotary evaporator.

The crude product was finally purified using column chromatography with silica gel as the stationary phase and a mixture of hexane: ethyl acetate (4:1) as the eluent. The final product was dried under vacuum, resulting in a yellow-dark powder with a yield of 60%.

The purity of the isolated MonPy was verified with different techniques. The ¹H and ¹³C NMR spectra (**Figure 3.1** and **Figure 3.2**, respectively) exhibited the expected peaks for MonPy without any evidence of residual material or contamination. The assignment of the signals is given in **Table 3.1**. 2D NMR techniques were also employed to accurately assign all the observed peaks (see **Appendix G**). Furthermore, analysis of a sample of MonPy by LC-MS in positive ion polarity yielded an M+1 signal of 457.1327, indicating the purity of MonPy.

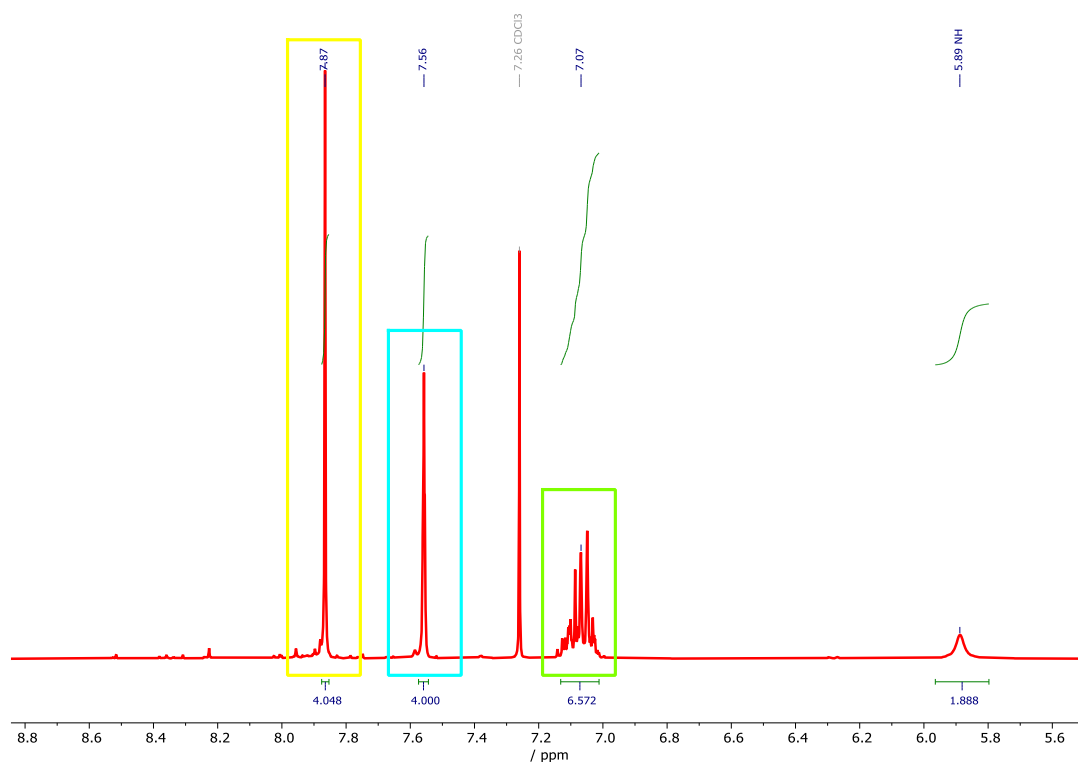


Figure 3.1 ^1H NMR of MonPy in deuterated chloroform. The peak attribution is made in Table 3.1.

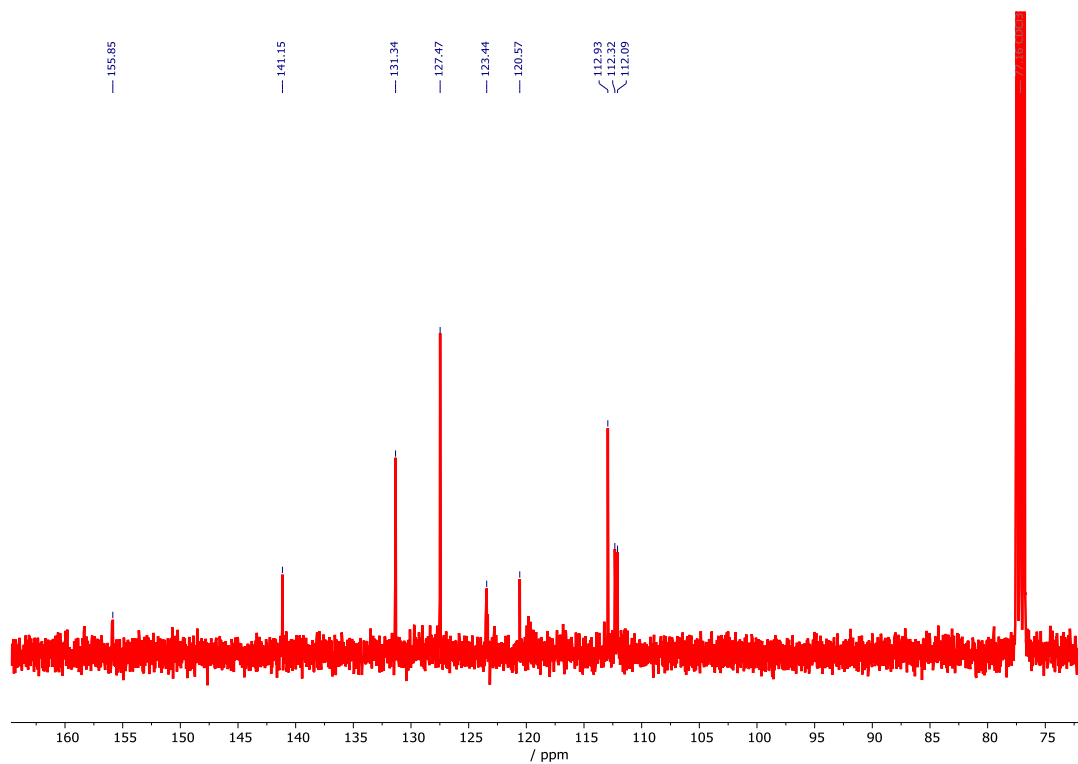
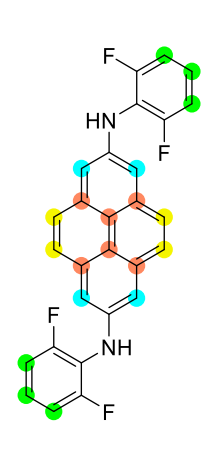


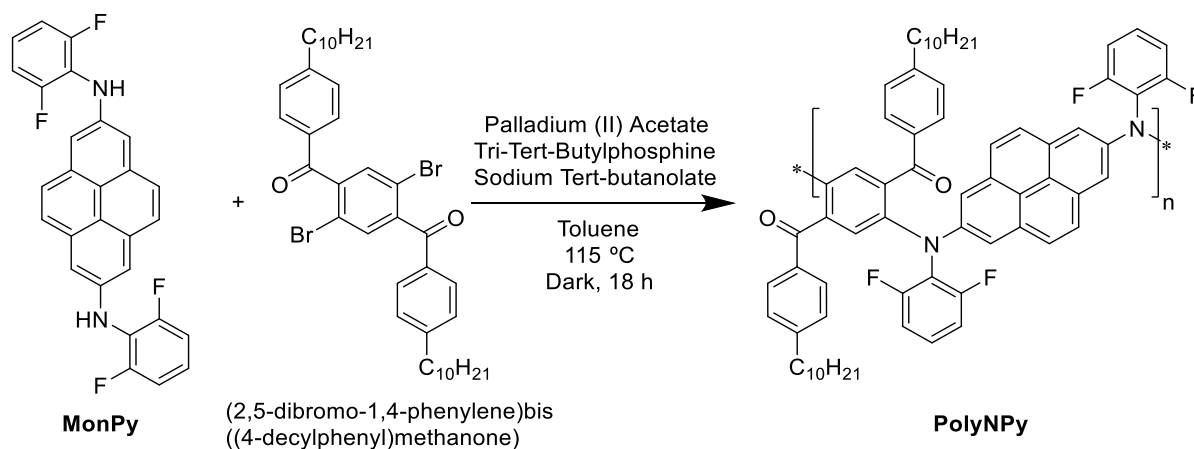
Figure 3.2 ^{13}C NMR of MonPy in deuterated chloroform. The peak attribution is made in Table 3.1.

Table 3.1. Attribution of signals of MonPy by ¹H and ¹³C NMR.

	Id.	Description	δ ¹H NMR / ppm	δ ¹³C NMR / ppm
	Green	C-H from <i>meta</i> and <i>para</i> position of 2,6-difluoroaniline	7.07 (m)	112.0 & 112.3
	Cyan	Protons from non-K-region in pyrene moiety	7.56 (s)	112.9
	Yellow	Protons from K-region in pyrene moiety	7.87 (s)	127.5
	Orange	Quaternary carbons in pyrene moiety		120.3 & 131.3
		N-H	5.89 (b)	
		C-N in pyrene moiety		141.1
		C-N in 2,6-difluoroaniline moiety		123.4
		C-F in 2,6-difluoroaniline moiety		155.9

N.O: Not observed; s:singlet; m: multiplet; b: broad.

The MonPy molecule was subsequently employed as a reagent to generate the precursor polymer containing pyrene (abbreviated as PolyNPy). The polymerization process involved the same type of reaction as the previous step, but in this case (2,5-dibromo-1,4-phenylene)bis((4-decylphenyl)methanone) was used as the complementary reagent. Please see **Scheme 3.2** for the schematic illustration of the synthetic procedure. The detailed synthetic procedure is described below.



Scheme 3.2 Polymerization of MonPy with (2,5-dibromo-1,4-phenylene)bis((4-decylphenyl)methanone).

A mixture containing an equimolar ratio of MonPy and 2,5-dibromo-1,4-phenylene)bis((4-decylphenyl)methanone) was placed in a microwave vessel under argon atmosphere. Sodium tert-butoxide (3 equivalents) and palladium (II) acetate (0.15 equivalents) were added, followed by tri-tert-butyl phosphine (0.45

equivalents) and dry toluene. The final molar concentration of the mixture was approximately 0.1 M. The reaction was stirred at 115 °C for 3 days in the absence of light.

For the workup, the mixture was diluted with chloroform at room temperature and washed twice with water and once with an aqueous NaCl solution. The organic phase was evaporated using a rotary evaporator. A saturated solution of the polymer was prepared by redissolving it in chloroform and precipitated in cold methanol at -20 °C. The precipitate was then subjected to extraction using a Soxhlet apparatus (see **Figure 3.3**), utilizing methanol, acetone, ethyl acetate, and chloroform as solvents, and avoiding exposure to light. The yield of the isolated PolyNPy in each fraction was 6% for acetone, 0.6% for ethyl acetate, and 14.5% for the chloroform fraction. PolyNPy exhibited a dark-yellow color.

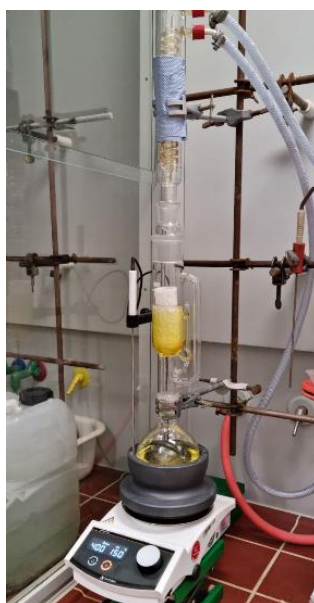


Figure 3.3 Soxhlet apparatus used for extraction of the different fractions of the PolyNPy polymers.

The ^1H NMR and ^{13}C NMR spectra of PolyNPy are shown in **Figure 3.4** and **Figure 3.5**, respectively. The analysis of these spectra is more complex due to the polymeric nature of the sample. In the proton NMR spectrum, the signals are broadened, reflecting the different chemical environments of the equivalent protons. In the ^1H NMR spectrum, two distinct regions can be identified: signals below 3 ppm correspond to the aliphatic side chain from the 4-decylphenyl group present in the expected PolyNPy polymer, while the signals in the aromatic region are more challenging to assign. Therefore, the aromatic signals were divided into four different groups, each representing a specific set of protons.

The ^{13}C NMR spectrum provides valuable information about the expected structure of PolyNPy. While attributing specific signals to each carbon can be challenging, three distinct regions can be observed. The lower chemical shift region corresponds to the aliphatic carbons in the side chain of the 4-decylphenyl group, while

signals around 100 – 160 ppm are associated with the aromatic carbons in the polymer structure. Additionally, a small signal at 193.5 ppm corresponds to the carbon in the carbonyl group of PolyNPy. Within the group of aromatic carbons, two subgroups can be attributed: the carbon directly bonded to the fluorine in the 2,6-difluoroaniline group, which should exhibit the highest chemical shift due to the inductive effect of fluorine, followed by the carbon directly attached to the nitrogen. **Table 3.2** shows the estimated attributions for PolyNPy.

The size of the isolated PolyNPy obtained from the acetone and chloroform fractions was determined using gel permeation chromatography (GPC) in chloroform with polystyrene calibration. The results for the acetone fraction indicated a number-average molecular weight (M_n) of 3,500 g/mol and a weight-average molecular weight (M_w) of 4,100 g/mol, with a polydispersity index (D, M_w/M_n) of 1.18. The chloroform fraction exhibited an M_n of 9,030 g/mol, an M_w of 11,800 g/mol, and a D ratio of 1.31. Considering that the molecular weight of a PolyNPy monomer is approximately 1,019 g/mol, the GPC data suggest that the acetone fraction consists of an oligomer composed of ca. 4 monomeric units per chain. In contrast, the chloroform fraction is composed of approximately 10 repeated monomeric units and can be designated as a polymer.

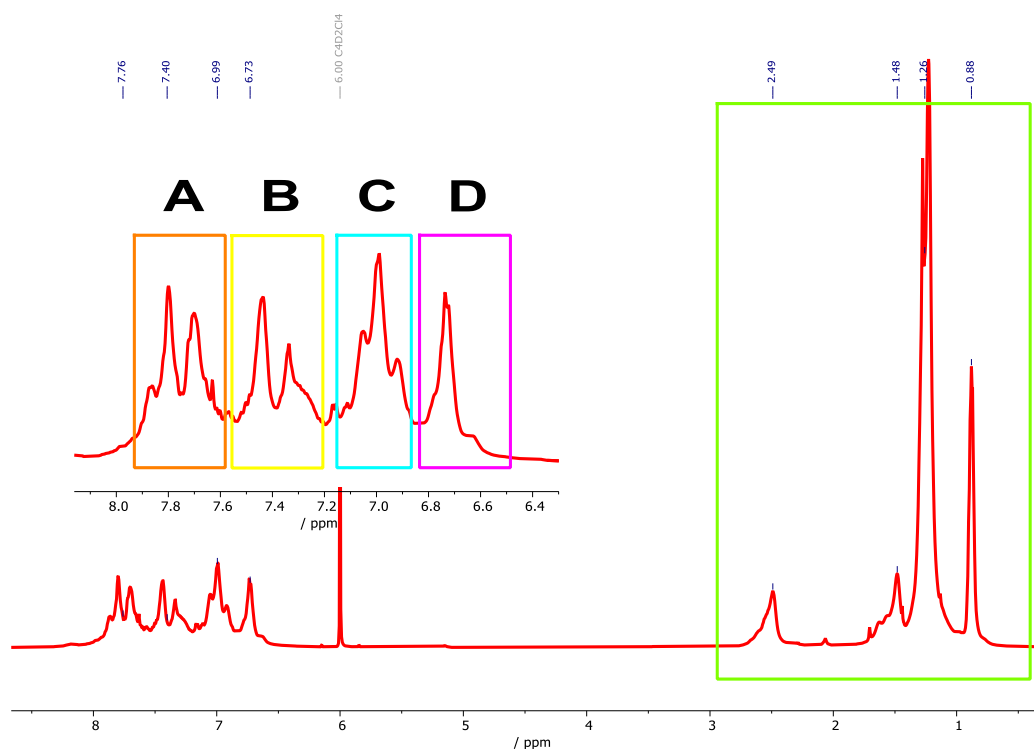


Figure 3.4 ¹H NMR of PolyNPy in 1,1,2,2-Tetrachloroethane-d₂. Expansion of the aromatic zone showed as inset. The colors match the attribution in Table 3.2.

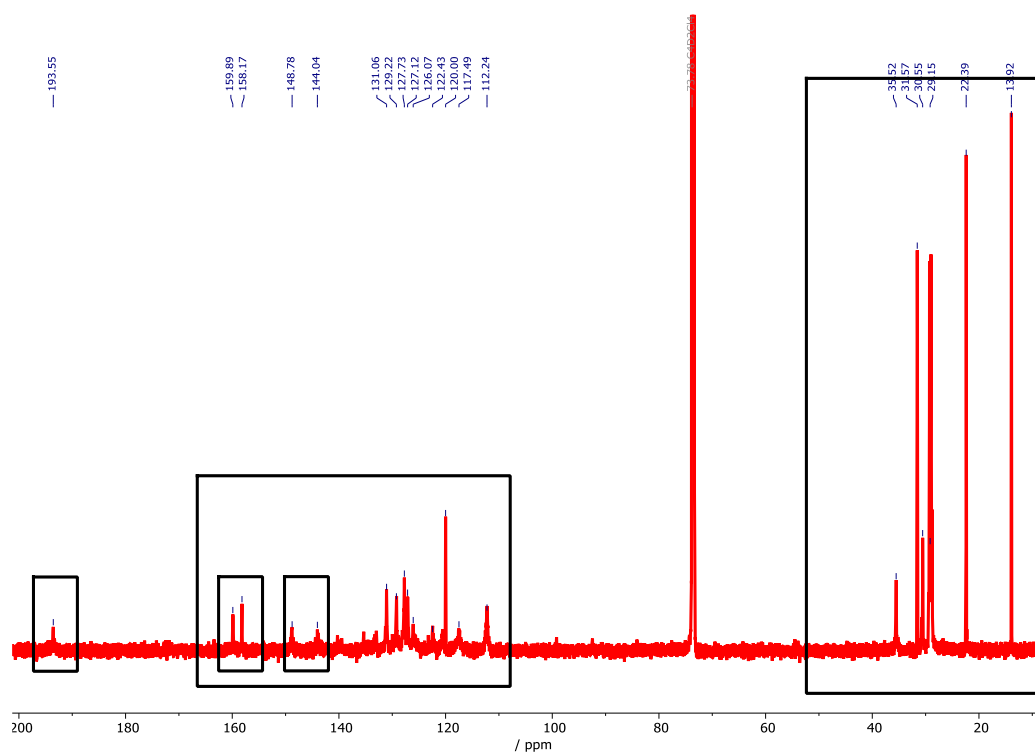
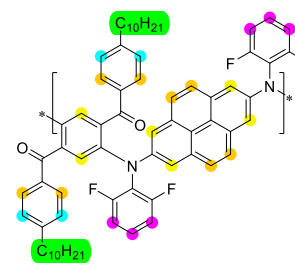


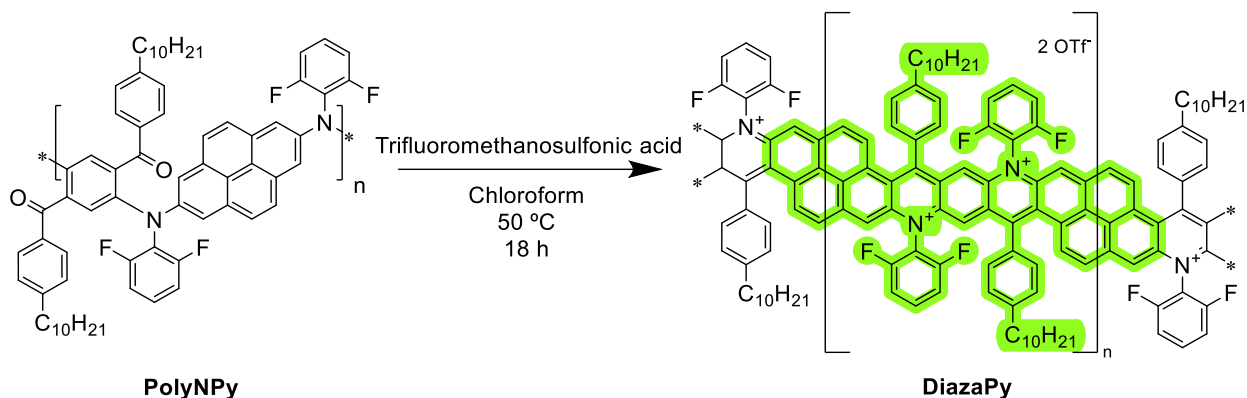
Figure 3.5 ^{13}C NMR of PolyNPY in 1,1,2,2-Tetrachloroethane- d_2 .

Table 3.2 Attribution of signals of PolyNPY by ^1H and ^{13}C NMR.

	Id.	Description	δ ^1H NMR/ ppm	δ ^{13}C NMR/ ppm
	Green	Aliphatic chain from 4-decylphenyl group	0.9 - 2.8	10 - 40
Purple	C-H from <i>meta</i> and <i>para</i> position of 2,6-difluoroaniline	c.a. 6.7	100 - 140	
Cyan	C-H from <i>meta</i> position in 4-decylphenyl group	c.a. 7.0		
Yellow	Protons from non-K-region in pyrene moiety and protons from phenylene ring	c.a. 7.4		
Orange	Protons from K-region in pyrene moiety and protons in <i>ortho</i> position in 4-decylphenyl group	c.a. 7.8		
		C-N		140 - 150
		C-F		150 - 160
		C=O		193

The post-polymerization of PolyNPY was performed through an acid-mediated cyclization to obtain a ladder-type diazacationic polymer, abbreviated as DiazaPy (Diaza- referring to diazacationic). Please see **Scheme 3.3** for an illustration of the synthetic procedure. To accomplish this, the PolyNPY obtained from the chloroform fraction was dissolved in chloroform in a heat-dried microwave vessel under an argon atmosphere. Then, 10

equivalents of trifluoromethanesulfonic acid were added dropwise to the reaction mixture. The reaction was kept at 50 °C for 18 hours with continuous stirring.



Scheme 3.3 Synthesis of diazacationic ladder-type polymer DiazaPy from PolyNPy.

After 18h, the flask was allowed to cool to room temperature, and the mixture was diluted with chloroform. It was then extracted twice with water and once with a saturated solution of NaCl. The solvent of the organic phase was removed under reduced pressure, and the remaining residue was precipitated in cold hexane (-20 °C), in a similar procedure to the one used for PolyNPy. Different fractions of DiazaPy were obtained by extraction using a Soxhlet with methanol and chloroform as solvents. The chloroform fraction was retained and reprecipitated in cold hexane (-20 °C). The final polymer was obtained as a dark green solid, yielding approximately 50%. The ¹H NMR and ¹³C NMR spectra are presented in **Figure 3.6** and **Figure 3.7**, respectively.

Comparing the ¹H NMR spectrum of DiazaPy with its precursor PolyNPy, it is possible to observe similarities in the signals from the aliphatic region, which corresponds to the side chain of the 4-decylphenyl group. In the aromatic region, the peaks become broader and less resolved, which is due to the complete conjugation of the ladder polymer. Consequently, the protons exhibit slight differences in their chemical environments, resulting in broad and poorly resolved signals. The ¹³C NMR spectrum also shows two notable differences compared to PolyNPy. Firstly, the signal associated with the carbonyl group is absent, indicating a successful electrophilic attack during the cyclization of the precursor polymer. Secondly, there are fewer signals in the aromatic carbon region (around 100 – 160 ppm), which may be attributed to the presence of a small number of radical cation species within DiazaPy, hindering the resolution of other NMR signals. This can be expected since the reduction potential of the dicationic species should be high, making it difficult to remove such radical cations even at trace levels. Further experiments in the next section were conducted to confirm the existence of radical cation species.

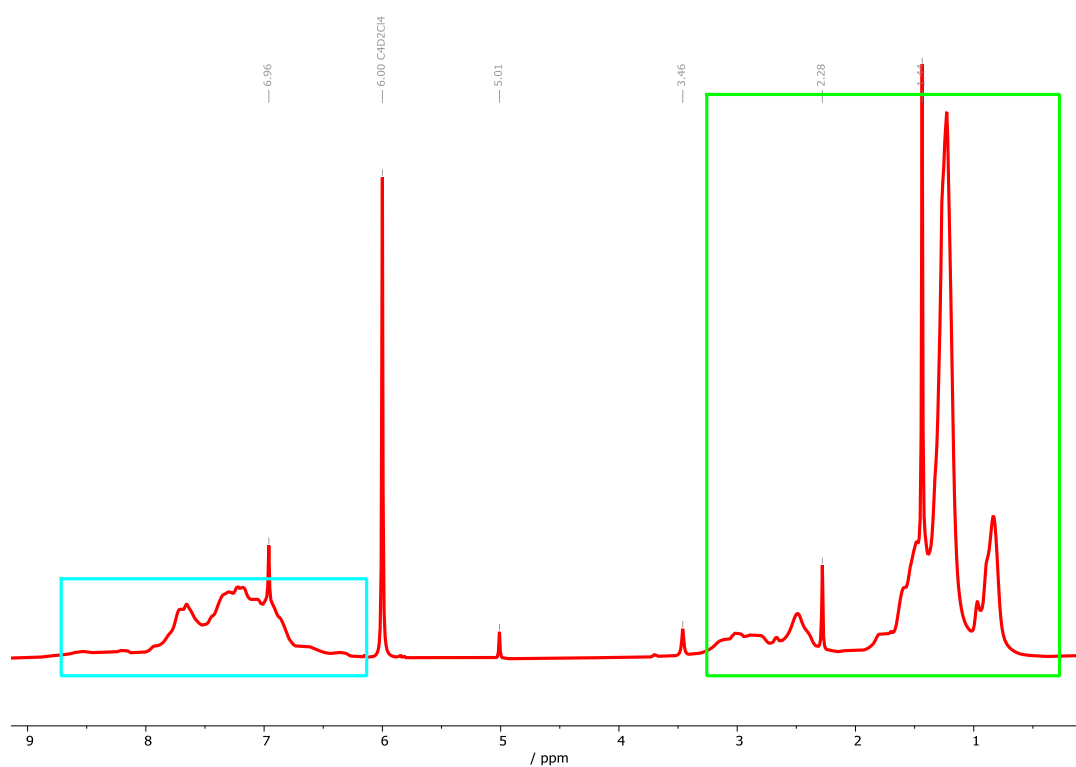


Figure 3.6 ^1H NMR of DiazaPy in $1,1,2,2\text{-Tetrachloroethane-}d_2$. Peaks marked as gray are residual solvents.

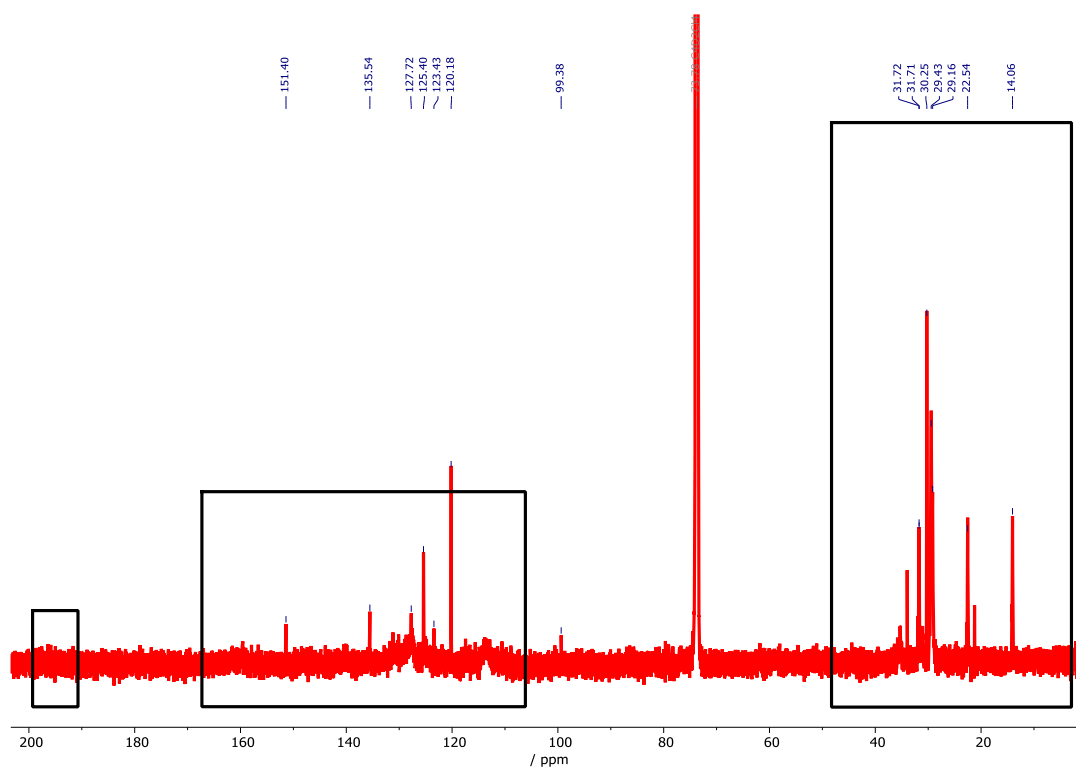


Figure 3.7 ^{13}C NMR of DiazaPy in $1,1,2,2\text{-Tetrachloroethane-}d_2$.

Table 3.3 Attribution of the ^1H and ^{13}C NMR signals of DiazaPy.

	Id.	Description	δ ^1H NMR/ ppm	δ ^{13}C NMR/ ppm
	Green	Aliphatic chain from 4-decylphenyl group	0.8 – 3.3	10 - 40
	Cyan	C-H attached to any aromatic system	6.5 – 8.5	90 - 160
		Quaternary carbons in the aromatic backbone		110 - 160

3.2 Results and Discussion

3.2.1 FTIR Characterization

Fourier-transform infrared spectra (FTIR) were recorded for each synthesized compound to substantiate the presence of significant distinctions between them and to verify the expected chemical reactions of the isolated products. As depicted in **Figure 3.8**, a comparative analysis of the FTIR spectra for MonPy, PolyNPy, and DiazaPy is presented.

In the MonPy spectrum, a discernible peak emerges around 3400 cm^{-1} associated with the stretching mode of the N-H group inherent in this molecule. However, following the polymerization step, this peak vanishes in both PolyNPy and DiazaPy due to the tri-substitution of the amine unit. Furthermore, in the PolyNPy spectrum, a relatively intense new peak is evident around 1680 cm^{-1} attributable to the stretching mode of the C=O group present in the previously functionalized (2,5-dibromo-1,4-phenylene)bis((4-decylphenyl)methanone).

In contrast, during the post-polymerization step, a nucleophilic attack occurs from the pyrene ring to the carbonyl group through an acid-mediated cyclization. This transformative reaction eliminates the functional group, consequently leading to the absence of the C=O stretching band in the FTIR spectra of the final DiazaPy polymer. The absence of this peak in the FTIR spectrum of the DiazaPy confirms the complete conversion of the carbonyl group, resulting in the desired ladder polymer.

It is noteworthy that all compound's FTIR spectra display the signals for the stretching vibrations of C-H bonds, observed at wavenumbers lower than 3000 cm^{-1} which supports the expected vibrational range for aromatic protons.

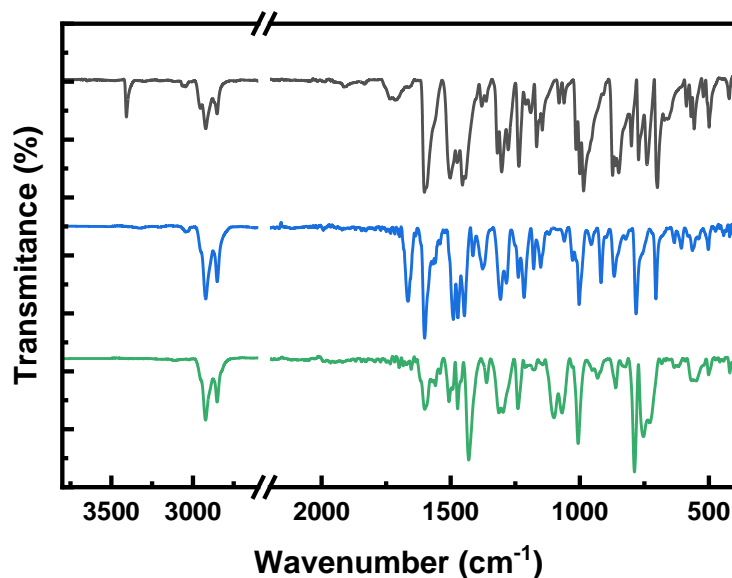


Figure 3.8 FTIR-ATR spectra of (black line) MonPy, (blue line) PolyNPY, and (green line) DiazaPy.

3.2.2 EPR measurements

References to previously documented literature reveal the existence of compounds analogous to DiazaPy, characterized by structural resemblance.² These compounds were identified as stable N, N'-diarylated radical cations. Confirmation of this hypothesis is obtained from ¹³C NMR data indicating the presence of radical cations. To provide additional support, electronic paramagnetic resonance (EPR) measurements were conducted.

As demonstrated in **Figure 3.9**, DiazaPy exhibits a distinct EPR signal lacking hyperfine splitting in chloroform ($g = 2.0019$) at 20°C. These findings indicate the presence of a radical cation in DiazaPy. Intriguingly, the signal intensity diminishes with time, ultimately becoming absent after 96 hours of sample preparation when exposed to daylight. Remarkably, when the solution is maintained in darkness for the same duration, the signal persists, an indicative signal of a ground-state radical that undergoes minimal photochemical degradation. Notably, EPR measurements in deaerated toluene yield similar results ($g = 2.0022$), showing that in the absence of oxygen, the signal remains stable even in the presence of light. The presence of a narrow signal is a definitive indication of a localized radical. The absence of hyperfine splitting further underscores the isolation of this radical from potential other radicals. Specifically, this points to the localization of the radical cation on the nitrogen atom.

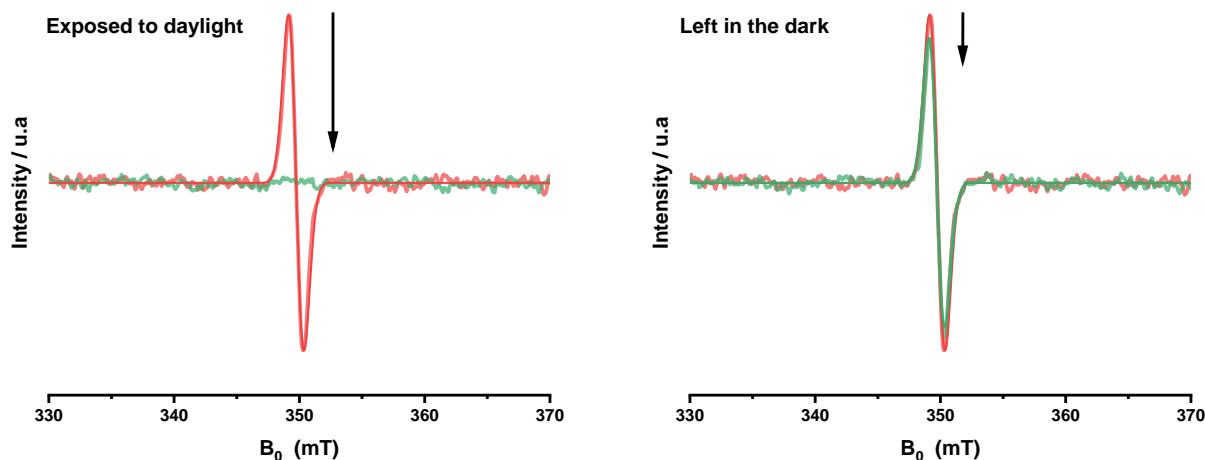


Figure 3.9 EPR spectra of DiazaPy in CHCl_3 (right) under exposition to room light and (left) and avoiding any type of radiation at time (red) 0 h and (green) 96 h.

3.2.3 UV-Vis and fluorescence characterization

Significant photochemical and photophysical characteristics are expected from all three synthesized compounds and polymers (MonPy, PolyNPy, and DiazaPy) due to the incorporation of pyrene into their molecular structures. As a result, a comprehensive analysis was conducted, employing steady-state and time-resolved techniques, in conjunction with other complementary methodologies and DFT calculations. The studies were carried out under deaerated conditions. However, notable changes in the absorption spectra of DiazaPy were observed with time. Consequently, the decision was made to use only the more promising solvent for a comparative analysis of the three samples studied in this chapter. All samples were freshly prepared prior to each measurement.

MonPy

As shown in **Figure 3.11**, the absorption spectra of MonPy exhibit negligible differences in the three solvents. Notably, two distinct electronic transitions are discernible: the $S_0 \rightarrow S_1$ transition occurring at around 430 nm and a more pronounced $S_0 \rightarrow S_2$ transition centered around 300 nm. The latter transition also displays vibronic resolution, with a peak near 344 nm. Concomitantly, the fluorescence emission, with its peak intensity maximum at approximately 445 nm, shows a characteristic mirror-image relationship with the $S_0 \rightarrow S_1$ transition according to Kasha's rule. It is worth noting that the Stokes shift (Δ_{ss}) for MonPy has a relatively low value. A more comprehensive summary of these parameters is provided in **Table 3.4**. Notably, MonPy exhibits a substantial fluorescence quantum yield (φ_f) of 0.48 ± 0.02 .

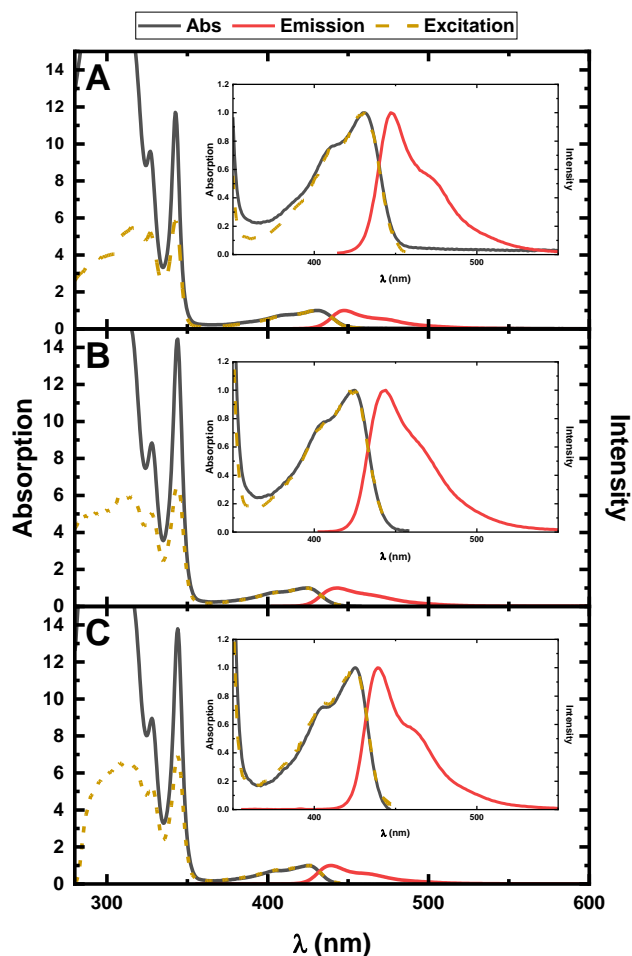


Figure 3.10 Normalized absorption, excitation and fluorescence emission of MonPy in (A) 2MeTHF, (B) CHCl_3 and (C) toluene. The fluorescence spectra were acquired using an excitation wavelength (λ_{exc}) of 350 nm, while the excitation spectra were obtained with an emission wavelength (λ_{em}) of 450 nm. Each spectrum is accompanied by an inset, providing an enlarged view of the $S_0 \rightarrow S_1$ transition and highlighting the mirrored relationship between absorption and fluorescence spectra.

Figure 3.11 illustrates the calculated (from TD-DFT calculations) spectrum that closely resembles the experimental UV-Vis spectrum of MonPy. These computational results not only predict the outcomes but also provide insights into the contributing orbitals for each transition. As demonstrated in Table 5.5, which presents selected relevant transitions and associated orbitals, the $S_0 \rightarrow S_1$ transition corresponds to a HOMO \rightarrow LUMO electronic transition. Consequently, the oscillator strength (f) for this transition appears relatively lower. Intriguingly, the most significant transitions driving the $S_0 \rightarrow S_2$ transition involve the HOMO-1 \rightarrow LUMO and HOMO \rightarrow LUMO+1 transitions. Notably, the intensity of these transitions is reasonably high.

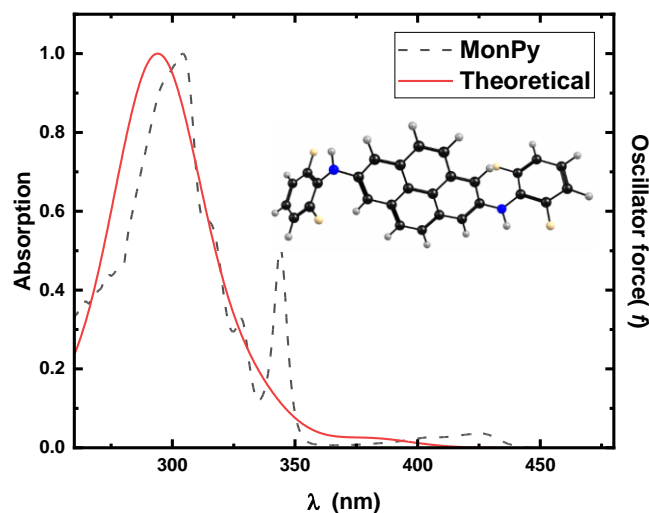


Figure 3.11 Absorption spectra predicted using TD-DFT with BPBE functional in toluene for MonPy, alongside inset of optimized structure. Dashed lines represent experimental absorption spectra for comparative analysis.

From time-resolved measurements, it was established that MonPy shows a mono-exponential fit of 20.6 ns in deaerated toluene. This data is obtained with excitation at 339 nm, and emission at 450 nm. For a more comprehensive detail of the time-resolved data, please see **Table 3.5**.

Time-resolved femtosecond transient absorption (fs-TA) measurements were conducted on MonPy using an excitation wavelength (λ_{exc}) of 380 nm. This compound shows a positive signal indicative of excited state absorption (ESA) in the spectral range of 450 – 650 nm, see **Figure 3.12**.³ The results of the global analysis corroborate this finding, demonstrating that the experimental traces across the entire spectral-temporal spectrum are well-fitted by the sum of three exponential components. Notably, one of these components exhibits an 'infinite' lifetime, potentially representing a long-lived state that falls beyond the temporal resolution limit of the technique (around 7.6 ns).

The fast decay component, characterized by a decay time of 52 ps, can be attributed to a new excited species. The second decay time of 5.0 ns can be associated with the non-radiative transition from S_n to S_1 . Considering that MonPy's fluorescence lifetime, as indicated in **Table 3.5**.

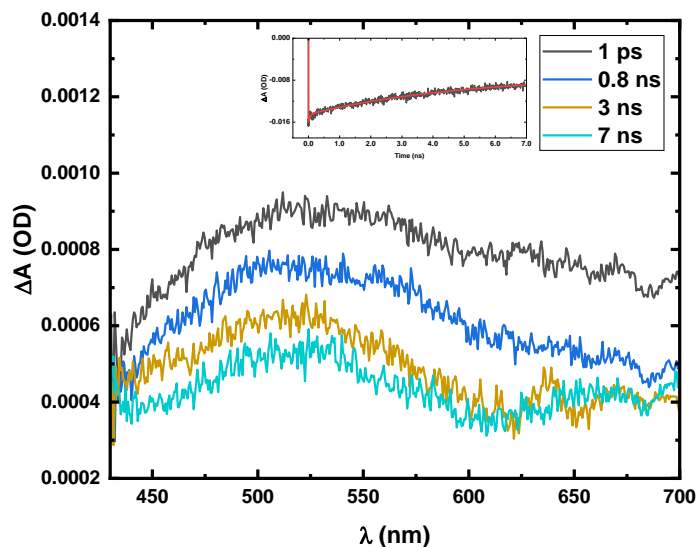


Figure 3.12 Time-resolved femtosecond transient absorption (fs-TA) of MonPy obtained with $\lambda_{\text{exc}} = 380$ nm in deaerated toluene at room temperature. Representative kinetic traces with fits from global analysis are presented as inset.

PolyNPy

The UV-Vis spectra of PolyNPy across various solvents are shown in **Figure 3.13**. PolyNPy, an alternating copolymer featuring MonPy as one of its constituents, departs significantly from the spectroscopic properties of the former. Its absorption spectrum remains relatively consistent across different solvents, and PolyNPy displays an emission that shifts towards longer wavelengths, ranging from 570 to 600 nm, depending upon the solvent. This emission shift is associated with the largest Stokes shift (Δ_{ss}) among the three studied samples (**Table 3.4**). Notably, PolyNPy excitation spectrum in CHCl_3 differs from its absorption profile, potentially indicating solvent-induced effects on the polymer's properties and solubility. However, for 2MeTHF and toluene, the excitation spectra mirror the absorption profile.

Furthermore, the fluorescence quantum yield (φ_{F}) of this polymer in deaerated toluene at 20°C is 0.190 ± 0.008 . This significant reduction in quantum yield can be attributed to the increment of the non-radiative contribution (number of degrees of freedom) as the polymer's size increases. This phenomenon likely contributes to the reduced radiative efficiency of PolyNPy.

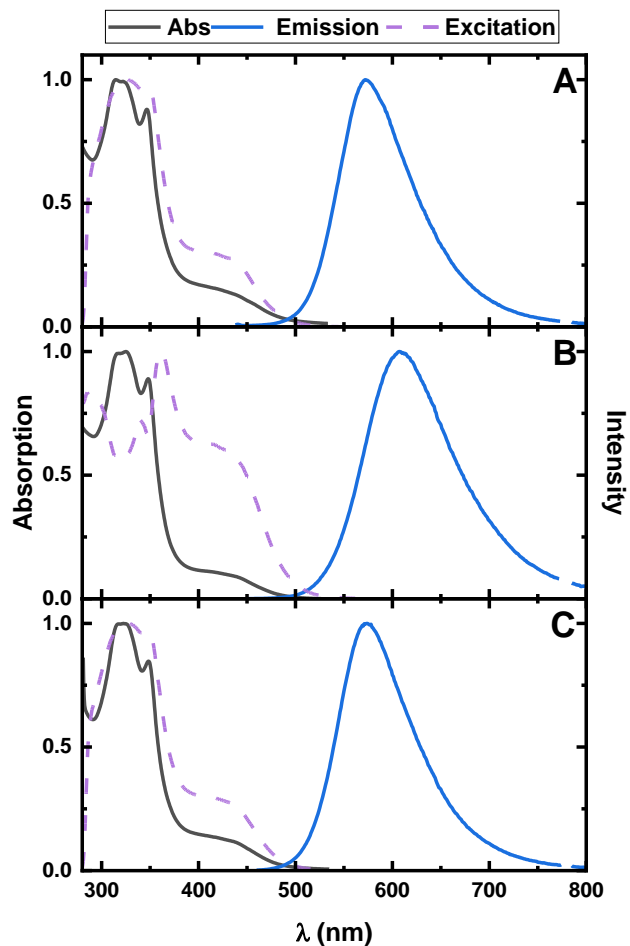


Figure 3.13 Normalized absorption, excitation and fluorescence emission of PolyNPy in (A) 2MeTHF, (B) CHCl_3 and (C) toluene. The fluorescence spectra were acquired using an excitation wavelength (λ_{exc}) of 390 nm, while the excitation spectra were obtained with an emission wavelength (λ_{em}) of 570 nm.

DFT calculations concerning the excited state properties were conducted on a proposed monomer of PolyNPy, as depicted in **Figure 3.14**, together with the predicted UV-Vis spectra. The results of these calculations indicated a poorly allowed HOMO \rightarrow LUMO transition at approximately 463 nm, characterized by a small oscillator strength (f) value. Additionally, two additional allowed transitions emerged at 350 nm and 318 nm, respectively. Notably, the orbitals involved in these transitions are predominantly localized within the pyrene moiety, as can be seen in **Table 5.5**.

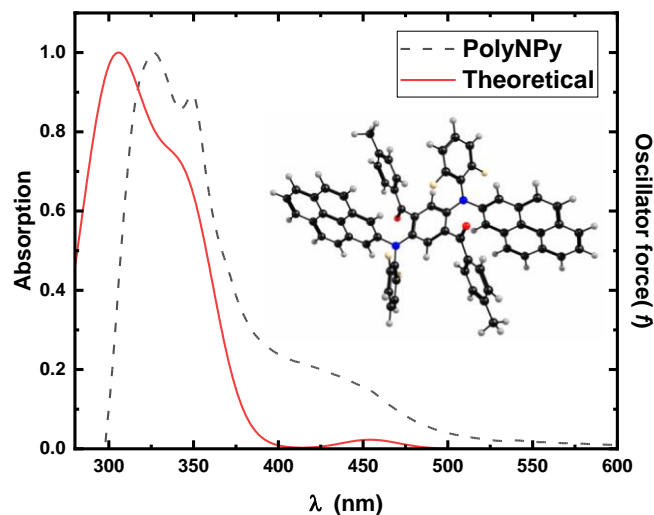


Figure 3.14 Absorption spectra predicted using TD-DFT with BPBE functional in toluene for PolyNPy, alongside inset of optimized structure. Dashed lines represent experimental absorption spectra for comparative analysis.

Time-resolved measurements, with two distinct excitation wavelengths (outlined in **Table 3.5**), unveiled the presence of two discrete excited species. These result from the bi-exponential fitting, resulting in two close but distinct lifetime values (~ 2 and ~ 6 ns). Interestingly, for both excitation wavelengths (λ_{exc}), the species with the longer decay lifetime governs the decay behavior. When excited at 339 nm, its contribution to the overall fluorescence is 71%. In contrast, upon excitation at 391 nm, this contribution amplifies significantly to 96%. This can be rationalized by considering the polymeric nature of the sample. Specifically, at 391 nm excitation, a significant portion of the polymeric chain is activated, leading to the dominance of the excited species characterized by the longer decay time.

For PolyNPy, an analysis was conducted using fs-TA under the same conditions employed for MonPy. This analysis revealed a positive transient absorption band in the range of 400 – 600 nm, which can be attributed to an ESA band, as depicted in **Figure 3.15**. The global trace analysis for this compound resulted in a bi-exponential fitting. One of the components was constrained to have an 'infinite' lifetime to optimize the fit to the experimental data, while the other lifetime was measured at 2.3 ns. This value is notably close to the two fluorescence lifetimes determined through time-correlated single photon counting (TCSPC).

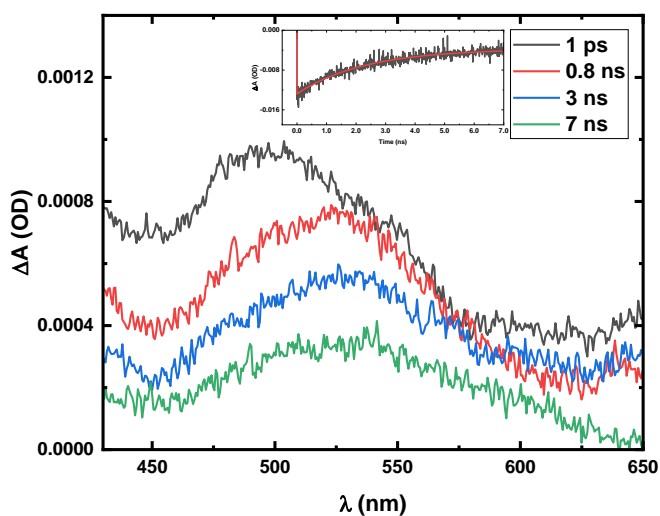


Figure 3.15 Time-resolved femtosecond transient absorption (fs-TA) of PolyNPy obtained with $\lambda_{\text{exc}} = 380$ nm in deaerated toluene at room temperature. Representative kinetic traces with fits from global analysis are presented as inset.

DiazaPy

The spectroscopic attributes of the final DiazaPy polymer were studied in different solvents, as depicted in **Figure 3.16**. Remarkably, the UV-Vis profile of this compound shows a remarkable similarity in all solvents in the spectral region below 500 nm. Intriguingly, in toluene, a distinctive characteristic emerges within the wavelength range of 600 nm to 800 nm, resulting in a band exhibiting vibronic resolution.

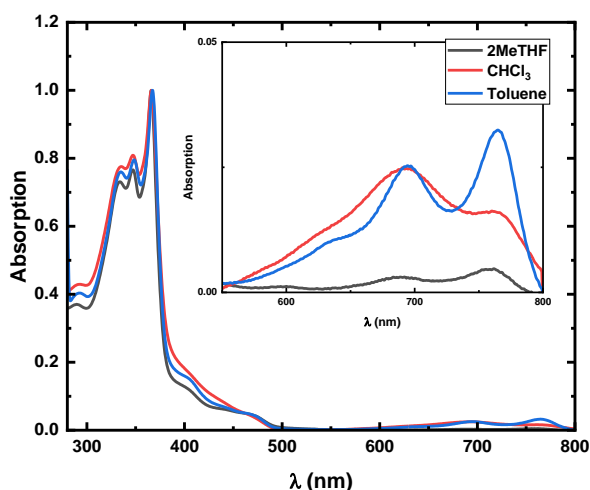


Figure 3.16 Normalized spectra of DiazaPy compound with a concentration of 35 ppm in different solvents.

When evaluating the same concentration of DiazaPy across different solvents, a noteworthy trend emerges. Specifically, this less energetic band becomes more pronounced in toluene. However, in chloroform, the profile of this band undergoes a complete transformation. This difference in behavior in different solvents underscores

the intricate interplay between DiazaPy spectral features and the solvent environment and highlights the role of solvent interactions in modulating the optical properties of the compound.

The fluorescence emission characteristics of the DiazaPy compound, as displayed in **Figure 3.17**, reveal a solvent-dependent emission pattern that alters its emission profile. The more intense emission band centered around 490 nm and bears a semblance to the emission band of MonPy, suggesting that this segment may constitute the primary fluorophore in the polymer. An even more intriguing behavior becomes apparent in toluene, where DiazaPy demonstrates a dual emission band, resulting in a novel, albeit less intense, emission peak around 780 nm. The excitation spectrum recorded in toluene for each emission band closely resembles the corresponding absorption spectrum.

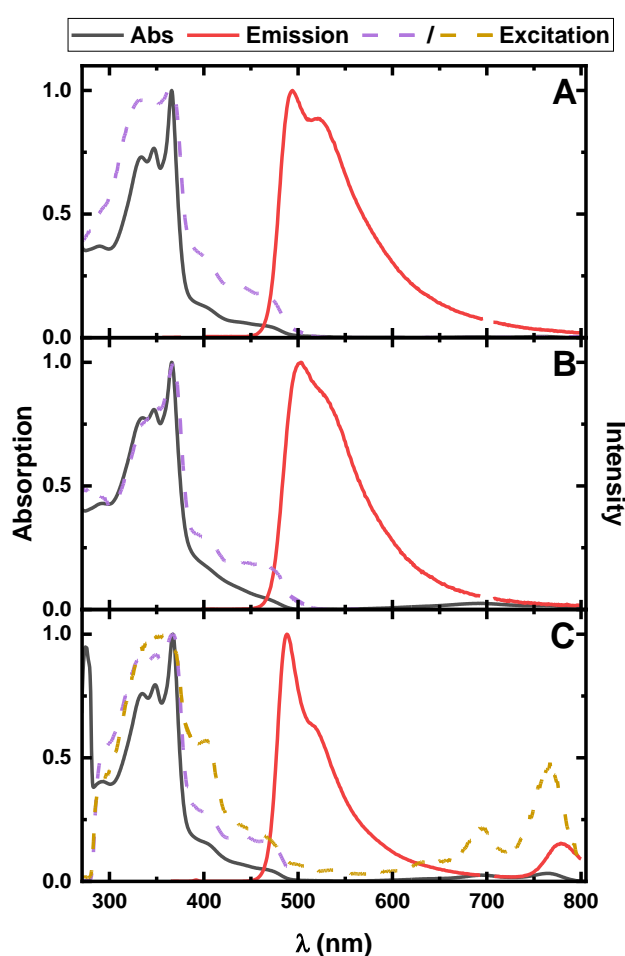


Figure 3.17 Normalized absorption, excitation and fluorescence emission of DiazaPy in (A) 2MeTHF, (B) CHCl_3 and (C) toluene. The fluorescence spectra were acquired using an excitation wavelength (λ_{exc}) of 350 nm, while the excitation spectra were obtained with an emission wavelength (λ_{em}) of (dashed purple) 510 nm and (dashed yellow) 780 nm.

To assess the possibility of aggregate formation in toluene, UV-Vis and fluorescence measurements were conducted, as shown in **Figure 3.18** and **Figure 3.19**, respectively. These analyses revealed a consistent pattern in both absorption and emission spectra, with the decrease in polymer concentration leading to a reduction in the intensity of the band. Notably, the shape of the bands remained unchanged. The less energetic band persisted even when the concentration of DiazaPy dropped below 0.5 ppm. Considering an estimated molecular weight (M_w) of 10,000 g/mol for DiazaPy, determined by analogy with PolyNPy, this concentration corresponds to approximately 10^{-8} M. This shows that this band cannot be associated with an aggregate and in contrast, is an inherent characteristic of the sample.

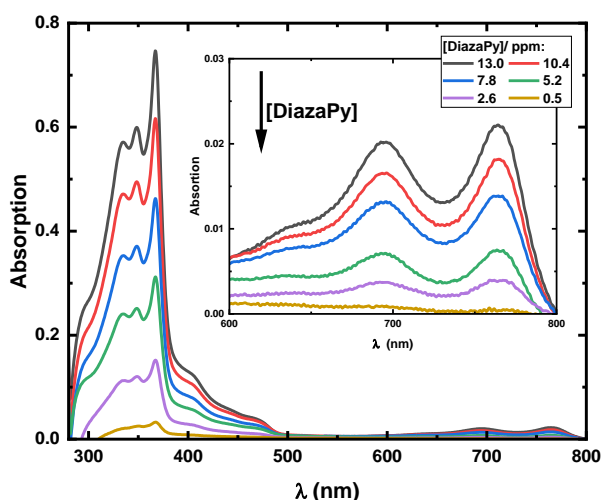


Figure 3.18 Absorption spectra of various concentrations of DiazaPy in toluene at 20 °C.

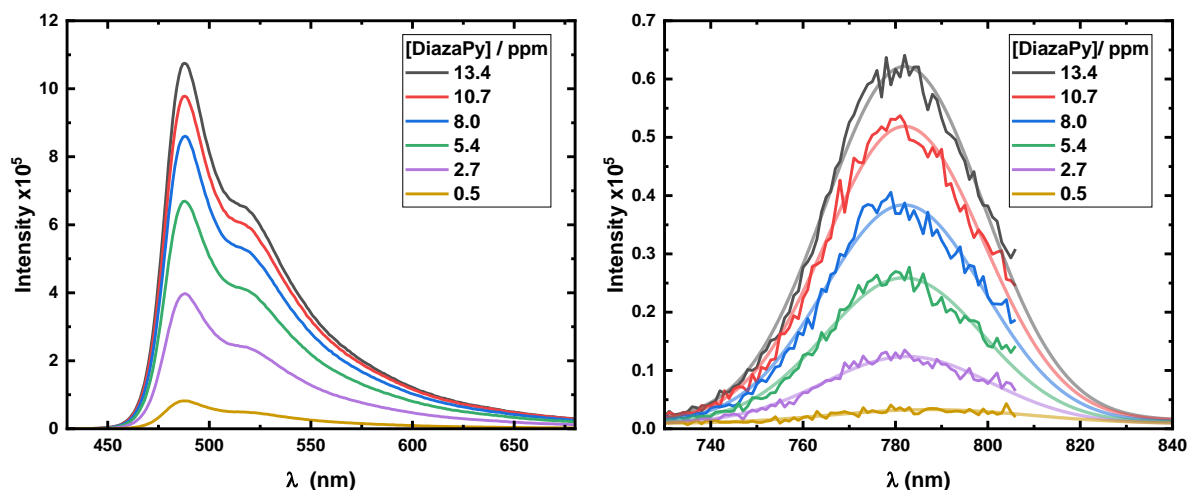


Figure 3.19 Emission spectra of different concentrations of DiazaPy in toluene at 20 °C using excitation wavelengths of (right) 350 nm and (left) 700 nm. A Gaussian fit was applied to the right spectrum to show the complete spectral profile since the correction factor is no longer valid for $\lambda > 810$ nm.

Employing a theoretical approach, the UV-Vis spectrum of a proposed DiazaPy monomer was predicted, as illustrated in **Figure 3.20**. Remarkably, this theoretical data exhibits a pronounced alignment with the experimental results. The computational analysis suggests that the HOMO→LUMO transition of this compound corresponds to the absorption band of lower energy in the experimental absorption spectra. This alignment indicates that this particular band is associated with the $S_0 \rightarrow S_1$ transition, confirming that is not related to any aggregate species.

The most pertinent transitions that closely correspond to the experimental data are summarized in **Table 5.5**. It is essential to emphasize that the more intense predicted transitions involve orbitals primarily localized within the pyrene moiety of the model molecule. This confirmation underscores the fact that the UV-Vis characteristics of DiazaPy are predominantly rooted in the pyrene moieties.

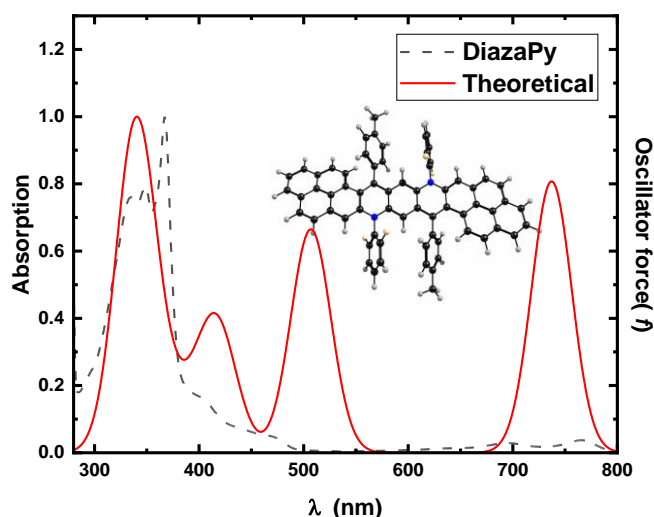


Figure 3.20 Absorption spectra predicted using TD-DFT with BPBE functional in toluene for DiazaPy, alongside inset of optimized structure. Dashed lines represent experimental absorption spectra for comparative analysis.

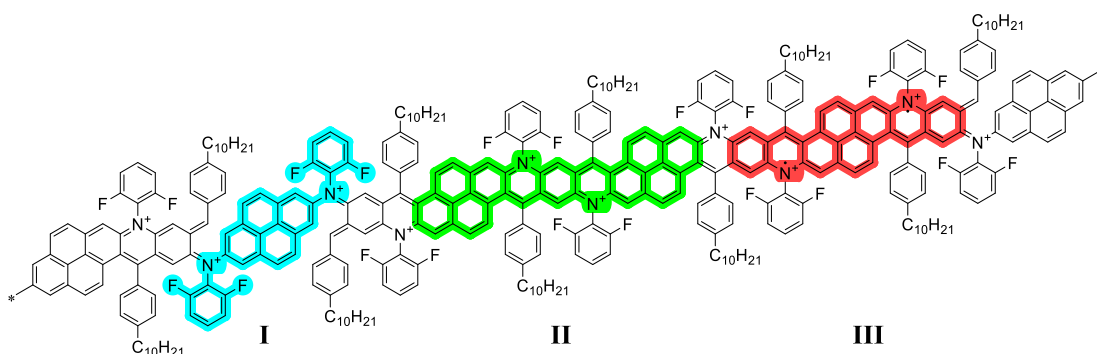
Analyzing results from steady-state, EPR, with theoretical predictions, and considering the challenges in achieving an ideal ladder polymer, it can be suggested that DiazaPy experiences bond cleavage in certain regions of its structure. This cleavage breaks the secondary bond needed for a perfect ladder polymer. The radical cationic nature of the polymer appears to promote this cleavage, potentially interacting with the solvent to introduce defects into its structure.

Interestingly, this cleavage exhibits solvent dependency, with toluene being the solvent where cleavage is less extensive. This fact is supported by the observation of emission around 780 nm, likely originating from the dicationic DiazaPy unit, which absorbs in the same region and was predicted by TD-DFT calculations.

Excitation spectra recovered from DiazaPy samples in toluene provide strong evidence for the existence of two different fluorophores within the compound. Despite some notable differences, both spectra follow a similar pattern in the $\lambda < 500$ nm region, which is an indication of being quite similar species. In addition, this solvent dependency can explain the slight changes observed in the absorption spectra in **Figure 3.16**.

We propose that the most probable cleavage occurs at the last C-C bond formed during the post-polymerization process, rather than cleaving the C-N bond. This preference allows for the formation of a pseudo-MonPy structure, highlighted in blue in **Scheme 3.4**. This structural hypothesis is supported by the resemblance of the more energetic emission band of the emission profile of MonPy, although with a slight bathochromic shift (ca. 40 nm) in its band maximum, which can be explained by the stabilization of the first excited state due an additional conjugation with the remaining polymeric structure (structures I, II and III in **Scheme 3.4**).

In the same Scheme, the dicationic structure of DiazaPy is highlighted in green, and since is expected to absorb at 780 nm, following Kasha's rule, it is also the probable emitting fluorophore in toluene in the same spectral region. Additionally, one of the probable radical cationic species in this compound is highlighted in red. It is important to note that these proposed structures are still suggestive. However, it is anticipated that further theoretical calculations, encompassing these diverse structures and others, could provide crucial insights into the DiazaPy structure and its electronic behavior.



Scheme 3.4 Illustration of possible structures in DiazaPy sample produced by defects in the polymer. These are highlighted to help in the discussion; see text for more details.

It is worth noting that for this sample, the determination of fluorescence quantum efficiency (φ_F) was pursued instead of fluorescence quantum yield. This distinction arises from the fact that since there is more than one chromophoric unit absorbing, and therefore emitting, the fluorescence efficiency is the result of more than one emission unit. In deaerated toluene at 20 °C, φ_F for this sample is determined to be 0.054 ± 0.005 , obtained from the integration of the 400 to 750 nm emission band.

TCSPC measurements were conducted on DiazaPy in deaerated toluene, with nanosecond (ns) and picosecond (ps) scales and performed at various excitation wavelengths as outlined in **Table 3.5**. The obtained results show

the presence of four distinct species in the excited state, corroborated by the identification of four discrete decay times. Notably, lifetimes around 1 ns and 6 ns consistently manifest across all measurements.

Specifically, when investigated at an emission wavelength (λ_{em}) of 510 nm, relative to the first emission band, the lifetime decay of approximately 6 ns assumes a more substantial role in the total fluorescence decay compared to the 1 ns decay lifetime. However, at λ_{em} of 780 nm (related to the second emission band), an inversion in the contribution is observed, with the 1 ns decay lifetime now exerting a greater influence on the total fluorescence decay. This empirical evidence sheds light on the fluorescence lifetime components of DiazaPy. The 6 ns decay lifetime aligns with the primary fluorescence lifetime of DiazaPy, while the 1 ns decay lifetime is attributed to a species of DiazaPy that emits at longer wavelengths.

The remaining two obtained decay lifetimes, approximately 15 ns and 200 ps pose more intricate challenges for identification. The former may be associated with locally excited species within the pyrene core, given its extended lifetime and relative proximity to the lifetime of MonPy. Conversely, the latter, spanning around 200 ps, could potentially originate from excited species emerging from the aryl side groups. However, further studies are required to corroborate and validate these findings conclusively.

DiazaPy was investigated using fs-TA with a λ_{exc} of 380 nm in deaerated toluene, mirroring the approach used for the other compounds. For DiazaPy, an ESA band spanning the 480 – 600 nm range was observed, attributed to the $S_1 \rightarrow S_n$ transition (**Figure 3.21**). A comprehensive analysis of the experimental traces within this spectral range necessitated a tetra-exponential fitting. One of these components was assigned an 'infinite' lifetime, essential for achieving optimal alignment with the experimental data.

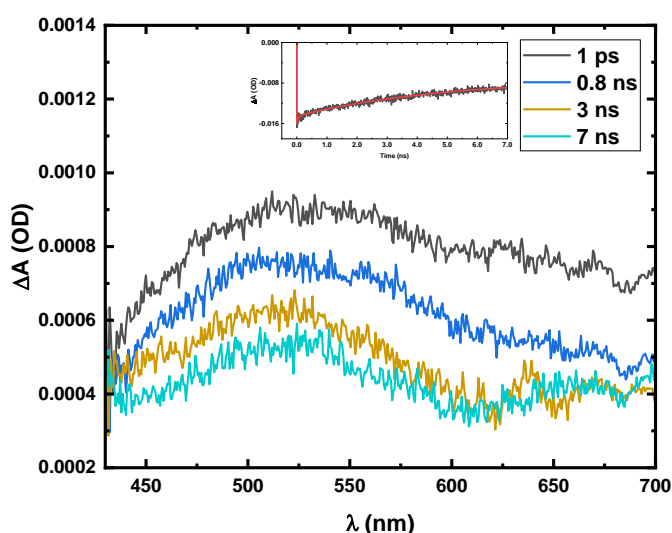


Figure 3.21 Time-resolved femtosecond transient absorption (fs-TA) of DiazaPy obtained with $\lambda_{exc} = 380$ nm in deaerated toluene at room temperature. Representative kinetic traces with fits from global analysis are presented as inset.

The other two obtained lifetimes were recorded at 131 ps and 2.1 ns. When compared with the fluorescence lifetime data provided in **Table 3.5** for DiazaPy, these values closely corresponded to the two shortest lifetimes found for this compound at 391 nm. It is plausible that the latter fs-TA lifetime is associated with the non-radiative deactivation of the excited state of the DiazaPy cation.

Table 3.4 Spectroscopic data (absorption, λ_{abs} , emission maxima, λ_{em} , and Stokes Shift, Δ_{SS} , and fluorescence quantum yields, φ_{F}) of the studied compound in different solvents at 20 °C.

Compound	Solvent	$\lambda_{\text{abs}} / \text{nm}$	$\lambda_{\text{em}} / \text{nm}$	$\Delta_{\text{ss}} / \text{cm}^{-1}$	φ_{F}
MonPy	2MeTHF	304/343/430	447	884	
	CHCl ₃	300/344/425	444	1007	
	Toluene	304/344/425	440	750	0.48 ± 0.02
PolyNPy	2MeTHF	315/347/440	572	5245	
	CHCl ₃	325/348/440	607	6253	
	Toluene	323/394/440	573	5306	0.190 ± 0.008
DiazaPy	2MeTHF	366/470/758	493	993	
	CHCl ₃	366/470/694	493	1396	
	Toluene	367/470/765 ^a	488/780 ^a	785/251 ^a	0.054 ± 0.005 ^b

^a Relate to the second emission band. ^b Quantum fluorescence efficiency since is not considered the second emission band.

Table 3.5 Emission lifetimes (τ_i) for studied compounds in deaerated toluene at 20 °C. Also presented are the associated pre-exponential factors (a_i) and the chi-square values (χ^2) for the judgment of the quality of the fit.

Compound	λ_{exc}	λ_{em}	τ_0 / ns	a_0^*	τ_1 / ns	a_1^*	τ_3 / ns	a_3^*	τ_4 / ns	a_4^*	χ^2
MonPy	339	450							20.6	1 (100)	1.05
PolyNPy	339	570					3.8	0.44 (29)	7.3	0.56 (71)	1.01
	391	570					1.2	0.15 (4)	5.7	0.85 (96)	0.95
DiazaPy	339	510			1.0	0.41 (6)	5.0	0.31 (24)	15.9	0.28 (70)	1.00
	391	510	0.12	0.51 (3)	1.4	0.22 (13)	7.2	0.27 (84)			1.00
	451	780	0.28	0.12 (3)	1.1	0.84 (83)	4.2	0.04 (14)			1.06

*Percentual fluorescence contribution (%C) of each amplitude is shown between parentheses.

3.2.4 Temperature dependence studies of PolyNPy and DiazaPy polymers

The spectral characteristics of a compound can be influenced by temperature, as non-radiative processes often exhibit temperature dependence. This phenomenon arises from the fact that elevated temperatures introduce greater thermal energy and molecular vibrations, which can perturb the excited state of fluorescent molecules and subsequently lead to non-radiative decay routes. Consequently, fluorescence emission can be reduced. To comprehensively analyze the impact of temperature on fluorescence emission intensity, an Arrhenius-type plot was constructed, following the principles outlined in **Equation 3.1**. This plot provides insights into the temperature-dependent behavior of fluorescence intensity, where I_F^0 represents the highest fluorescence intensity typically attained at the lowest temperature, and E_a denotes the energy of activation. This methodology is particularly useful in elucidating the underlying mechanisms of temperature-related effects on fluorescence behavior.^{4,5}

$$\ln\left(\frac{I_F^0}{I_F} - 1\right) = \ln A - \frac{E_a}{R} \cdot \frac{1}{T} \quad 3.1$$

For PolyNPy, the emission spectra were recorded at various temperatures, and the results are displayed in **Figure 3.22**. These observations are further detailed in **Figure 3.23**, which reveals that the emission maxima experiences a hypochromic shift as the temperature increases. Additionally, the fluorescence emission intensity demonstrates a decline up to 70°C, followed by an unexpected increase in intensity within the temperature range of 70-90°C.

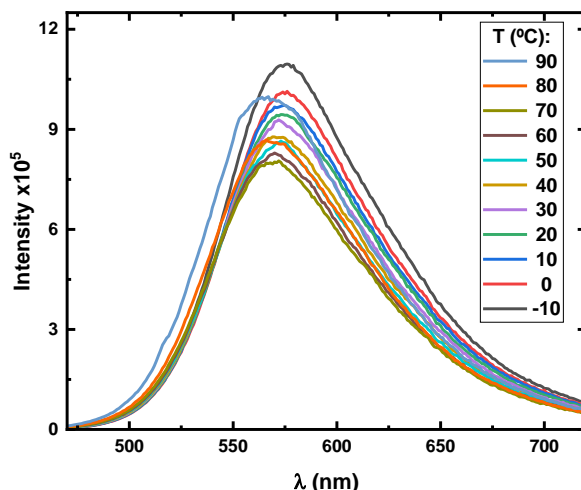


Figure 3.22 Emission spectra of PolyNPy at different temperatures with $\lambda_{exc} = 390$ nm.

In organic donor-acceptor (D-A) molecules, the presence of locally excited (LE) and twisted intramolecular charge-transfer (TICT) states is greatly influenced by solvent polarity and viscosity. Notably, certain TICT-

activated fluorophores exhibit a distinctive response to temperature, wherein additional vibrational modes become activated, leading to a blue-shift in the emission peak and subsequent modifications in their emission characteristics.⁶⁻⁸

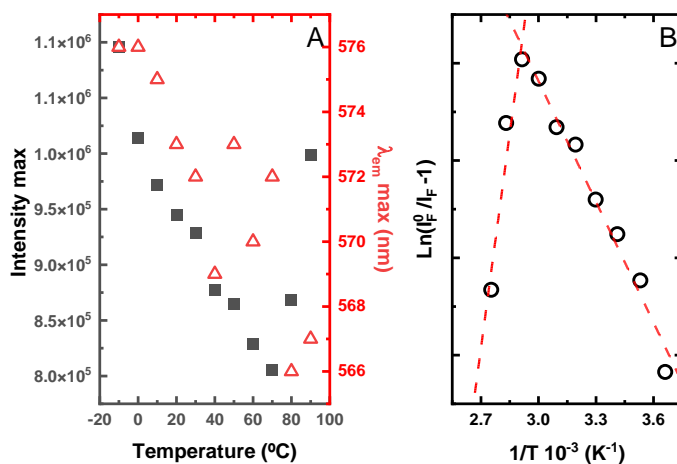


Figure 3.23 (Left) Depiction of maximum emission intensity and corresponding emission wavelength as functions of temperature for PolyNPy in toluene with excitation wavelength (λ_{exc}) of 390 nm. **(Right)** Arrhenius plot illustrating experimental data for PolyNPy tracked at emission wavelength (λ_{em}) of 573 nm.

PolyNPy, characterized by its D-A polymer nature, can be conceptualized as a system where charge transfer (CT) can take place from the diketone core to the pyrene core, a concept that can be deduced from the characteristics of the HOMO-LUMO orbitals illustrated in **Table 5.5**. Additionally, there is evidence suggesting that the 2,7-disubstituted pyrene can function as a compound with a CT state.⁹

The intriguing findings shown in **Figure 3.23** point to a scenario where upon excitation at varying temperatures, distinct behaviors manifest, marked by two regimes, and where the polymeric structure of PolyNPy undergoes conformational reorganization. The first regime, in accordance with standard behavior, displays a decrease in emission intensity as the temperature rises, attributed to the increase in the contribution of the non-radiative deactivation. In contrast, the second regime, which emerges beyond 70°C, presents a significant departure from conventional behavior. This regime introduces the activation of a TICT-active fluorophore with temperature, resulting in an amplified fluorescence intensity as the temperature increases.

It is important to emphasize that while these observations provide valuable insights, further experiments conducted in various solvent environments are imperative to validate and confirm this unconventional behavior. Such investigations would contribute to a more comprehensive understanding of the intricate interplay between PolyNPy's structural attributes, solvent dynamics, and the effects induced by temperature.

Figure 3.24 presents the emission spectra of DiazaPy at varying temperatures. Given its dual emission nature, both emission bands were monitored to track their behavior with changing temperatures. As shown in **Figure**

3.25, a consistent trend emerges where the fluorescence intensity fades as temperature rises for both emission bands. Furthermore, in the first emission band, the wavelength of maximum emission remains relatively stable despite temperature changes. However, in the second and less emissive band, the maximum emission peak experiences a blue shift of approximately 10 nm.

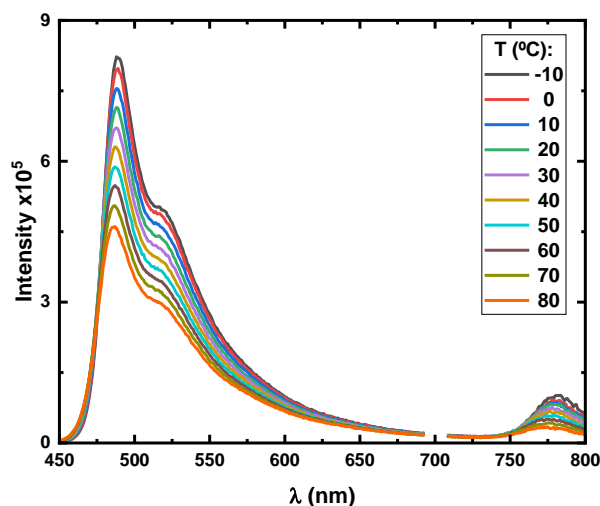


Figure 3.24 Emission spectra of DiazaPy at different temperatures with $\lambda_{exc} = 350$ nm.

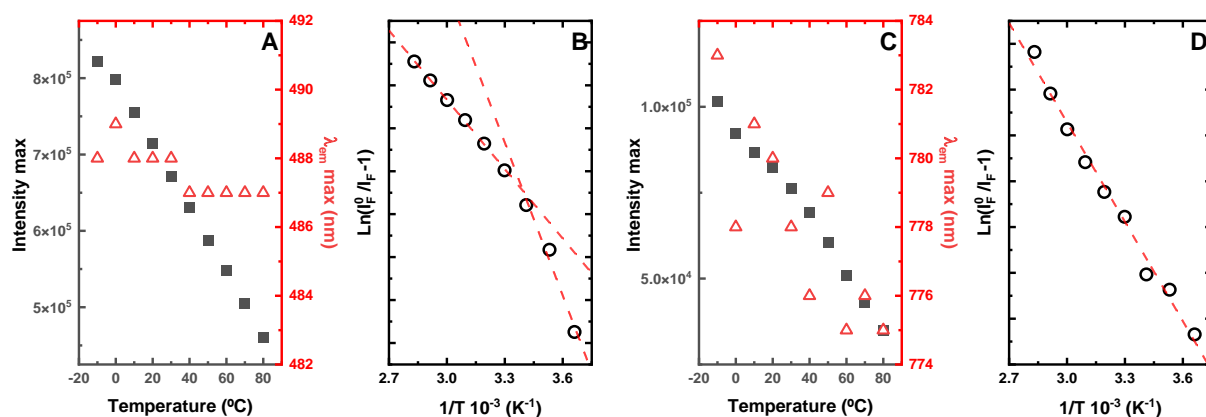


Figure 3.25 (A) Depiction of maximum emission intensity in the first emission band of DiazaPy and corresponding emission wavelength as functions of temperature in toluene with excitation wavelength (λ_{exc}) of 350 nm. (B) Arrhenius plot illustrating experimental data of first emission band for DiazaPy tracked at emission wavelength (λ_{em}) of 488 nm. (C) Depiction of maximum emission intensity in the second emission band of DiazaPy and corresponding emission wavelength as functions of temperature in toluene with excitation wavelength (λ_{exc}) of 350 nm. (D) Arrhenius plot illustrating experimental data of second emission band for DiazaPy tracked at emission wavelength (λ_{em}) of 780 nm.

The respective Arrhenius plots for each emission band highlight distinctive behaviors. In the case of the first band, a bending tendency in the Arrhenius plot indicates the presence of two distinct regimes. Conversely, the Arrhenius behavior for the second band remains linear. **Table 3.6** provides a summary of the key parameters

extracted from the Arrhenius linear fit, which was applied to the experimental data for both studied polymers. This comprehensive analysis sheds light on the intricate temperature-dependent fluorescence characteristics of DiazaPy and offers insights into the underlying factors driving its behavior.

Table 3.6 Summary of key information extracted from Arrhenius-type plots for various compounds in temperature-dependent experiments.

Compound	λ_{em} /nm	Solvent	Crossing point/ °C	E_a / kJ·mol ⁻¹
PolyNPy	573	Toluene	70	17 (0 – 60 °C)
				-61 (70 – 90 °C)
DiazaPy	488	Toluene	21	22 (0 - 50 °C)
				49 (60 – 80 °C)
	780	Toluene		30 (0 – 80 °C)

Conclusion

Three new compounds containing pyrene were successfully synthesized and characterized through various spectroscopic techniques. Initially, a 2,7-diamino pyrene monomer (MonPy) was achieved using the Buchwald-Hartwig catalyzed cross-coupling amination method. This process yielded a respectable 60 % yield. MonPy exhibited a relatively low Stokes shift (below 1000 cm⁻¹) in different solvents, along with a monoexponentially fluorescence lifetime of 20.6 ns in deaerated toluene.

Furthermore, an alternating copolymer, denoted as PolyNPy, was also synthesized via the same cross-coupling amination approach, utilizing the previously synthesized MonPy and a specific diketone compound. PolyNPy displayed a molecular weight (M_w) of 11,800 g/mol, determined post-extraction with chloroform and purification from the raw product. Notably, this polymer demonstrated a substantial Stokes shift in different solvents, accompanied by a ϕ_F of 0.190 ± 0.008 . Time-resolved techniques unveiled its association with two distinct fluorescent species in the excited state, characterized by relatively close lifetimes. Intriguingly, PolyNPy exhibited non-conventional thermally twisted intermolecular charge transfer active (TICT-active) properties, resulting in enhanced emission in toluene at temperatures exceeding 70 °C.

To achieve the desired ladder-type diazaacenes family polymer known as DiazaPy, a post-polymerization step via acid-mediated cyclization was applied to PolyNPy. The resultant polymer, DiazaPy, exhibited a ϕ_F' value of 0.054 ± 0.005 when dissolved in toluene. Surprisingly, EPR measurements unveiled a sharp signal, indicating a radical cationic nature, contrary to the expected cationic state. Steady-state experiments unveiled an unusual

dual emission phenomenon, observed in toluene. It was suggested that this observation in DiazaPy is the result of different fluorophores, stemming from defects present in its structure.

The dual emission behavior can be attributed to toluene's superior solvent capabilities in stabilizing the cationic structure of the polymer. DFT and TD-DFT calculations suggest that the less energetic emission band is probably produced by a ladder structure of DiazaPy and the more energetic emission band from a potential pseudo-MonPy structure derived from the heterolytic cleavage of the preceding C-C bond formed during the post-polymerization reaction. Nonetheless, further theoretical investigations will be conducted to gain a more comprehensive understanding of the possible fluorophore structures within DiazaPy.

Characterization of the compound using time-resolved techniques necessitated the use of at least four exponential components to accurately fit the experimental decay. These components varied with the excitation wavelength, underscoring the complexity of the polymeric structure. This complexity arises from the potential presence of structural defects, which give rise to new fluorophores.

For all three compounds, ultrafast time-resolved techniques, particularly fs-Transient Absorption (fs-TA), were employed, revealing positive signals indicative of excited state absorption (ESA) beyond ground state absorption. Global analysis of the traces for all compounds necessitated the inclusion of an 'infinite' lifetime to achieve accurate fitting of the experimental data. This extended lifetime signifies processes with durations surpassing 7 ns, the technique's experimental limit. Further investigations incorporating ns-TA setups are planned to comprehensively unravel the nature of these long-lived species.

Bibliography

1. Wetterling, D.; Forster, M.; AC, B. R.; Seixas de Melo, J. S.; Scherf, U., Cationic Diazapentacenium Polymers Made in a Sequence of C-N Cross Coupling Polymerization and Acid-Mediated Postpolymerization Cyclization. *Macromol Rapid Commun* **2021**, *42* (19), e2100370.
2. Xie, G.; Bojanowski, N. M.; Brosius, V.; Wiesner, T.; Rominger, F.; Freudenberg, J.; Bunz, U. H. F., Stable N,N'-Diarylated Dihydrodiazacene Radical Cations. *Chemistry* **2021**, *27* (6), 1976-1980.
3. Rodrigues, A. C. B.; Eckert, A.; Pina, J.; Scherf, U.; Seixas de Melo, J. S., Polymeric near infrared emitters with bay-annulated indigo moieties. *Materials Advances* **2021**, *2* (11), 3736-3743.
4. Cunha, C.; Klein, P.; Rosenauer, C.; Scherf, U.; Seixas de Melo, J. S., Fluorescence Studies on a Thermoresponsive PNIPAM-Polyfluorene Graft Copolymer. *Macromolecules* **2021**, *54* (16), 7612-7620.
5. Kirby, E. P.; Steiner, R. F., Influence of solvent and temperature upon the fluorescence of indole derivatives. *The Journal of Physical Chemistry* **2002**, *74* (26), 4480-4490.
6. Chandrasekharan, N.; Kelly, L. A., A dual fluorescence temperature sensor based on perylene/excimer interconversion. *J Am Chem Soc* **2001**, *123* (40), 9898-9.
7. Cao, C.; Liu, X.; Qiao, Q.; Zhao, M.; Yin, W.; Mao, D.; Zhang, H.; Xu, Z., A twisted-intramolecular-charge-transfer (TICT) based ratiometric fluorescent thermometer with a mega-Stokes shift and a positive temperature coefficient. *Chem Commun (Camb)* **2014**, *50* (99), 15811-4.
8. Kundu, A.; Karthikeyan, S.; Sagara, Y.; Moon, D.; Anthony, S. P., Temperature-Controlled Locally Excited and Twisted Intramolecular Charge-Transfer State-Dependent Fluorescence Switching in Triphenylamine-Benzothiazole Derivatives. *ACS Omega* **2019**, *4* (3), 5147-5154.
9. Ji, L.; Lorbach, A.; Edkins, R. M.; Marder, T. B., Synthesis and photophysics of a 2,7-disubstituted donor-acceptor pyrene derivative: an example of the application of sequential Ir-catalyzed C-H borylation and substitution chemistry. *J Org Chem* **2015**, *80* (11), 5658-65.

Chapter 4:

Experimental Techniques

Summary

The upcoming chapter will delve into the discussion of the instrumental setups and the defined parameters essential for conducting all measurements and experiments outlined in **Chapter 2: Chitosan Polymer Randomly Labeled with Pyrene**, and **Chapter 3: Diazacationic Ladder-type Polymers with Pyrene**.

Instrumentation and techniques

4.1.1 Nuclear Magnetic Resonance

Nuclear Magnetic Resonance (NMR) spectroscopy is a technique rooted in the transitions occurring between distinct energy levels associated with permissible orientations of nuclear spins when exposed to an external magnetic field. Due to the relatively modest energy differential, NMR instruments must possess the capability to generate an intense and uniform magnetic field across the specimen. The salient advantage of this technique stems from the fact that the resonance signals of nuclei do not manifest as solitary occurrences, but rather manifest as an array of signals. These signals, collectively, offer insights into the local environments of the nuclei under observation. Consequently, they facilitate the extraction of spectra, which, in turn, can yield invaluable information regarding the molecular structure in the presence of observed nuclei endowed with angular momentum.¹

Experimental conditions: NMR measurements were executed using a Bruker Avance III spectrometer, which was equipped with a 5mm BBFO probehead featuring automatic frequency tuning (ATM). The operational frequency was tailored to the specific nuclei under examination: 400.13 MHz for ¹H and 100.61 MHz for ¹³C, with tetramethyl silane (TMS) serving as the reference compound unless otherwise specified. For ¹⁹F, the measurement frequency was set at 376.50 MHz, with CFC₃ as the reference material. Subsequent data analysis was carried out using the MNova software. The distinct conditions for each sample are outlined below.

In the investigation detailed in **Chapter 2** concerning ChiNPy Polymers, all samples were dissolved in a solution containing 1% v/v of DCl in D₂O. Additionally, 3-(Trimethylsilyl)propionic-2,2,3,3 acid sodium salt (TSP-d₄) was introduced as an internal reference ($\delta = 0.00$ ppm). This process was conducted at a temperature of 50 °C, and data acquisition comprised a total of 256 scans.

Moving on to **Chapter 3**, the following conditions were employed: MonPy was dissolved in CDCl₃ and subjected to a series of NMR analyses, including ¹H NMR (16 scans), ¹³C NMR (1024 scans), and ¹⁹F NMR (32

scans). Furthermore, 2D analyses were carried out mirroring the ^1H conditions, and these analyses were conducted at a temperature of 18 °C. For PolyNPy and DiazaPy, both polymers were dissolved in deuterated tetrachloroethane ($\text{C}_2\text{H}_2\text{Cl}_4$, $\delta = 6.00$ ppm) at a concentration of no less than 40 mg/mL. Consequently, these samples underwent ^1H NMR (256 scans) and ^{13}C NMR (16384 scans) analyses, with both analyses being conducted at a temperature of 18 °C as well.

4.1.2 Liquid Chromatography - Mass Spectrometry

Liquid chromatography (LC) serves as a technique utilized for the separation, identification, and quantification of components that share close associations within mixtures. Across diverse chromatographic methodologies, the sample is dissolved within a mobile phase and subsequently impelled through an immiscible stationary phase. During this process, the constituents present in the mobile phase engage in interactions with the stationary phase, causing them to be retained due to their affinity for the latter. This differential interaction prompts a temporary halt in their progression. Consequently, this strategic pause facilitates the selective isolation of individual compounds from the mixture.²

The mass spectrometer operates through the conversion of the analyte into an ionized state, followed by the subsequent analysis of these ions as well as any fragment ions generated during the ionization process. This analysis is predicated on the mass-to-charge ratio (m/z) of the ions. The ionization of the sample can be achieved using diverse methods; one such method is Atmospheric Pressure Chemical Ionization (APCI). In the case of APCI, a liquid sample is pumped through a capillary and nebulized at its tip. This nebulization leads to a discharge involving gas and solvent molecules within the ion source, resulting in their ionization. These ions then engage with the analyte, inducing ionization via charge transfer.³

The integration of liquid chromatography (LC) and mass spectrometry (MS) constitutes a powerful tandem approach. LC facilitates the isolation of compounds from a complex mixture, while MS enables their subsequent analysis based on mass-to-charge ratios (m/z). This symbiotic coupling ensures that the presence of a targeted analyte within a sample can be both effectively isolated and accurately confirmed. The utilization of these two techniques in tandem offers an ultimate strategy for comprehensive analysis and identification of specific compounds within complex samples.

Experimental conditions: The precise mass of MonPy was ascertained using a tandem liquid chromatography-mass spectrometer (LC-MS), specifically the Bruker MicrOTOF model. This analysis was conducted in the positive ion polarity mode, with an Atmospheric Pressure Chemical Ionization (APCI) Source facilitating flow injection. The LC-MS system was procured from Bergische Universität Wuppertal.

The experimental setup entailed a nebulizer pressure of 3.0 Bar, a dry heater maintained at 200 °C, and a dry gas flow rate set at 5.0 l/min. The collected data underwent analysis via the Bruker Compass DataAnalysis 4.2 software.

4.1.3 Fourier Transform Infrared and Raman Spectroscopy

Fourier Transform Infrared spectroscopy (FTIR) stands as an invaluable analytical technique, providing essential insights into molecular vibrations. Infrared spectra serve as a common tool for discerning functional groups present in a sample, allowing for the correlation of peak signals with underlying molecular structures. The foundational principle underpinning FTIR resides in the absorption of infrared (IR) radiation by molecules. Specifically, molecules could absorb IR radiation at precise frequencies aligned with their unique vibrational modes. These vibrational modes encompass stretching and bending motions intrinsic to chemical bonds within the molecule's composition. Upon the absorption of IR radiation, the molecule's vibrational energy levels undergo alteration, thereby generating an absorption spectrum.

The amalgamation of FTIR with an attenuated total reflectance (ATR) module introduces a specialized dimension to the technique. This integration enables the measurement of infrared absorption across a sample through multiple internal reflections at the sample-crystal interface. ATR, therefore, allows for the direct examination of solid, liquid, gel, and even powdered samples without requiring extensive preparatory procedures. This innovation significantly expedites the analytical process, enhancing the applicability of FTIR for various material types.

In IR spectroscopy, the resonance-driven interaction involves the coherent coupling of electromagnetic radiation with the vibrational modes of the molecule. This coupling arises primarily due to the electric dipole moments associated with molecular vibrations. As a result, the incident radiation induces transitions between vibrational energy levels, enabling the extraction of information regarding molecular structures and functional groups.⁴

The fundamental principle behind Raman spectroscopy is the inelastic scattering of light. When a sample is exposed to a monochromatic light source (typically laser light), some of the incident photons are scattered with an energy shift due to interactions with molecular vibrations. This energy shift corresponds to the vibrational modes of the sample molecules. The difference in energy between the incident and scattered photons produces the Raman spectrum, a plot of intensity versus the energy shift (Raman shift) from the incident light.

Conversely, the Raman technique capitalizes on an off-resonance dynamic, where incident light interacts with the molecule's vibrational modes without invoking resonance. This interaction leads to a small portion of the scattered light experiencing energy shifts, known as Raman scattering. The Raman scattering phenomenon,

driven by the Raman polarizability of the molecule, provides insights into molecular vibrations and offers complementary information to that obtained through IR spectroscopy.

In essence, both IR and Raman techniques serve as pivotal tools for investigating molecular vibrations, yet they differentiate themselves through the nature of energy exchange mechanisms and the specific molecular aspects they unveil. ⁵

Experimental conditions: Infrared spectra of solid samples were acquired using a Thermo Scientific Nicolet IS5 Fourier-Transform Infrared Spectrometer (FTIR), which was coupled with an ATR module model iD7. The measurements were conducted with 128 scans, and a spectral resolution of 1 cm⁻¹ was employed, accompanied by background subtraction.

Raman spectra were obtained using the Raman Horiba LabRam HR Evolution system. The excitation wavelength utilized was $\lambda = 785$ nm, which was generated by a solid-state laser capable of delivering power within the range of 5-20 mW. The laser beam, featuring a spot diameter of approximately 1 μm , was precisely focused onto the sample through the utilization of a 50 \times long-working-distance objective and a 100 \times objective.

To generate the ultimate spectra, a total of 100 to 250 accumulations of individual spectra were collected during time intervals ranging from 10 to 100 seconds. These accumulations were performed with a spectral resolution of 0.5 cm⁻¹. Notably, the system underwent calibration using the silicon crystal Raman peak located at 520.5 cm⁻¹, which served as a reference point.

4.1.4 Electron Paramagnetic Resonance

Electron paramagnetic resonance (EPR) spectroscopy pertains to the investigation of magnetic dipole transitions induced by microwave irradiation of a paramagnetic system situated within a static magnetic field. When a paramagnetic sample containing unpaired electrons is subjected to an external magnetic field, the electrons can absorb energy from electromagnetic radiation and transition between different energy levels. This absorption of energy corresponds to the resonance condition, where the energy difference between two electron spin states matches the energy of the applied radiation. The energy associated with the spin's alignment relative to the magnetic field is influenced by the Zeeman effect, which describes how the magnetic field affects the energy levels of the electron. An electron with a parallel alignment to the field has lower energy than one with an antiparallel alignment. The resonance condition is satisfied when the Zeeman effect, caused by the external magnetic field, matches the energy gap between spin states, **Equation 4.1**.

$$\Delta E = g \cdot \mu_B \cdot B_0 \cdot \Delta m_s \quad 4.1$$

Here, μ_B represents the Bohr magneton, B_0 is the strength of the applied magnetic field, and Δm_s is the change in the spin projection quantum number, which is either +1 or -1 for allowed transitions. The factor of proportionality, referred to as the gyromagnetic ratio, deviates from the classically predicted value due to the g-factor. For a free electron, this value is known with remarkable precision ($g_e = 2.0023193043608252$). In the context of systems under scrutiny, where electrons are bound to the system, the g-factor deviates from g_e . However, for organic radicals, this deviation is minor, generally less than 0.5%. Notably, the g-factor serves as a distinctive characteristic, akin to a material's fingerprint.

When the resonance condition is met, the unpaired electrons absorb energy and transition from the lower energy state to the higher energy state. This absorption of energy is detected as a decrease in microwave power passing through the sample. The intensity of the absorbed microwave radiation is recorded and plotted against the strength of the magnetic field. This generates an EPR spectrum, which is a plot of absorption intensity (or sometimes derivative of intensity) against magnetic field strength.⁶

Experimental conditions: The inquiry into the presence of a radical in DiazaPy encompassed studies performed in both CHCl_3 and toluene solvents. These investigations employed the Bruker X-band EMX EPR spectrometer, which operated at a microwave frequency of 9.77 GHz. The power input was set at 3.98 mW, accompanied by a modulation amplitude of 16.00 G. Data accumulation involved the collection of 32 scans, all conducted at room temperature and the experimental data were subjected to fitting using the MATLAB® toolbox EasySpin.⁷

4.1.5 UV-visible spectrophotometry and Steady-State Fluorescence measurements

As elaborated extensively in **Section 1.1**, a molecule can undergo promotion from its ground electronic state to an electronically excited state through the absorption of a photon. The process of absorbing a monochromatic beam of light by a substance dissolved in a transparent medium is expounded by the Beer-Lambert law, as defined by **Equation 4.2**.

$$A = \log\left(\frac{I_0}{I}\right) = \epsilon lc \quad 4.2$$

Where I and I_0 represent the intensity of transmitted and incident light, respectively, ϵ denotes the molar absorption coefficient (in $\text{M}^{-1}\cdot\text{cm}^{-1}$), l signifies the optical path, and c represents the molar concentration of the solution.

A spectrophotometer operates by dispersing light into its constituent wavelengths using either a prism or a grating monochromator. It utilizes a deuterium lamp for the UV region and a tungsten lamp for the visible region, enabling continuous variation of measurements across the entire spectrum. Two common configurations exist: the single-beam and double-beam instruments. The former operates based on the substitution principle, where the reference and sample are placed consecutively. In the latter setup, the incident beam is divided and directed along two paths that intersect the reference and sample simultaneously.⁸

The emission of a photon from the electronically excited state to the ground state can be categorized into two types: fluorescence and phosphorescence, contingent on the nature of the excited state. Fluorescence emanates from singlet excited states, whereas phosphorescence results from photon emission from the triplet excited state. The energy emitted is typically lower than the absorbed energy, a distinction termed the Stokes Shift, often quantified in cm^{-1} and represented by **Equation 4.3**, where the maximum of emission and absorption ($\lambda_{\text{max}}^{\text{em}}$ and $\lambda_{\text{max}}^{\text{abs}}$) are given in cm .

$$\Delta_{ss} (\text{cm}^{-1}) = \frac{1}{\lambda_{\text{max}}^{\text{abs}}} - \frac{1}{\lambda_{\text{max}}^{\text{em}}} \quad 4.3$$

A standard spectrofluorometer is capable of recording both excitation and emission spectra. To provide a concise explanation, an emission spectrum entails the distribution of wavelengths measured at a constant excitation wavelength. Conversely, an excitation spectrum refers to the variation in emission intensity, measured at a fixed emission wavelength, as a range of excitation wavelengths is scanned.⁹

The fluorescence quantum yield (ϕ_F) is defined as the ratio between the number of emitted fluorescence quanta and the number of absorbed quanta for a given singlet excited state. This parameter experimentally can be determined by comparing the sample with a reference compound whose quantum yield is already established (ϕ_F^{ref}). The reference compound is typically chosen to absorb within the same spectral region as the sample, or as closely as possible. In practical terms, the absorption of both the sample and the reference should be sufficiently low to prevent inner filter effects. The fluorescence quantum yield (ϕ_F) can be determined using **Equation 4.4**.¹⁰

$$\phi_F^{\text{sample}} = \frac{\int I(\lambda)^{\text{sample}} d\lambda}{\int I(\lambda)^{\text{ref}} d\lambda} \cdot \frac{DO_{\text{ref}}}{DO_{\text{sample}}} \cdot \frac{n_{\text{sample}}^2}{n_{\text{ref}}^2} \cdot \frac{f_{O_2}^{\text{sample}}}{f_{O_2}^{\text{ref}}} \cdot \phi_F^{\text{ref}} \quad 4.4$$

Here, DO represents the optical density of the sample, n stands for the refractive index of the solvent, and f_{O_2} is a correction parameter accounting for the measurement of dissolved oxygen content in both the sample and reference compounds.

Experimental conditions: Absorption spectra for all investigated compounds were captured using a double-beam Shimadzu UV-2600 UV-Vis spectrophotometer. Hellma quartz cuvettes, featuring optical path lengths of either 0.5 or 1 cm, were employed for the measurements. All spectra were recorded at room temperature unless explicitly stated otherwise. A slit width of 2 nm was used, covering the wavelength range from 200 to 800 nm.

Emission and excitation spectra were acquired using a spectrofluorometer, specifically the Jobin Yvon-Spex-Fluorolog 3-2.2, with corrections applied for the instrumental response. This instrument was integrated with a Quantum model thermal bath, maintaining a precise temperature of $20\text{ }^{\circ}\text{C} \pm 0.2\text{ }^{\circ}\text{C}$. All measurements were conducted in Hellma quartz cuvettes with a 1 cm optical path length, utilizing a $90\text{ }^{\circ}\text{C}$ acquisition geometry. A time integration of 0.5 s and slits set at 2 nm were employed.

The fluorescence quantum yield was determined following the procedure outlined below. However, it is important to note that the f_{O_2} parameter was assumed to be 1, given that all measurements were conducted under deoxygenated conditions. For each measurement, a series of triplicate experiments were conducted to obtain a quantification of the associated error for this parameter.

For data interpretation, the OriginPro 2021b software was employed.

4.1.6 Time-Correlated Single Photon Counting Techniques

Time-Correlated Single Photon Counting (TCSPC) is founded on the principle of detecting individual photons within a periodic light signal. This technique capitalizes on the inherent characteristic of low-intensity, high-repetition-rate signals, where the likelihood of detecting multiple photons within a single signal period is negligible. The temporal gap between the excitation pulse and the detection of a photon is quantified and recorded in a histogram. Over an accumulation period, this histogram captures the temporal profile of the decay process.

Time-resolved fluorescence data exhibit a degree of complexity that generally precludes graphical analysis. In response, numerous analytical methods have been introduced to dissect the intensity decay. Among these, the multi-exponential decay model stands out, postulating that decay is the summation of individual single exponential decays, as exemplified in **Equation 4.5**.^{9,11}

$$I(t) = \sum_{i=1}^n \alpha_i \exp(-t / \tau_i) \quad 4.5$$

Here, τ_i corresponds to the decay times, a_i denotes the amplitudes of the components at $\tau = 0$, and n signifies the number of decay times. This model proves valuable in examining mixtures of fluorophore species, with each species associated with a distinct decay time τ_i .

In certain cases, such as in macromolecular systems, polymers, and biomolecules, intensity decays often manifest as multi-exponential or non-exponential. While these can be fitted with the multi-exponential model, comprehending the results through the examination of decay times and amplitudes can be challenging. Consequently, the analysis of decays in terms of lifetime distributions becomes beneficial.

The application of the maximum entropy method (MEM) allows the recovery of lifetime distributions without imposing assumptions about the shape of the components. Although mathematically intricate, MEM is rooted in the maximization of a function called the Skilling-Jaynes entropy function, illustrated in **Equation 4.6**.

$$S = \int_0^{\infty} \alpha(\tau) - m(\tau) - \alpha(\tau) \log \frac{\alpha(\tau)}{m(\tau)} d\tau \quad 4.6$$

In this context, $a(t)$ represents the recovered distribution, while $m(t)$ stands for an assumed starting model that maintains a flat distribution in log space. The fitting process is conducted concurrently with the χ^2 parameter to ensure the consistency of the fit with the data.⁹

Experimental Conditions: Fluorescence decay times (τ_F) were measured using two distinct types of equipment. First, a custom-built nanosecond time-correlated single-photon counting (ns-TCSPC) setup and a picosecond time-correlated single-photon counting (ps-TCSPC) instrument, as described elsewhere, both equipped with 1024 channels.^{10, 12-14} All measurements were conducted at room temperature. The instrumental response was calibrated using a diluted scattering solution, commonly colloidal silica (Ludox).

Polymers from **Chapter 2: Chitosan Polymer Randomly Labeled with Pyrene**, were dissolved in Acetic Acid (HAc) 5% v/v, under standard conditions and measured under continuous stirring at 20 °C. In the case of the molecules discussed in **Chapter 3: Diazacationic Ladder-type Polymers with Pyrene**, toluene was used as the solvent, which was deaerated before the measurements and measured at 20 °C.

The acquired fluorescence decays were subjected to analysis using the SAND program, which employs the modulation functions method developed and implemented by Striker et al.¹⁵ This technique involves the summation of discrete exponentials. Additionally, for ChiNPy polymers, the maximum entropy method (MEM) was employed for analysis.¹⁵⁻¹⁷

4.1.7 Pump-probe femtosecond Transient Absorption

Ultrafast Transient Absorption (TA), also known as pump/probe spectroscopy, is a nonlinear spectroscopy technique centered around the measurement of alterations in the absorption spectrum of a system after excitation. In this method, samples are subjected to photoexcitation using a femtosecond (fs) pulse referred to as the pump, while changes in absorption are gauged using a subsequent pulse known as the probe. The probe pulse is generally spectrally broad, allowing simultaneous recording of spectrum modifications over a wide range. Additionally, variations in the spectrum are captured at distinct time intervals between the two pulses, producing kinetic traces of time-dependent absorption. Pump-probe TA spectroscopy is a potent technique employed to investigate ultrafast dynamics in diverse materials, including molecules, nanoparticles, and biological systems. It offers insights into structural and electronic changes occurring within exceedingly short timescales, often within the femtosecond to picosecond range.

In this approach, the pump pulse resonates with one of the electronic transitions of the sample to elevate it to an excited state. Transient Absorption is conveyed as the differential optical density (ΔOD), which is formulated as shown in **Equation 4.7**.¹⁸⁻¹⁹

$$\Delta OD = \frac{1}{2.303} \frac{I_u - I_p}{I_u} \quad 4.7$$

Where I_u and I_p represent the probe light intensity through the unexcited (u) and photoexcited (p) samples, respectively. In this spectroscopy approach, three distinct signals can be observed: two negative signals attributed to ground-state bleaching (GSB) and stimulated emission (SE), and one positive signal stemming from excited-state absorption (ESA).¹⁸

Experimental conditions: Time-resolved ultrafast TA measurements were conducted using a broadband HELIOS spectrometer (350-1600 nm) from Ultrafast System, as detailed elsewhere.²⁰ TA data was acquired with excitation at 380 nm and probing in the 400-760 nm range. Measurements in solution were performed in a 2 mm quartz cuvette, with an optical density of approximately 0.5 at the pump excitation wavelength. To ensure sample homogeneity and avoid photodegradation, a motorized translating sample holder was employed for continuous movement. The spectral data was corrected and analyzed using the software Surface Explorer version 4.5.3 from Ultrafast Systems, with the instrumental response function (IRF) set to 250 fs.

4.1.8 Theoretical Calculations

The Density-Functional Theory (DFT), initially formulated by Hohenberg and Kohn, posits that the electronic energy within the ground state can be comprehensively determined without necessitating a wave function.

Instead, the electron density establishes a direct correspondence with energy, thereby underscoring the intrinsic connection between them. However, it was Kohn and Sham who subsequently refined its practical application, devising a calculation methodology that exhibits a structural resemblance to the Hartree-Fock methods.²¹

Within the framework of the Kohn-Sham approach to DFT, the incorporation of a density functional alongside the kinetic energy operator becomes essential to acquire correlation and exchange energies. These quantities, while essential, cannot be obtained directly and necessitate specific treatment. The realm of available functionals for conducting such calculations is expansive, encompassing those fashioned from first principles (*ab initio* methods) as well as those derived from parameterized functions utilizing empirical values. The latter often exhibit a superior capacity to replicate experimental outcomes.²¹⁻²²

For addressing excited electronic states, the Time-Dependent Density Functional Theory (TD-DFT) emerges as an indispensable avenue. This approach yields notably accurate values when juxtaposed with empirical measurements, boasting the added advantage of being computationally more efficient in comparison to alternative methodologies. The foundation of TD-DFT rests upon a theorem arising from the time-dependent Schrödinger equation, necessitating the utilization of a corresponding functional.²²

Experimental conditions: Theoretical computations encompassing the ultraviolet-visible (UV-visible) spectral range were executed utilizing Density Functional Theory (DFT) with the software GAMESS-US 2018R3.²³ The chosen approach involved the application of the LC-BPBE functional ($\omega = 0.20$).²⁴⁻²⁵ For Time-Dependent DFT (TD-DFT) assessments of Franck-Condon (FC) excitations, the solvent's dielectric constant was partitioned into two components: a "bulk" element and a swift component, denoting the square of the refractive index. Under "adiabatic" conditions, solely the static dielectric constant was employed. Both DFT and TD-DFT calculations were conducted using a 6-31G** basis set.

The outcomes attained through the employment of the LC-BPBE(20) functional present unprocessed, unscaled data derived from the computations. In instances of $S_0 \rightarrow S_n$ transitions, a minor correction of 0.05 eV was introduced to rectify the variance between the zero-point and the initial vibronic level. Subsequently, optimized geometries were ascertained, followed by the execution of time-dependent DFT calculations (employing the identical functional and basis set as previous assessments) for forecasting the vertical electronic excitation energies. Molecular orbital distributions were visualized utilizing the ChemCraft 1.7 software. Furthermore, a frequency analysis was undertaken for each compound, revealing the absence of imaginary frequencies, signifying that the molecular structures correspond to, at the very least, a local energy minimum on the potential energy surface.

Due to the extensive volume of computations conducted, a succinct illustration of the model templates employed will be provided as follows:

```

! DFT for optimization of ground-state structure of ChiNPy polymers*, MonPy & PolyNPy
$CONTRL SCFTYP=RHF RUNTYP=OPTIMIZE MAXIT=200 MULT=1
DFTTYP=BPBE NOSYM=1 $END
$$SYSTEM TIMLIM=525600 MEMORY=1000000000 $END
$BASIS GBASIS=N31 NGAUSS=6 NDFUNC=1 NPFUNC=1 $END
$$SCF DIRSCF=.TRUE. $END
$DFT LC=.T. MU=0.2 $END
$PCM solvnt=toluene smd=.true. $END
$TD-DFT NSTATE=10 MULT=1 $END
$$STATPT OPTTOL=0.0001 NSTEP=300 $END
$DATA
NAME
C1
      COORDINATES GAMESS-US FORMAT
END

```

```

! TD-DFT for excited state of ChiNPy polymers*, MonPy & PolyNPy
$CONTRL SCFTYP=RHF RUNTYP=ENERGY MAXIT=200 ICHARG=+2 MULT=1
DFTTYP=BPBE NOSYM=1 TD-DFT=EXCITE $END
$$SYSTEM TIMLIM=525600 MEMORY=1000000000 $END
$BASIS GBASIS=N31 NGAUSS=6 NDFUNC=1 NPFUNC=1 $END
$$SCF DIRSCF=.TRUE. $END
$DFT LC=.T. MU=0.2 $END
$PCM SOLVNT=toluene smd=.true. $END
$TD-DFT NSTATE=15 MULT=1 $END
$$STATPT OPTTOL=0.0001 NSTEP=300 $END
$DATA
NAME
C1
      OPTIMIZED COORDINATES GAMESS-US FORMAT
END

```

**Notes: For ChiNPy polymers solvent in PCM model was change for water*

```

! DFT for optimization of ground-state structure of DiazaPy
$CONTRL SCFTYP=RHF RUNTYP=OPTIMIZE MAXIT=200 ICHARG=+2 MULT=1
DFTTYP=BPBE NOSYM=1 $END
$$SYSTEM TIMLIM=525600 MEMORY=1000000000 $END
$BASIS GBASIS=N31 NGAUSS=6 NDFUNC=1 NPFUNC=1 $END
$$SCF DIRSCF=.TRUE. $END
$DFT LC=.T. MU=0.2 $END
$PCM solvnt=toluene smd=.true. $END
$TD-DFT NSTATE=10 MULT=1 $END
$$STATPT OPTTOL=0.0001 NSTEP=300 $END
$DATA
NAME
C1
      COORDINATES GAMESS-US FORMAT
END

```

```

! TD-DFT for excited state for DiazaPy
$CONTRL SCFTYP=RHF RUNTYP=ENERGY MAXIT=200 ICHARG=+2 MULT=1
DFTTYP=BPBE NOSYM=1 TD-DFT=EXCITE $END
$$SYSTEM TIMLIM=525600 MEMORY=1000000000 $END
$BASIS GBASIS=N31 NGAUSS=6 NDFUNC=1 NPFUNC=1 $END
$$SCF DIRSCF=.TRUE. $END
$DFT LC=.T. MU=0.2 $END
$PCM SOLVNT=toluene smd=.true. $END
$TD-DFT NSTATE=15 MULT=1 $END
$$STATPT OPTTOL=0.0001 NSTEP=300 $END
$DATA
NAME
C1
      OPTIMIZED COORDINATES GAMESS-US FORMAT
END

```

Bibliography

1. Gonsalves, A. R.; Pinho, T., *Espectroscopia de ressonância magnética e nuclear*. Imprensa da Universidade de Coimbra/Coimbra University Press: 2007.
2. Skoog, D. A.; Holler, F. J.; Crouch, S. R., *Principles of instrumental analysis*. Cengage learning: 2017.
3. Pitt, J. J., Principles and applications of liquid chromatography-mass spectrometry in clinical biochemistry. *Clin Biochem Rev* **2009**, *30* (1), 19-34.
4. Smith, B. C., *Fundamentals of Fourier transform infrared spectroscopy*. CRC press: 2011.
5. Larkin, P., *Infrared and Raman spectroscopy: principles and spectral interpretation*. Elsevier: 2017.
6. Stoll, S.; Goldfarb, D., *EPR spectroscopy: fundamentals and methods*. John Wiley & Sons: 2018.
7. Stoll, S.; Schweiger, A., EasySpin, a comprehensive software package for spectral simulation and analysis in EPR. *J Magn Reson* **2006**, *178* (1), 42-55.
8. Perkampus, H.-H., *UV-VIS Spectroscopy and its Applications*. Springer Science & Business Media: 2013.
9. Lakowicz, J. R., *Principles of fluorescence spectroscopy*. Springer: 2006.
10. Seixas de Melo, J. S.; Pina, J.; Dias, F. B.; Maçanita, A. L., Experimental Techniques for Excited State Characterisation. In *Applied Photochemistry*, Evans, R. C.; Douglas, P.; Burrow, H. D., Eds. Springer Netherlands: Dordrecht, 2013; pp 533-585.
11. Becker, W., *Advanced time-correlated single photon counting applications*. Springer: 2015; Vol. 111.
12. Seixas de Melo, J., The influence of oxygen on the lifetime of luminescent probes. A simple device for degassing solutions for fluorescence measurements. *Chem. Educ* **2005**, *10* (05), 29-35.
13. Pina, J.; Seixas de Melo, J.; Burrows, H. D.; Maçanita, A. L.; Galbrecht, F.; Bunnagel, T.; Scherf, U., Alternating Binaphthyl-Thiophene Copolymers: Synthesis, Spectroscopy, and Photophysics and Their Relevance to the Question of Energy Migration versus Conformational Relaxation. *Macromolecules* **2009**, *42* (5), 1710-1719.
14. Rodrigues, A. C. B.; Eckert, A.; Pina, J.; Scherf, U.; Seixas de Melo, J. S., Polymeric near infrared emitters with bay-annulated indigo moieties. *Materials Advances* **2021**, *2* (11), 3736-3743.
15. Striker, G.; Subramaniam, V.; Seidel, C. A. M.; Volkmer, A., Photochromicity and Fluorescence Lifetimes of Green Fluorescent Protein. *The Journal of Physical Chemistry B* **1999**, *103* (40), 8612-8617.
16. Berberan-Santos, M. N.; Valeur, B., Luminescence decays with underlying distributions: General properties and analysis with mathematical functions. *Journal of Luminescence* **2007**, *126* (2), 263-272.
17. Shaver, J. M.; McGown, L. B., Maximum Entropy Method for Frequency Domain Fluorescence Lifetime Analysis. 1. Effects of Frequency Range and Random Noise. *Analytical Chemistry* **1996**, *68* (1), 9-17.
18. Sciortino, A.; Messina, F., Ultrafast Optical Spectroscopies. *Spectroscopy for Materials Characterization* **2021**, 65-95.
19. Ruckebusch, C.; Sliwa, M.; Pernot, P.; de Juan, A.; Tauler, R., Comprehensive data analysis of femtosecond transient absorption spectra: A review. *Journal of Photochemistry and Photobiology C: Photochemistry Reviews* **2012**, *13* (1), 1-27.

20. Pina, J.; Queiroz, M. J.; Seixas de Melo, J., Effect of substitution on the ultrafast deactivation of the excited state of benzo[b]thiophene-arylamines. *Photochem Photobiol Sci* **2016**, *15* (8), 1029-38.
21. Young, D., *Computational chemistry: a practical guide for applying techniques to real world problems*. John Wiley & Sons: 2004.
22. Jensen, F., *Introduction to computational chemistry*. John Wiley & sons: 2017.
23. Barca, G. M. J.; Bertoni, C.; Carrington, L.; Datta, D.; De Silva, N.; Deustua, J. E.; Fedorov, D. G.; Gour, J. R.; Gunina, A. O.; Guidez, E.; Harville, T.; Irlé, S.; Ivanic, J.; Kowalski, K.; Leang, S. S.; Li, H.; Li, W.; Lutz, J. J.; Magoulas, I.; Mato, J.; Mironov, V.; Nakata, H.; Pham, B. Q.; Piecuch, P.; Poole, D.; Pruitt, S. R.; Rendell, A. P.; Roskop, L. B.; Ruedenberg, K.; Sattasathuchana, T.; Schmidt, M. W.; Shen, J.; Slipchenko, L.; Sosonkina, M.; Sundriyal, V.; Tiwari, A.; Galvez Vallejo, J. L.; Westheimer, B.; Wloch, M.; Xu, P.; Zahariev, F.; Gordon, M. S., Recent developments in the general atomic and molecular electronic structure system. *J Chem Phys* **2020**, *152* (15), 154102.
24. Perdew, J. P.; Burke, K.; Ernzerhof, M., Generalized gradient approximation made simple. *Physical review letters* **1996**, *77* (18), 3865.
25. Adamo, C.; Barone, V., Toward reliable density functional methods without adjustable parameters: The PBE0 model. *The Journal of chemical physics* **1999**, *110* (13), 6158-6170.

Chapter 5:

Appendix

Appendix A. ^1H NMR of ChiNPy Polymers

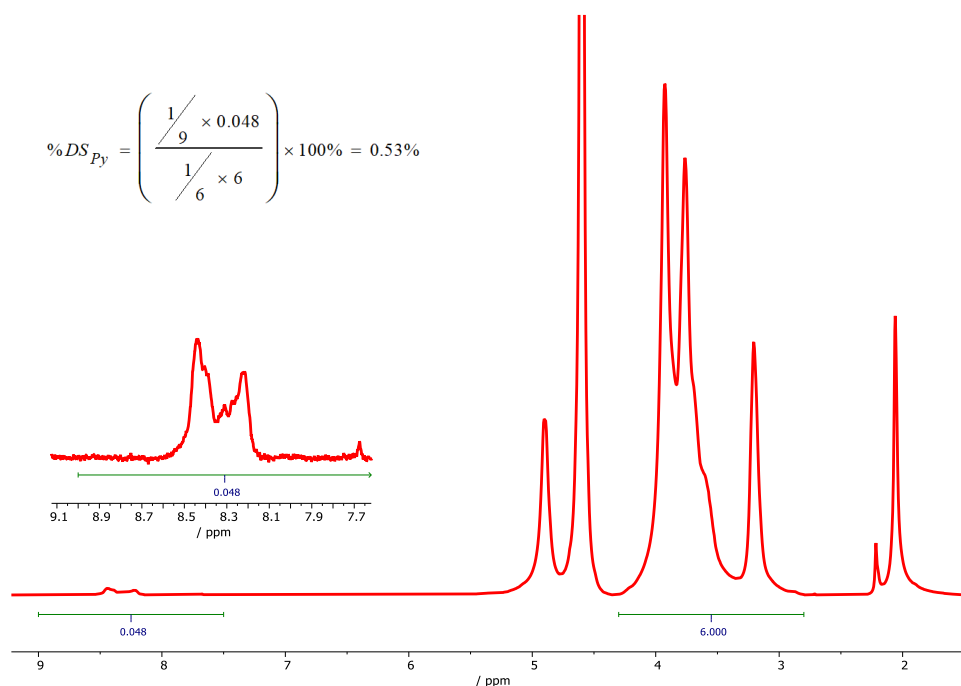


Figure 5.1 ^1H NMR of ChiNPy-A at 50 °C in D_2O : DCI 1% solution. The degree of substitution determined by this technique is shown as inset.

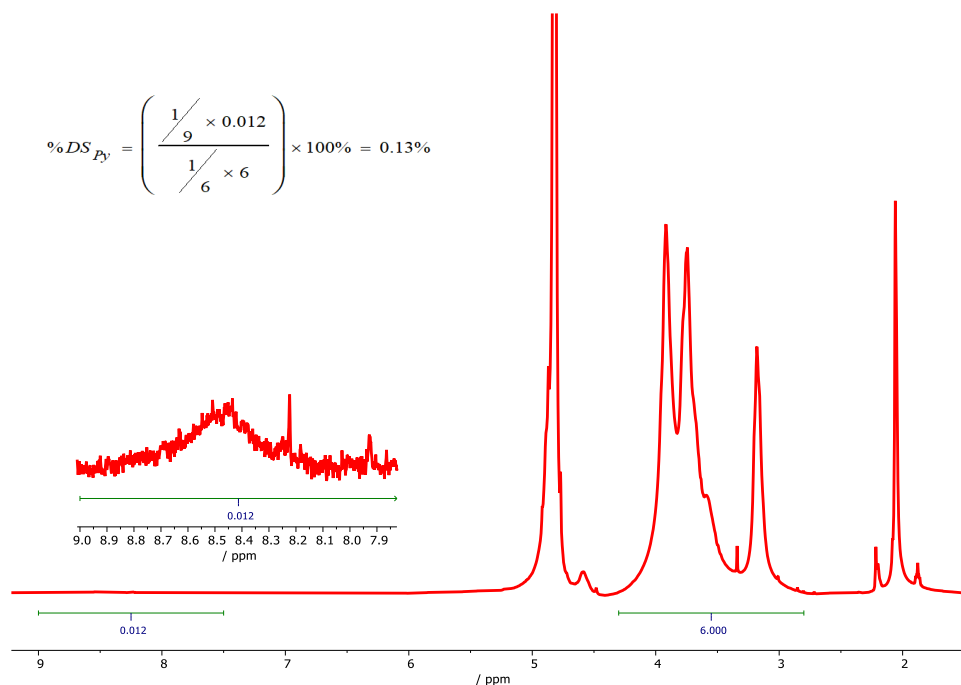


Figure 5.2 ^1H NMR of ChiNPy-A at 50 °C in D_2O : DCI 1% solution. The degree of substitution determined by this technique is shown as inset.

Appendix B. Determination of molar extinction coefficient

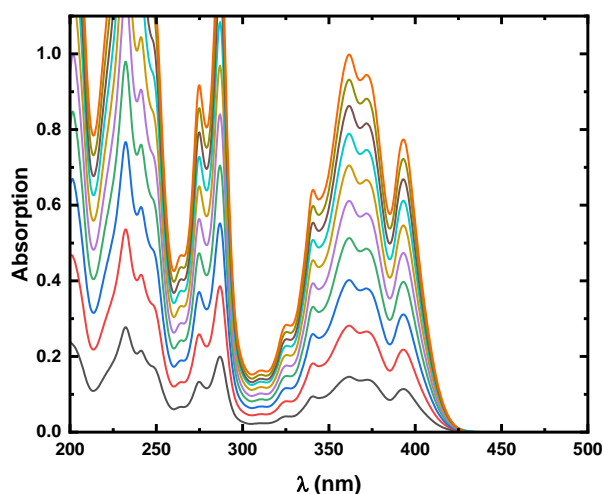


Figure 5.3 Representation of UV-Vis spectra of 1-pyrenecarboxyaldehyde for determination of molar extinction coefficient in methanol at 20 °C.

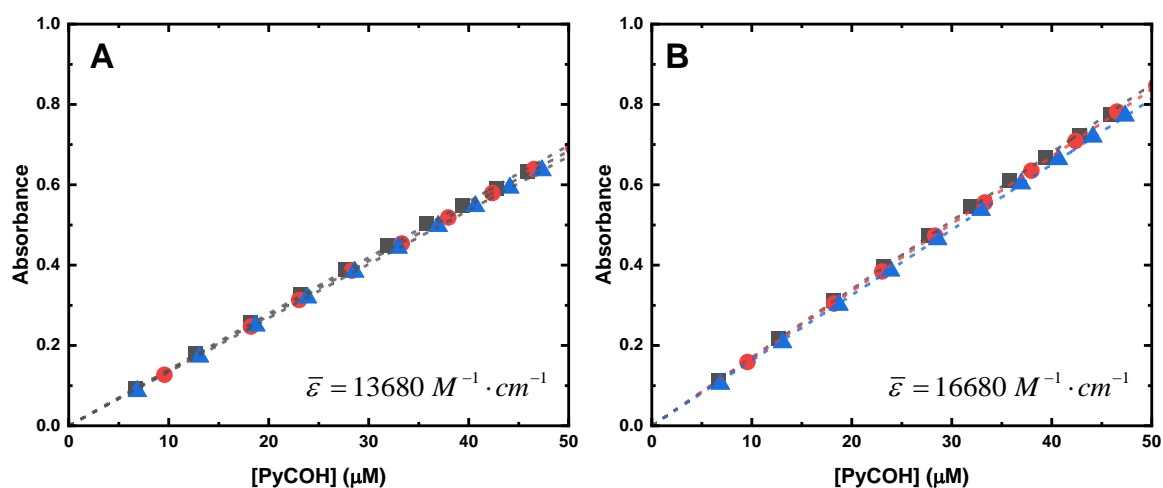


Figure 5.4 Determination of molar extinction coefficient of 1-pyrenecarboxyaldehyde in methanol at (A) 340 nm and (B) 393 nm.

Appendix C. Determination of %DS_{Py} by UV-Vis techniques

%DS_{Py} is obtained by UV-Vis as the average of independent measurements and its confidence limits are given by **Equation 5.1** for a small population with $P=0.05$ and $n-1$ freedom degrees, with a two-tailed t student distribution.

$$\bar{x} \pm t_{n-1} \cdot \frac{s}{\sqrt{n}} \quad 5.1$$

Table 5.1 Resume of experiments for determination of the degree of substitution with pyrene (%DS_{Py}) for ChiNPy-A by UV-Vis techniques.

	[Polymer]/ mg·mL ⁻¹	y _{Py} Imine	x _{Py} Amine	P _{AC}	w _{DA}	%DS _{Py}
ChiNPy-A	0.710	1	5	210	1045	0.47
	0.893	1	6	259	1291	0.47
	0.798	1	6	248	1236	0.47
	0.922	1	6	264	1315	0.44
	0.968	1	5	243	1209	0.44
	Avg	1	6	258	1287	0.46 ± 0.02
	Pyrene units	1		Other units	c.a. 230	

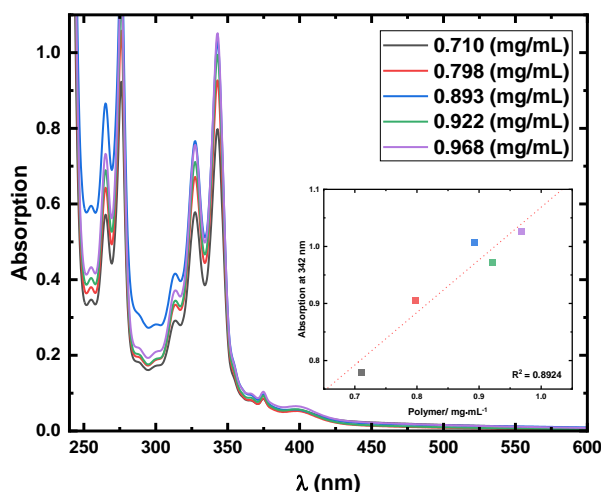


Figure 5.5 Absorption spectra of ChiNPy-A solutions used for determination of %DS_{Py}.

Table 5.2 Resume of experiments for determination of the degree of substitution with pyrene (%DS_{Py}) for ChiNPy-B by UV-Vis techniques.

	[Polymer]/ mg·mL ⁻¹	y _{Py} Imine	x _{Py} Amine	P _{AC}	w _{DA}	%DS _{Py}
ChiNPy-B	0.090	1	3	15	65	4.48
	0.049	1	2	10	44	4.63
	0.067	1	2	12	54	4.48
	0.046	1	2	11	51	4.44
	0.037	1	2	13	59	4.18
	Avg	1	2	12	52	4.4 ± 0.2
	Pyrene units	1		Other units	c.a. 20	

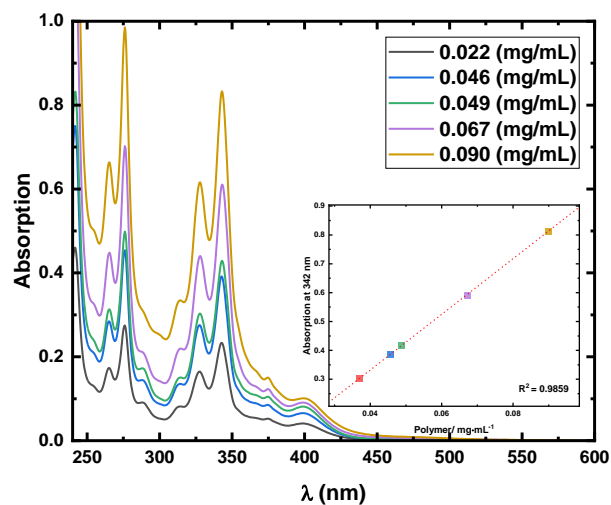


Figure 5.6 Absorption spectra of ChiNPy-B solutions used for determination of its %DS_{Py}.

Table 5.3 Resume of experiments for determination of the degree of substitution with pyrene (%DS_{Py}) for ChiNPy-Imine by UV-Vis techniques.

	[Polymer]/ mg·mL ⁻¹	Y _{Py Imine}	P _{AC}	w _{DA}	%DS _{Py}
ChiNPy-Imine	0.648	1	0	123	619
	0.845	1	0	134	676
	0.847	1	0	129	650
	0.711	1	0	128	645
	0.821	1	0	142	712
	Avg	1	138	694	0.13 ± 0.01
	Pyrene units	1	Other units	c.a. 830	

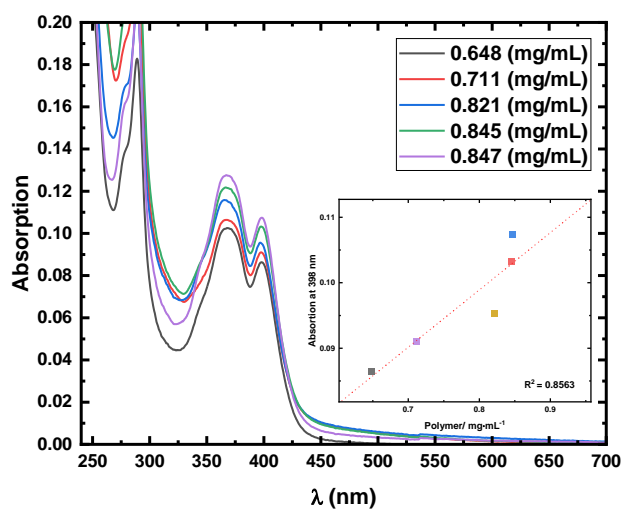


Figure 5.7 Absorption spectra of ChiNPy-Imine solutions used for determination of its %DS_{Py}.

Appendix D. Fluorescence quenching

Fluorescence quenching pertains to any process that reduces the fluorescence intensity of a sample. This phenomenon can arise from a diverse array of interactions involving the fluorophore. One form of quenching is collisional quenching, which is mathematically characterized by the Stern-Volmer equation:

$$\frac{F_0}{F} = 1 + k_q \tau_0 [Q] \quad 5.2$$

In **Equation 5.2**, the symbols F_0 and F represent the fluorescence intensities in the absence and presence of the quencher, respectively. The parameter k_q denotes the bimolecular quenching constant, while τ_0 signifies the lifetime of the fluorophore in the absence of the quencher. The concentration of the quencher is represented by the symbol Q .

A linear Stern-Volmer plot typically suggests the presence of a single type of fluorophore that is equally accessible to the quencher. This form of quenching is often referred to as static quenching, wherein the interaction occurs exclusively with the excited state of the fluorophore. However, if there are two distinct populations of fluorophores, the Stern-Volmer plot will deviate from linearity, showing a shift towards the x-axis.

An upward deviation from linearity signifies the coexistence of static and dynamic quenching. In this scenario, dynamic quenching becomes prominent due to a subset of fluorophores undergoing quenching through the formation of a dynamic ground-state complex. Consequently, the fractional fluorescence remaining (F/F_0) can be expressed as the product of the fraction that is not in complex with the quencher and the fraction that remains unquenched. This relationship leads to the formulation expressed by **Equation 5.3**. The dynamic portion (K_D) of the observed quenching can be determined through time-resolved measurements.¹⁻²

$$\frac{F_0}{F} = 1 + (K_D + K_S)[Q] + K_D K_S [Q]^2 \quad 5.3$$

In cases where a Stern-Volmer plot displays a downward curvature, it implies the presence of two distinct populations, one of which is not readily accessible to the quencher due to physical hindrances. This type of quenching tends to manifest in macromolecular systems such as polymers and proteins, where not all the fluorophores are uniformly exposed to the quencher. This phenomenon leads to a self-protection mechanism against quenching, resulting in a consistent residual fluorescence emission. In such scenarios, the Stern-Volmer plot is adapted according to **Equation 5.4**, wherein f_a represents the fraction of the initial fluorescence

accessible to the quencher, and K_a signifies the Stern-Volmer quenching constant associated with the accessible fraction. ¹

$$\frac{F_0}{\Delta F} = \frac{1}{f_a K_a [Q]} + \frac{1}{f_a} \quad 5.4$$

Appendix E. Statistical parameter of Stern-Volmer plots

Table 5.4 Summary of relevant parameters obtained by the linear fit of the alternative Stern-Volmer plot for the different quenchers tested with ChiNPy-B at 25 °C.

Quencher	Intercept		Slope		Adj. R-Square
	Value	Standard Error	Value	Standard Error	
Cl ⁻	5.16	0.44	500.3	17.0	0.990
NO ₃ ⁻	1.89	0.18	92.8	4.0	0.984
I ⁻	1.32	0.25	103.6	2.7	0.994
Cu ²⁺	2.61	0.48	363.2	10.2	0.993
Hg ²⁺	2.66	0.40	89.8	2.7	0.992
Pb ²⁺	1.51	0.12	34.4	0.8	0.995

Appendix F. Prediction of electronic transitions of MonPy, PolyNPy, and DiazaPy

Table 5.5 Most relevant predicted transition for compound MonPy, PolyNPy, and DiazaPy and representation of the orbital evolved in the respective transition.

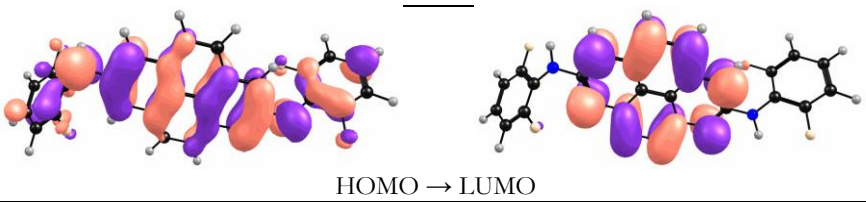
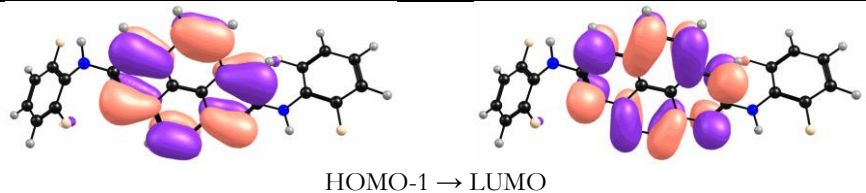
Compound	λ_{abs} /nm (f)	Electronic transition	
MonPy	386 (0.0642)	 HOMO → LUMO	
MonPy	332 (0.4266)	 HOMO-1 → LUMO	

Table 5.5 (continue) Most relevant predicted transition for compound MonPy, PolyNPy, and DiazaPy and representation of the orbital evolved in the respective transition.

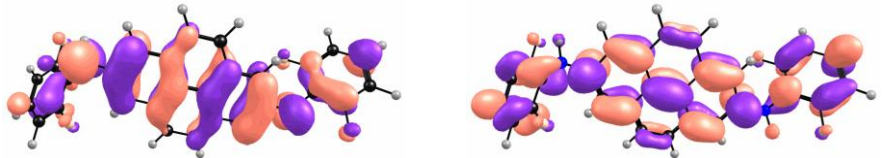
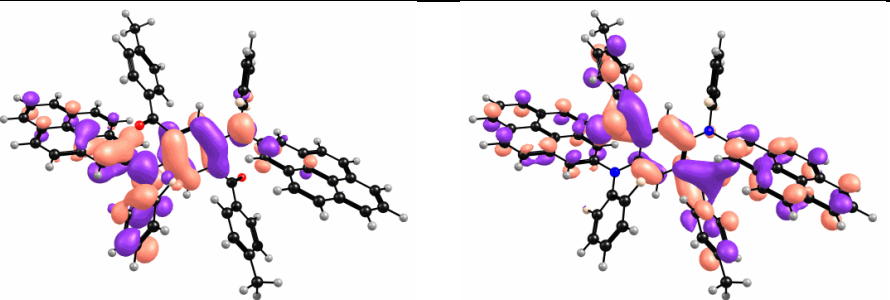
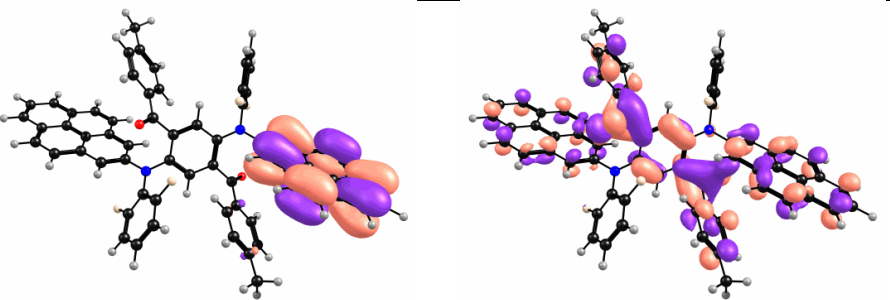
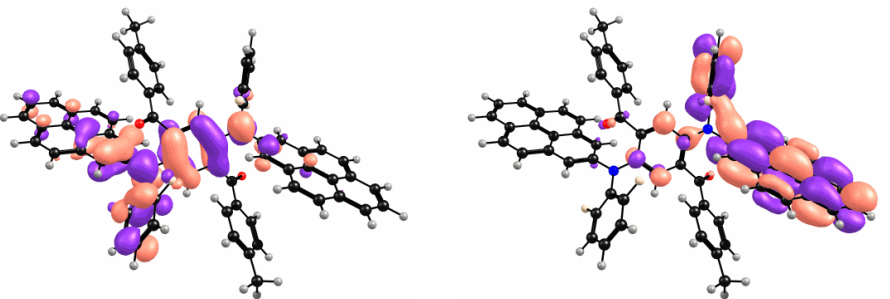
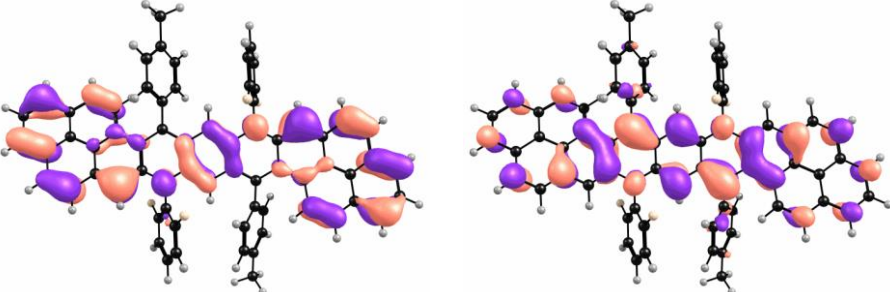
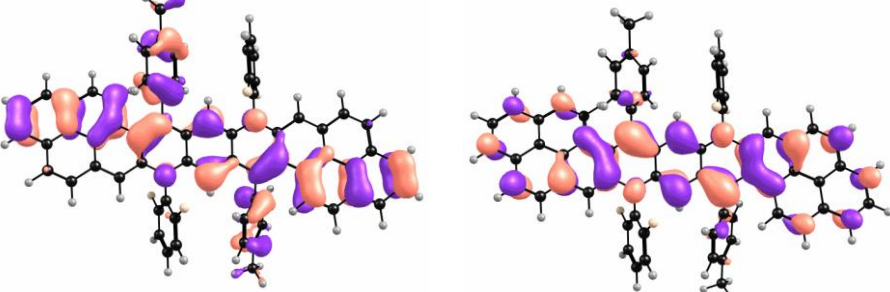
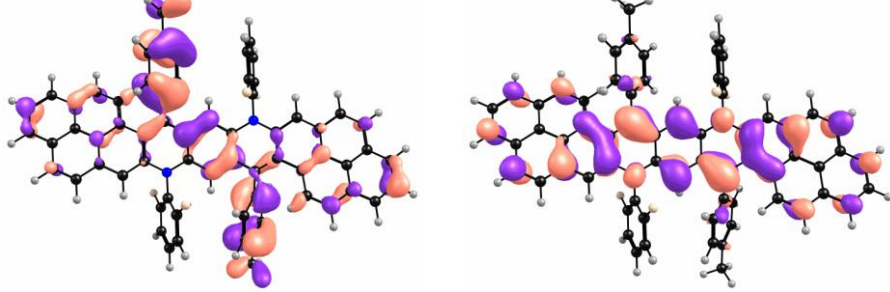
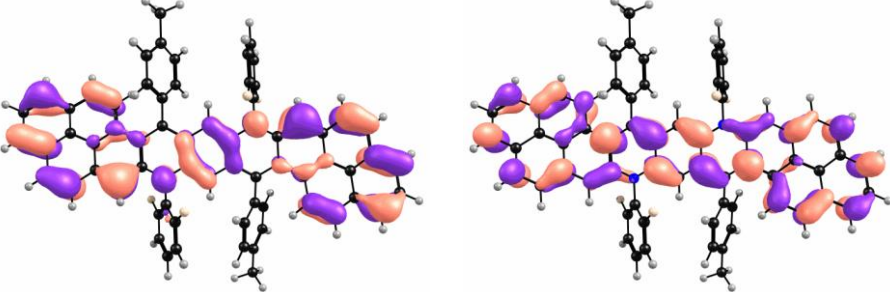
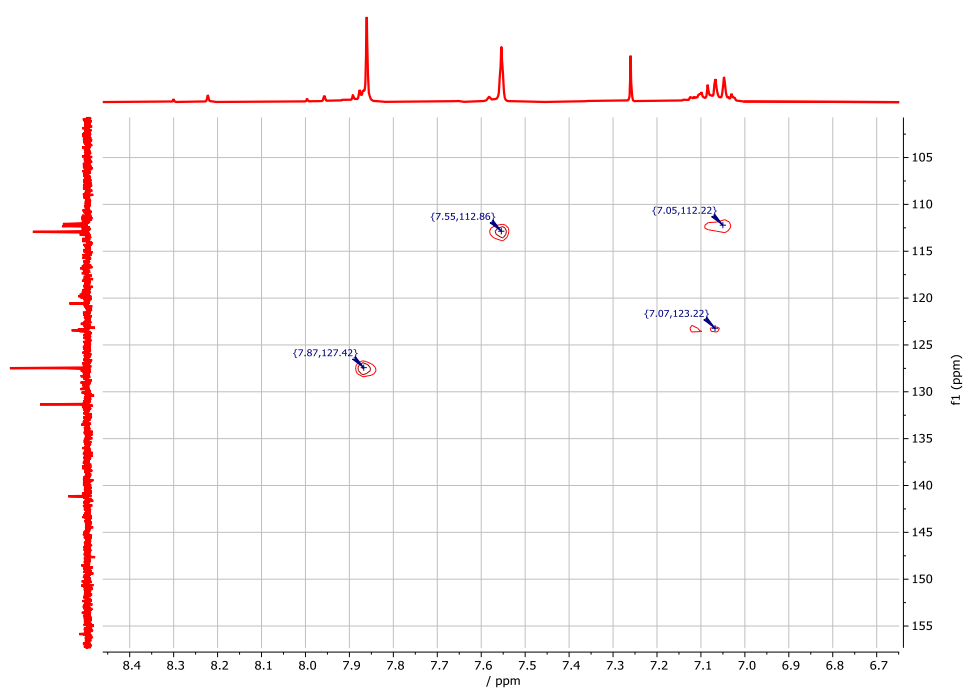
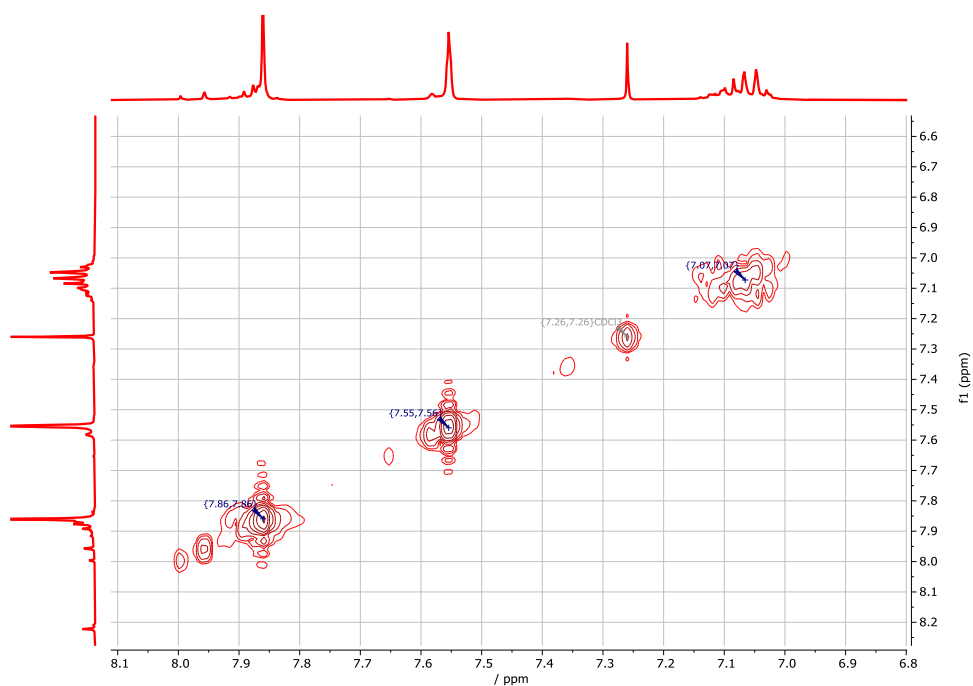
Compound	λ_{abs} /nm (<i>f</i>)	Electronic transition	
	297 (2.2475)	 <p data-bbox="874 741 1114 768">HOMO \rightarrow LUMO+1</p>	
PolyNPy	463 (0.0456)	 <p data-bbox="890 1077 1098 1104">HOMO \rightarrow LUMO</p>	
	350 (0.9061)	 <p data-bbox="879 1417 1109 1444">HOMO-2 \rightarrow LUMO</p>	
	318 (0.7667)	 <p data-bbox="874 1758 1114 1785">HOMO \rightarrow LUMO +4</p>	

Table 5.5 (continue) Most relevant predicted transition for compound MonPy, PolyNPy and DiazaPy and representation of the orbital evolved in the respective transition.

Compound	$\lambda_{\text{abs}} / \text{nm}$ (f)	Electronic transition
DiazaPy	760 (0.9487)	 <p style="text-align: center;">HOMO \rightarrow LUMO</p>
	518 (0.7805)	 <p style="text-align: center;">HOMO-2 \rightarrow LUMO</p>
	425 (0.3845)	 <p style="text-align: center;">HOMO-4 \rightarrow LUMO</p>
	344 (0.10928)	 <p style="text-align: center;">HOMO \rightarrow LUMO+2</p>

Appendix G. 2D-NMR of MonPy



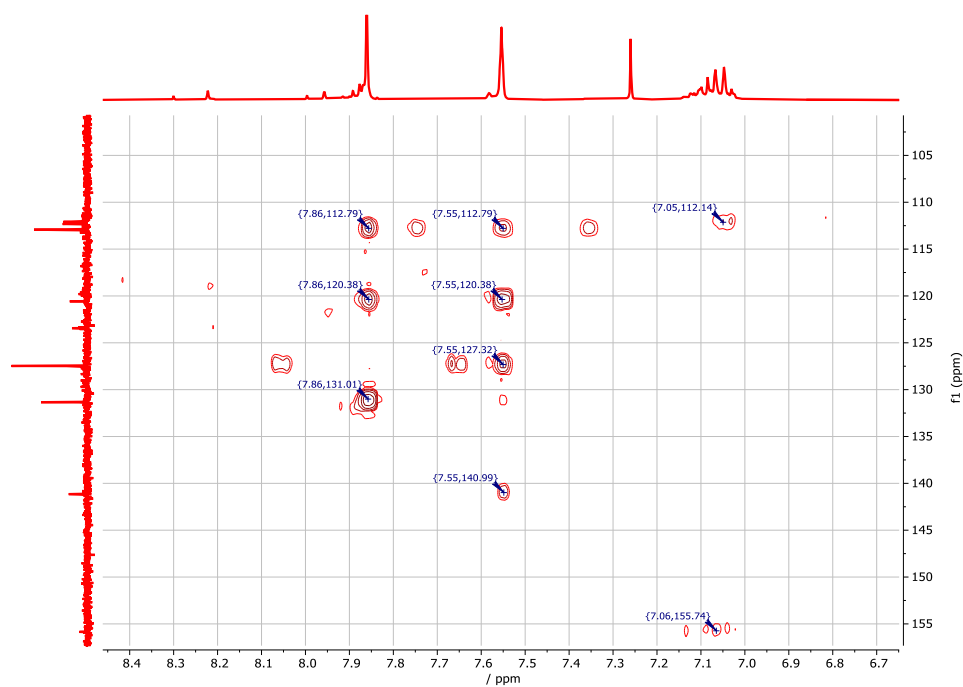


Figure 5.10 ^1H - ^{13}C HMBC NMR spectra of MonPy in CDCl_3 .

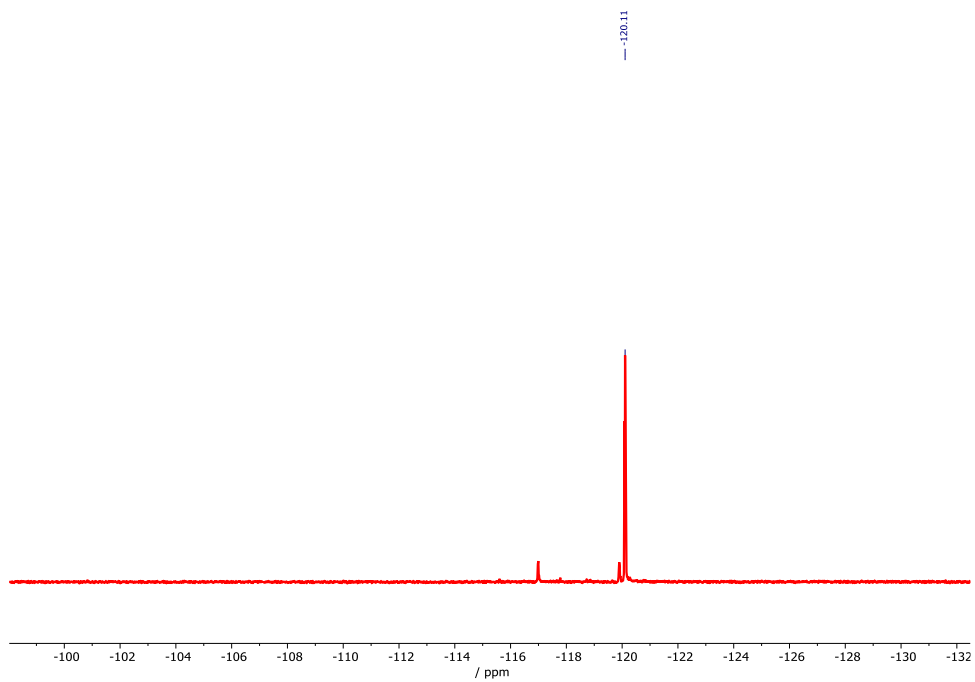


Figure 5.11 ^{19}F NMR spectra of MonPy in CDCl_3 .

Bibliography

1. Lakowicz, J. R., *Principles of fluorescence spectroscopy*. Springer: 2006.
2. Valeur, B.; Berberan-Santos, M. N., *Molecular fluorescence: principles and applications*. John Wiley & Sons: 2012.